NASA CR-179648
GARRETT 21-6355

National
Aeronautics and
Space
Administration

THERMAL BARRIER COATING LIFE-PREDICTION MODEL DEVELOPMENT

FINAL REPORT

by

T.E. STRANGMAN
J. NEUMANN
A. LIU

GARRETT TURBINE ENGINE COMPANY
A DIVISION OF THE GARRETT CORPORATION
PHOENIX, ARIZONA

Prepared for

NATIONAL AERONAUTICS AND SPACE ADMINISTRATION
NASA-LERC (CONTRACT NAS3-23945)

1. Report No.	2. Government Accession No.	3. Recipient's Catalog No.
CR-179648		

4. Title and Subtitle	5. Report Date
Thermal Barrier Coating Life - Prediction Model Development Final Report	October 30, 1987
	6. Performing Organization Code

7. Author(s)	8. Performing Organization Report No.
T. E. Strangman A. Liu J. Neumann	21-6355
	10. Work Unit No.

9. Performing Organization Name and Address	11. Contract or Grant No.
Garrett Turbine Engine Company 111 S. 34th Street, P.O. Box 5217 Phoenix, AZ 85010	NAS3-23945
	13. Type of Report and Period Covered
	Final, All Years

12. Sponsoring Agency Name and Address	14. Sponsoring Agency Code
NASA - Lewis Research Center	

15. Supplementary Notes

Project Manager: R. A. Miller
NASA-Lewis Research Center
Cleveland, Ohio 44135

16. Abstract

This program focused on predicting the lives of two types of strain-tolerant and oxidation-resistant thermal barrier coating (TBC) systems that are produced by commercial coating suppliers to the gas turbine industry. The plasma-sprayed TBC system is composed of a low-pressure plasma-spray (LPPS), or an argon shrouded plasma-spray (ASPS) applied oxidation resistant NiCrAlY (or CoNiCrAlY) bond coating, and an air-plasma-sprayed yttria (8 percent) partially stabilized zirconia insulative layer. It is applied by both Chromalloy (Orangeburg, New York), Klock (Manchester, Connecticut), and Union Carbide (Indianapolis, Indiana). The second type of TBC is applied by the electron beam - physical vapor deposition (EB-PVD) process by Temescal (Berkeley, California).

The primary objective of the program was successfully accomplished with the development, calibration, and demonstration of a mechanistic thermochemical model, which rapidly predicts TBC life as a function of engine, mission, and material parameters. The design models have been calibrated for three plasma sprayed and EB-PVD TBC systems and demonstrated for three TFE731 turbofan engine cycles.

In addition to the primary objective of demonstrating the proficiency of this preliminary TBC life model, significant progress was achieved in the development of a thermomechanical stress-based, finite-element micromodel.

Substantial burner rig and mechanical properties data were obtained to support the development and calibration of the above-mentioned thermochemical and thermomechanical life prediction models.

Feasibility of using nondestructive evaluation (NDE) to verify critical TBC properties (thickness and flaw size) was also demonstrated.

Finally, the TBC systems investigated were run concurrently on a TFE731-5 engine to gain experience and provide validation of the TBC life model.

17. Key Words (Suggested by Author(s))	18. Distribution Statement
Thermal Barrier Life Prediction Development Program	

19. Security Classif. (of this report)	20. Security Classif. (of this page)	21. No. of Pages	22. Price*
Unclassified	Unclassified	172	

* For sale by the National Technical Information Service, Springfield, Virginia 22161

TABLE OF CONTENTS

LIST OF FIGURES

LIST OF FIGURES (Contd)

LIST OF FIGURES (Contd)

LIST OF FIGURES (Contd)

LIST OF FIGURES (Contd)

LIST OF FIGURES (Contd)

LIST OF FIGURES (Contd)

LIST OF TABLES

FOREWORD

This report was prepared for the National Aeronautics and Space Administration (NASA), Lewis Research Center. It presents the results of a program conducted to establish mission-analysis-capable life prediction models for thermal barrier coatings (TBCs) on turbine airfoils. The program was conducted as part of the Turbine Engine Hot Section Technology (HOST) Program under Contract NAS3-23945.

The authors wish to acknowledge the assistance and guidance of R.A. Miller of the NASA-Lewis Research Center. In addition, the contributions of our commercial coating suppliers (Chromalloy, Klock, Temescal, and Union Carbide) are hereby acknowledged. Program Management functions at Garrett Turbine Engine Company (GTEC) were ably performed by J. Mays and B. O'Halloran. Burner rig testing was conducted under the direction of G. Capek, G. Curbishley, and J. McIver. Development of the computer life prediction models was assisted by P. Solfest and E. Miller.

THERMAL BARRIER COATING
LIFE-PREDICTION MODEL DEVELOPMENT

1.0 SUMMARY

Thermal barrier coatings (TBCs) for high-performance engine turbine airfoils represent advanced materials technology with both performance and durability benefits. The greatest TBC benefit is the reduction of heat transferred into air-cooled components, allowing higher turbine operating temperatures and/or reduced component cooling for improved engine performance. Recognizing the benefits of TBCs, the Garrett Turbine Engine Company (GTEC) has developed mechanistic thermochemical and thermomechanical life models in this program to facilitate reliable exploitation of TBC benefits.

This program focuses on predicting the lives of two types of strain-tolerant and oxidation-resistant TBC systems that are produced by commercial coating suppliers to the gas turbine industry. The plasma-sprayed (APS) TBC system, composed of a low-pressure plasma spray (LPPS), or an argon-shrouded plasma spray (ASPS) applied oxidation-resistant NiCrAlY (or CoNiCrAlY) bond coating, and an air-plasma-sprayed yttria (8 percent) partially stabilized zirconia insulative layer (Figure 1), is applied by Chromalloy (Orangeburg, New York), Klock (Manchester, Connecticut), and Union Carbide (Indianapolis, Indiana). The second type of TBC is applied by the electron beam evaporation-physical vapor deposition (EB-PVD) process by Edwards-Temescal (Berkeley, California).

The primary objective of this program was to develop an operative TBC design model for life prediction. This objective was successfully accomplished with the development, calibration, and demonstration of a mechanistic thermochemical model, which rapidly predicts TBC life as a function of engine, mission, and materials system parameters (Figure 2). This thermochemical design model

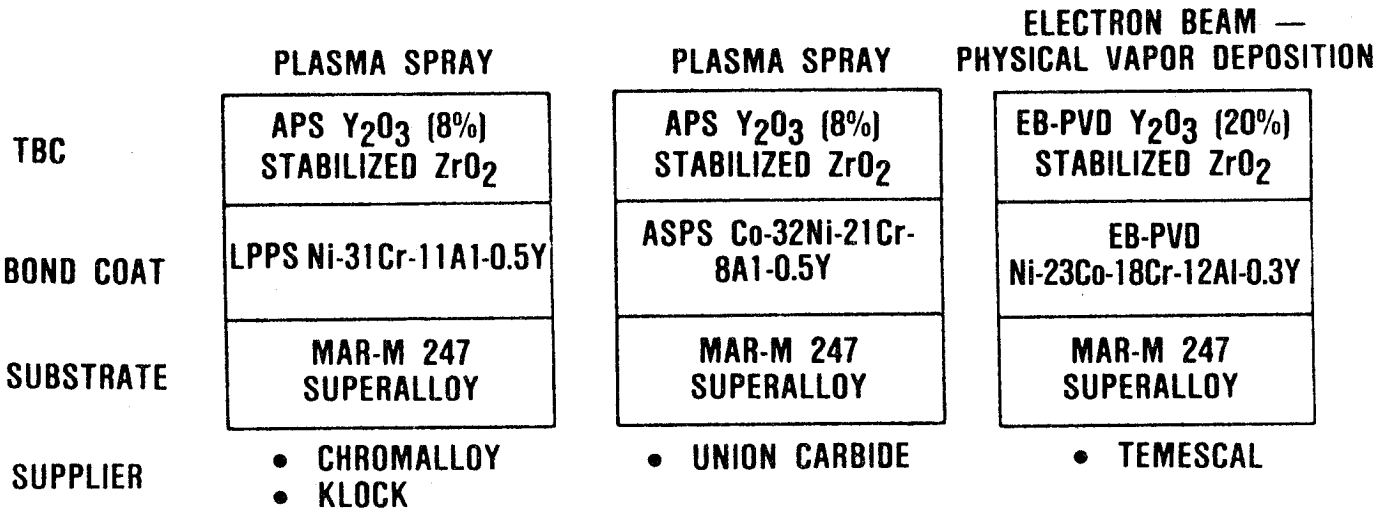

Figure 1. Life Prediction Models are Calibrated for Plasma-Sprayed and EB-PVD TBC Systems.

PRELIMINARY TBC LIFE ANALYSIS METHOD

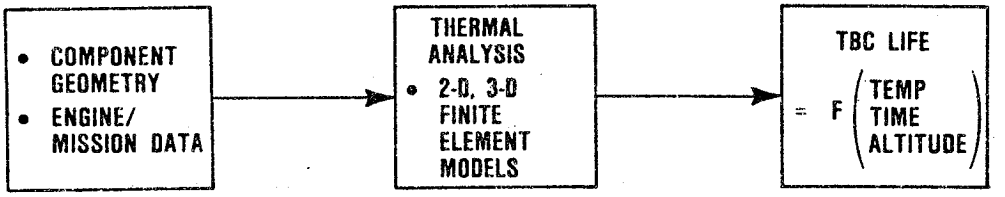

THERMOCHEMICAL MODEL CALIBRATION

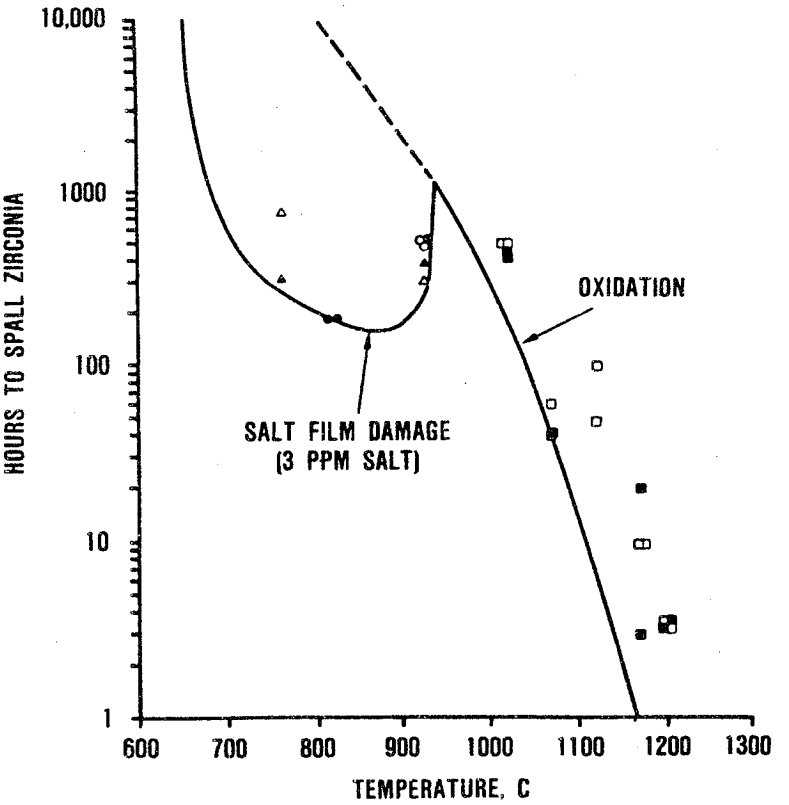

MISSION ANALYSIS CAPABILITY HAS BEEN DEMONSTRATED

TBC SYSTEM	BUSINESS JET	MARITIME SURVEILLANCE
PLASMA SPRAY		
CHROMALLOY	16,517 HOURS	9843 HOURS
UNION CARBIDE	6656 HOURS	5207 HOURS
KLOCK	49,644 HOURS	29,973 HOURS
EB-PVD		
TEMESCAL	55,607 HOURS	2106 HOURS

G7012-21

Figure 2. Inexpensive Design Analysis Iterations are Facilitated by Thermochemical TBC Life Model.

accounts for the three operative TBC damage modes (bond coating oxidation, zirconia toughness reduction, and molten salt film damage), which all contribute to spalling of the insulating zirconia layer. The model has been calibrated for three plasma-sprayed systems and one EB-PVD TBC system, which are applied by commercial sources. The GTEC preliminary design TBC life-prediction system has been demonstrated for three TFE731 turbofan engine cycles (busines aircraft, maritime surveillance, and factory endurance test).

It should be noted that the preliminary TBC life model is primarily driven by the thermal analysis for the component and the anticipated mission usage of the aircraft. This feature permits the designer to economically consider the TBC early in the component design process, which facilitates full incorporation and exploitation of its benefits for turbine airfoil applications.

In addition to achieving the primary objective, significant progress was achieved in the development of a thermomechanical stress-based, finite-element micromodel, which has the potential to more accurately model TBC spalling mechanisms for improved final design life predictions (Figure 3). As presently developed, the micromodel is capable of calculating localized stresses within the TBC system, which arise from ceramic-metal thermal expansion mismatch, thermal, and centrifugal strains. The micromodel is further designed to have sufficient flexibility for future incorporation of refinements, such as analysis of:

- Time- and temperature-dependent changes in local stresses arising from bond-coating oxidation
- Stress redistribution associated with bond-coating creep (stress relaxation)
- Zirconia sintering shrinkage
- Cyclic crack propagation in the zirconia

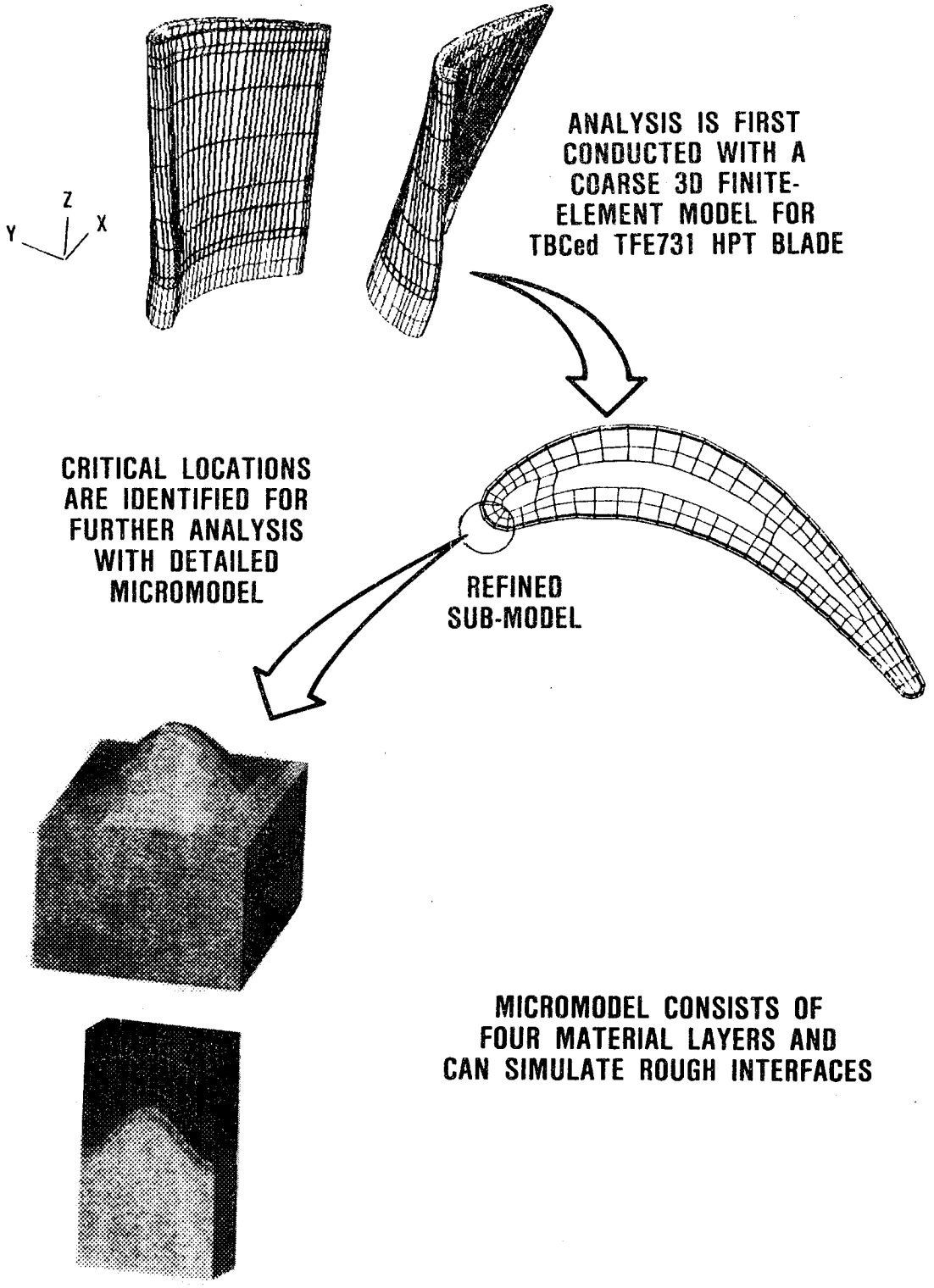

Figure 3. Three-Dimensional Finite-Element Thermomechanical Micromodel Is Interfaced with a Design Grade Coarse Model.

Substantial burner rig and mechanical properties data (Figures 2 and 4) have been obtained to facilitate development and calibration of these thermochemical and thermomechanical life prediction models. Interestingly, it was observed that the toughness of plasma-sprayed zirconia coatings remained stable during short exposures at high temperatures, but transitioned to lower values after longer exposures. Furthermore, the approximate transition time to the lower toughness value was similar to average spalling lives for the TBC system that were observed in burner rig tests in the 1100 to 1150C temperature range, where comparable data were obtained. Zirconia sintering densification ("mud-flat" cracking) and interfacial oxide scale growth (Union Carbide TBC specimens only) appeared to be associated with the reduced level of zirconia toughness.

Thermal conductivity is the critical design property of TBCs, which govern heat transfer into air-cooled turbine components. Component metal temperatures and thermal strains are dependent on the thermal conductivity of the zirconia layer. Consequently, thermal conductivity data were obtained for both plasma-sprayed and EB-PVD zirconia coatings. These data are presented in Figure 5 and are in excellent agreement with published data from other NASA-sponsored programs. They indicate that yttria-stabilized zirconia coatings have thermal conductivities that are lower by about a factor of 30 than typical superalloys.

Finally, effective exploitation of TBCs requires that critical materials properties be verified. The insulative TBC system capability is dependent on thickness. Mechanical integrity of TBCs is dependent on the size of critical flaws. Therefore, feasibility of using nondestructive evaluation (NDE) to verify critical TBC properties (thickness and flaw size) was demonstrated. Eddy current analysis was verified to be a viable method for measuring zirconia

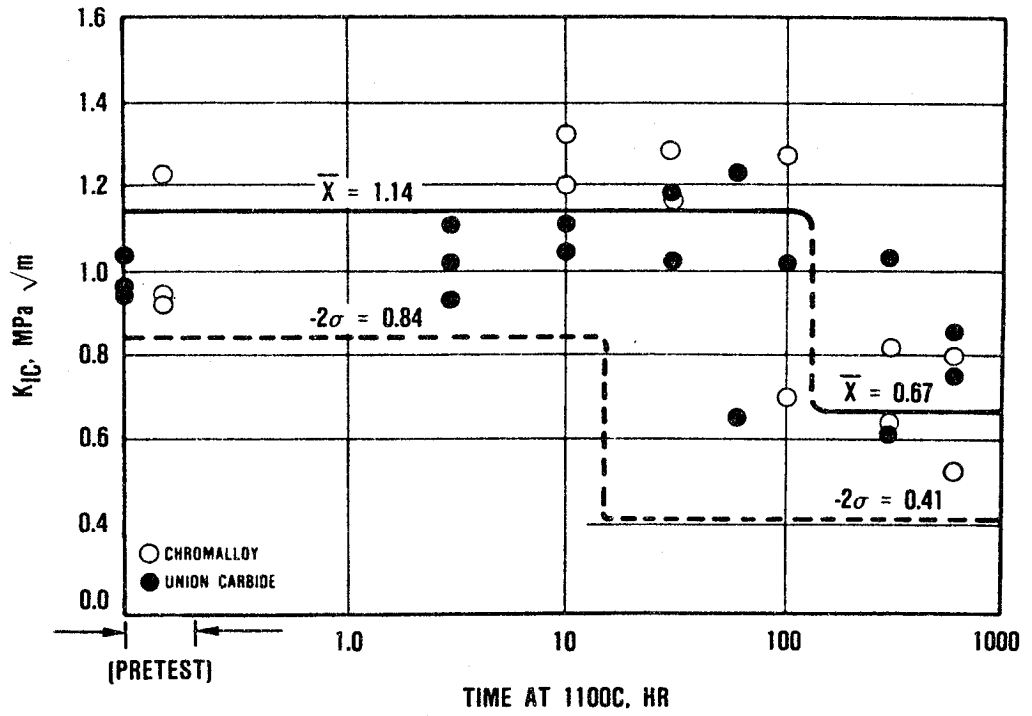

Figure 4. Fracture Toughness of Plasma-Sprayed, Yttria-Stabilized Zirconia Coating is Reduced After Long Exposures at High Temperatures.

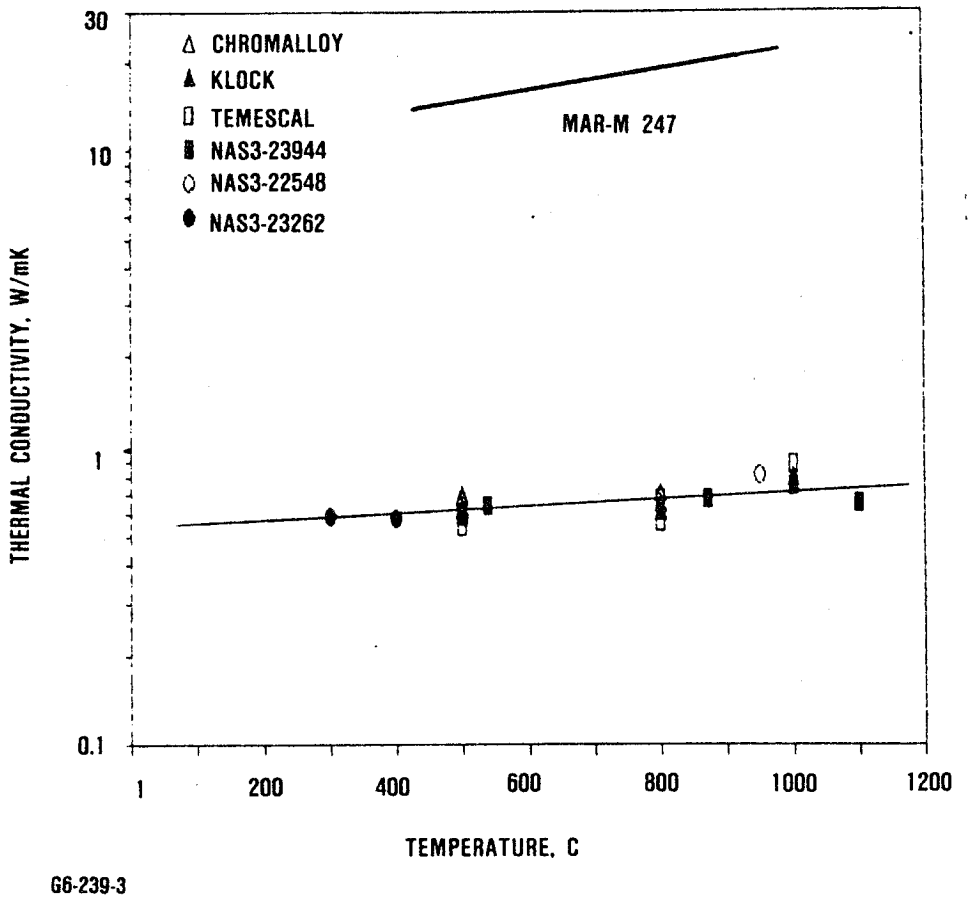

Figure 5. Plasma-Sprayed and EB-PVD TBCs Have Equivalent Thermal Conductivity.

thickness. High-frequency ultrasonics showed promise in detecting flaws at the ceramic-metal interface.

2.0 INTRODUCTION

TBCs for turbine airfoils in high-performance engines represent an advanced materials technology that has both performance and durability benefits. The greatest TBC benefit is the reduction of heat transferred into air-cooled components. However, to achieve these benefits, the TBC system must be predictable because the life of the turbine component will be dependent upon the integrity of the TBC. Therefore, mechanistic, efficient life prediction models and appropriate calibration data were required for the reliable exploitation of TBC benefits on gas turbine airfoils. This program succeeded in fulfilling these requirements.

GTEC strategy for this program comprised the following objectives:

- Development of mission-analysis-capable TBC life models that recognize operative failure modes and account for all significant mission, engine, and component design factors

- Development of rapid computation approaches for estimating TBC life during preliminary design iterations

- Calibration of the TBC life models with data for plasma-sprayed and EB-PVD TBC systems produced by commercial suppliers to the gas turbine industry; i.e., Chromalloy, Klock, Union Carbide, and Temescal

- Establish feasibility that life-critical TBC parameters can be verified by appropriate NDE techniques

The approach to this program involved the following activities:

- Review available TBC technology literature to identify operative degradation modes (Appendix A).

- Select TBCs and procure specimens (Section 3.0).

- Characterize TBC systems sufficiently to develop materials models for operative TBC failure mechanisms (Section 4.0). Mechanical tests included zirconia strength and fracture toughness, spalling strain, and elastic moduli. Burner rig environmental tests were conducted with and without ingestion of sea salt. Thermal conductivity was measured to facilitate stress calculations. NDE feasibility was assessed for verification of thickness and detection of interfacial flaws.

- TBC life models were developed and calibrated with data for each of the commercial TBC systems (Section 5.0). Procedures were established for interfacing these life models with GTEC's airfoil design tools.

- TFE731 high-pressure (HP) turbine blades were coated with the program's TBC systems and evaluated in a factory test engine to facilitate validation of the TBC life model (Section 6.0).

3.0 TBC SYSTEMS AND SPECIMEN PROCUREMENT

The objective of this program was to develop life prediction methods for plasma-sprayed and EB-PVD TBC systems. This effort focused on the following TBC systems applied by four commercial suppliers:

Chromalloy - NiCrAlY (LPPS) + 8 percent Y_2O_3 stabilized ZrO_2 (APS)

Klock - NiCrAlY (LPPS) + 8 percent Y_2O_3 stabilized ZrO_2 (APS)

Union Carbide - CoNiCrAlY (ASPS) + 8 percent Y_2O_3 stabilized ZrO_2 (APS)

Temescal - NiCoCrAlY (EB-PVD) + 20 percent Y_2O_3 stabilized ZrO_2 (EB-PVD)

Compositions and microstructures of these TBC systems are reviewed in the following paragraphs.

Low-pressure plasma-spray (LPPS) and argon-shrouded plasma-spray (ASPS) processes were used to apply the oxidation-resistant bond coating. The insulative 8 percent Y_2O_3 - ZrO_2 layers were applied by air plasma-spray (APS). Specimens were coated using the fixed (proprietary) processes of Chromalloy Research and Technology in Orangeburg, New York; Klock in Manchester, Connecticut; and Union Carbide, in Indianapolis, Indiana. Microstructures of the Chromalloy, Klock, and Union Carbide plasma-sprayed TBC systems are provided in Figures 6, 7 and 8, respectively.

EB-PVD coatings were applied by Temescal in Berkeley, California using their established (proprietary) fixed process. The EB-PVD TBC system featured a columnar grained EB-PVD-applied yttria (20 percent), fully-stabilized, cubic zirconia insulative layer on

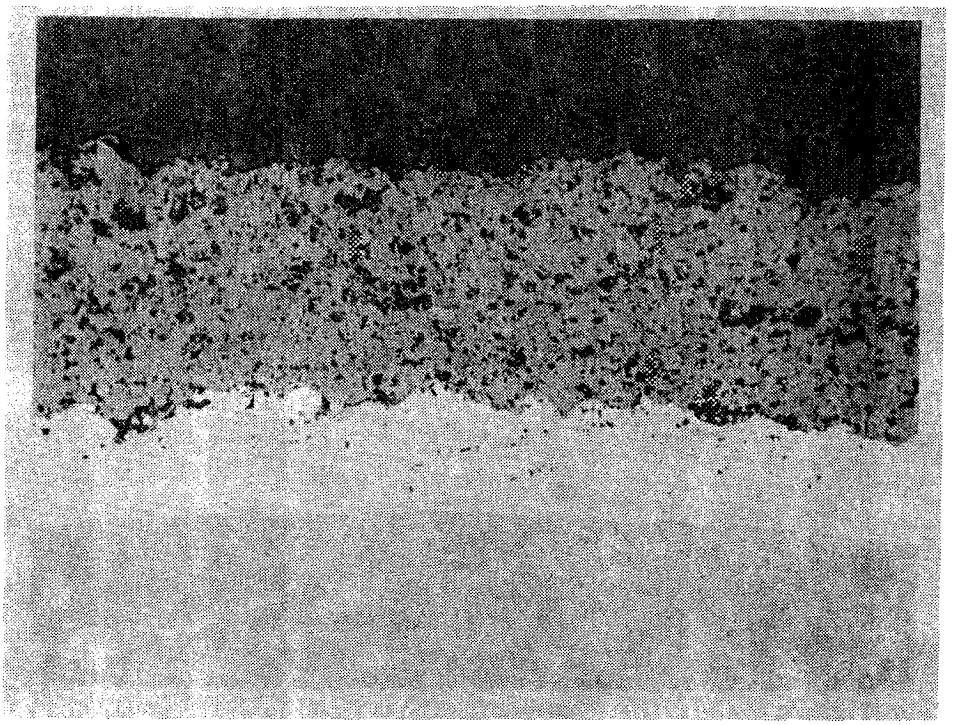

G7106-7

Figure 6. Pretest Microstructure of Chromalloy Plasma-Sprayed Ni-31Cr-11Al-0.5Y Plus Y_2O_3 (8 Percent) Stabilized ZrO_2 TBC System, 200X Magnification.

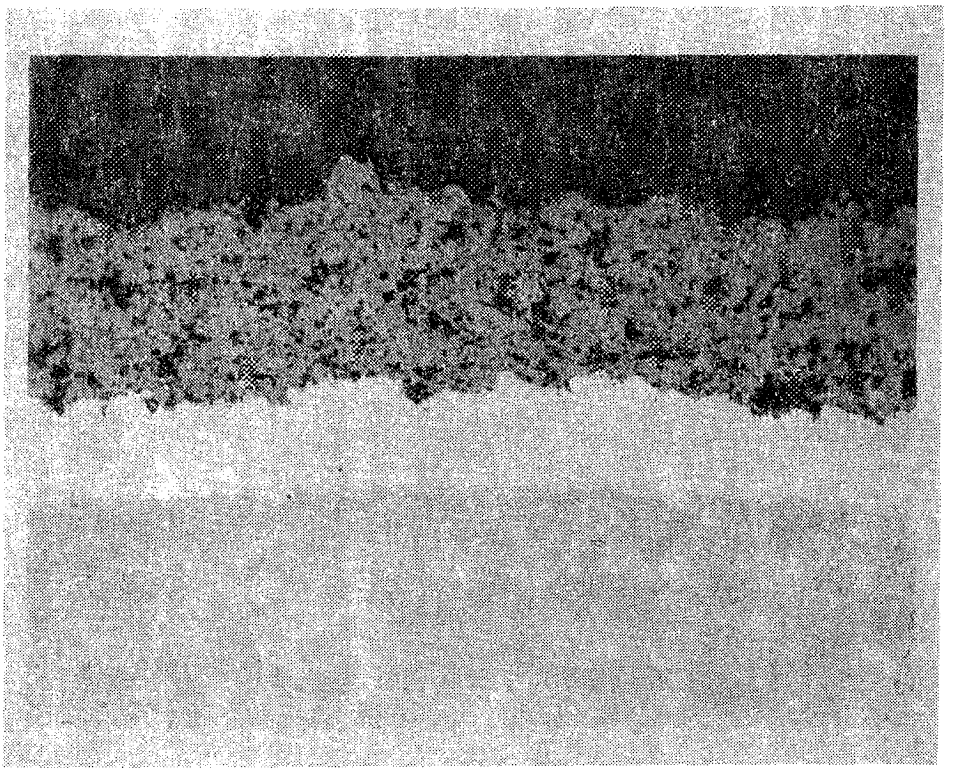

G7106-8

Figure 7. Pretest Microstructure of Klock Plasma-Sprayed Ni-31Cr-11Al-0.5Y Plus Y_2O_3 (8 Percent) Stabilized ZrO_2 TBC System, 200X Magnification.

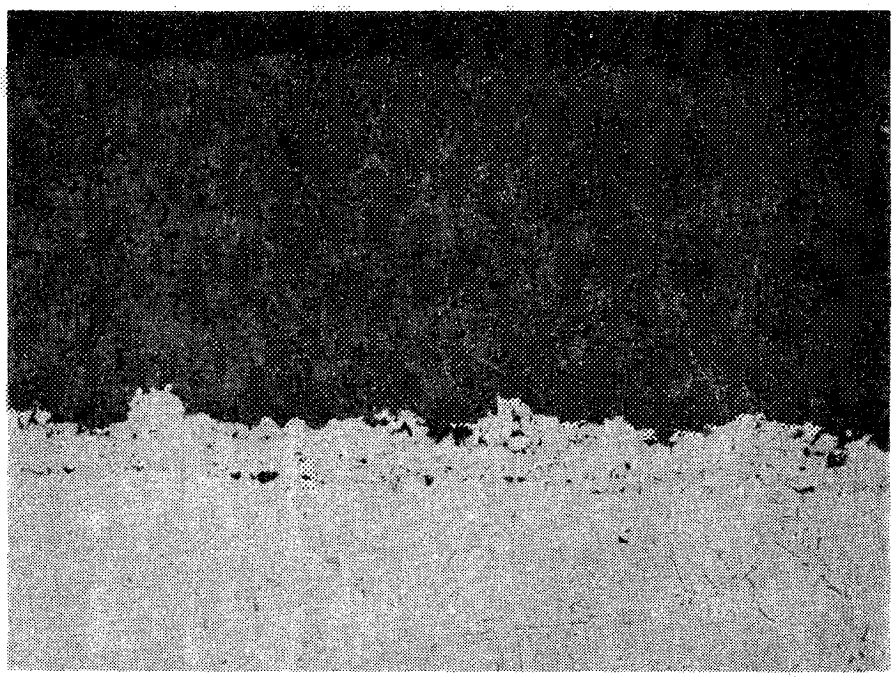

G7106-9

Figure 8. Pretest Microstructure of Union Carbide Plasma-Sprayed 39Co-32Ni-21Cr-8Al-0.5Y Plus Y_2O_3 (8 Percent) Stabilized ZrO_2 TBC System, 200X Magnification.

top of a Ni-23Co-18Cr-12Al-0.3Y EB-PVD oxidation-resistant bond coating. The microstructure of the EB-PVD TBC system is provided in Figure 9.

Capabilities of these TBC systems were established on several types of specimens machined from Mar-M 247 superalloy castings. The composition of this alloy is provided in Table 1. The cast Mar-M 247, which is used in the equiaxed and directionally solidified conditions for turbine airfoils, was selected for all specimens because of its stability at elevated temperature for long exposure times. Burner rig test specimen, cohesive/interfacial strength and toughness specimens, thermal conductivity samples, tension and compression spalling strain samples, and the modulus specimen are shown in Figures 10 through 14. The cohesive strength specimen was also used for evaluating nondestructive evaluation (NDE) feasibility.

Table 1. Composition of MAR-M 247 Superalloy (Weight Percent)

	Mo	W	Ta	Al	Ti	Cr	Co	Hf	Zr	C	B	Ni
Mar-M 247	0.65	10.0	3.3	5.5	1.05	8.4	10.0	1.4	0.055	0.15	0.015	Balance

The solid Mar-M 247 spalling strain specimens were used to replace IN718 tube specimens (ref. 1)*, which were prone to wall thickness variations, buckling concurrent with zirconia spalling in compression, and metallurgical instability during post-coating exposures at high temperatures.

*A list of references is provided at the end of this report.

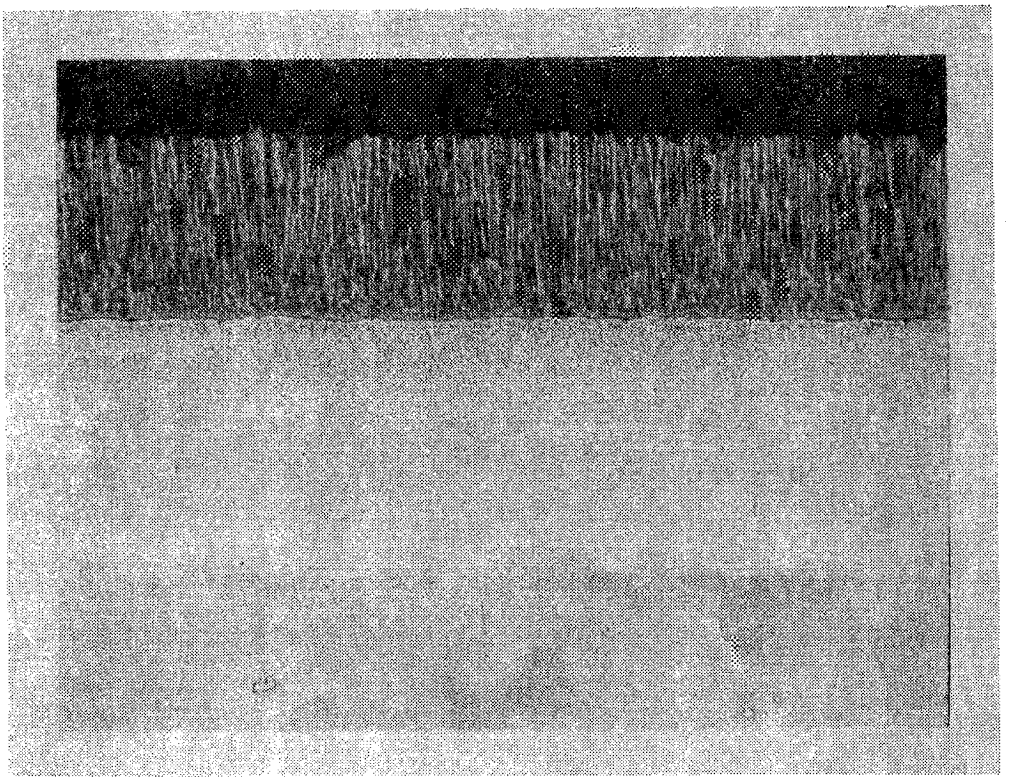

G7106-10

Figure 9. Pretest Microstructure of Temescal EB-PVD Ni-23Co-18Cr-12Al-0.3Y Plus Y_2O_3 (20 Percent) Stabilized ZrO_2 TBC System, 200X Magnification.

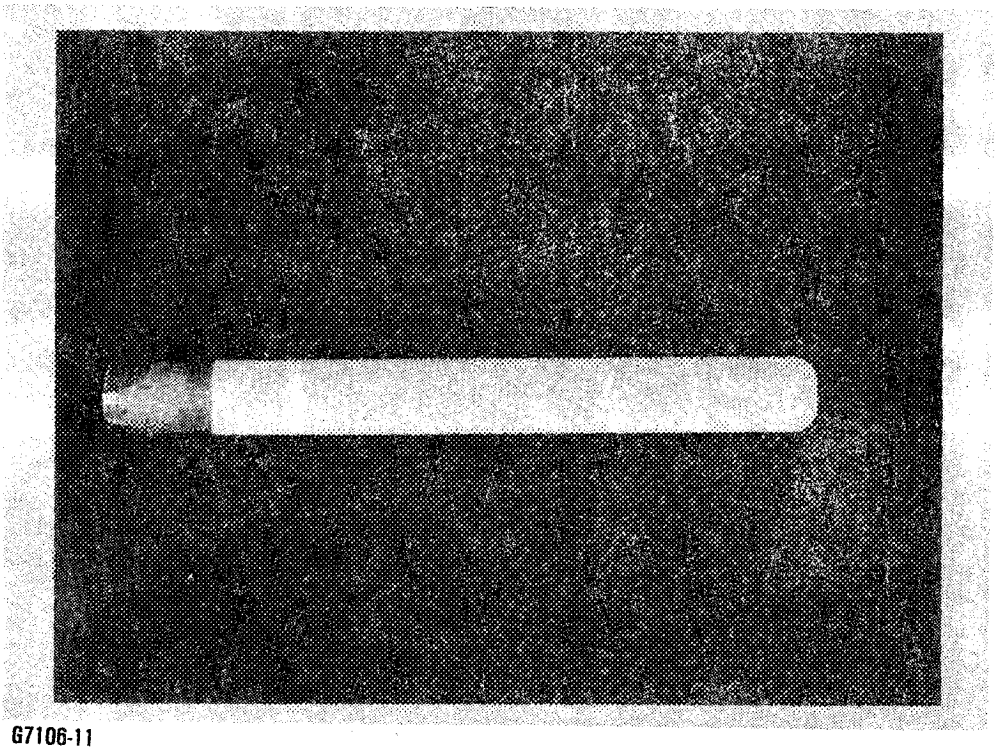

G7106-11

Figure 10. Burner Rig Specimens Were Used to Calibrate Environmental Life Model.

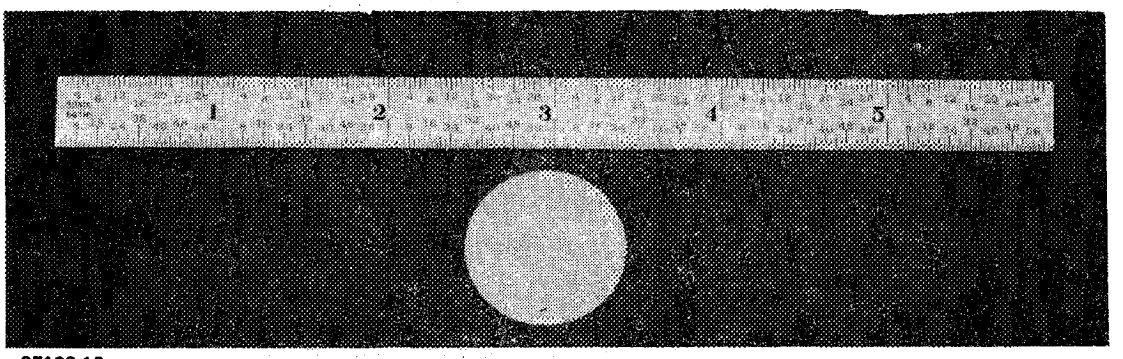

G7106-12

Figure 11. Cohesive (Interfacial) Strength and Toughness Specimen Was Used to Obtain Fracture Mechanics Data. This Specimen Was Also Used for NDE Feasibility Studies.

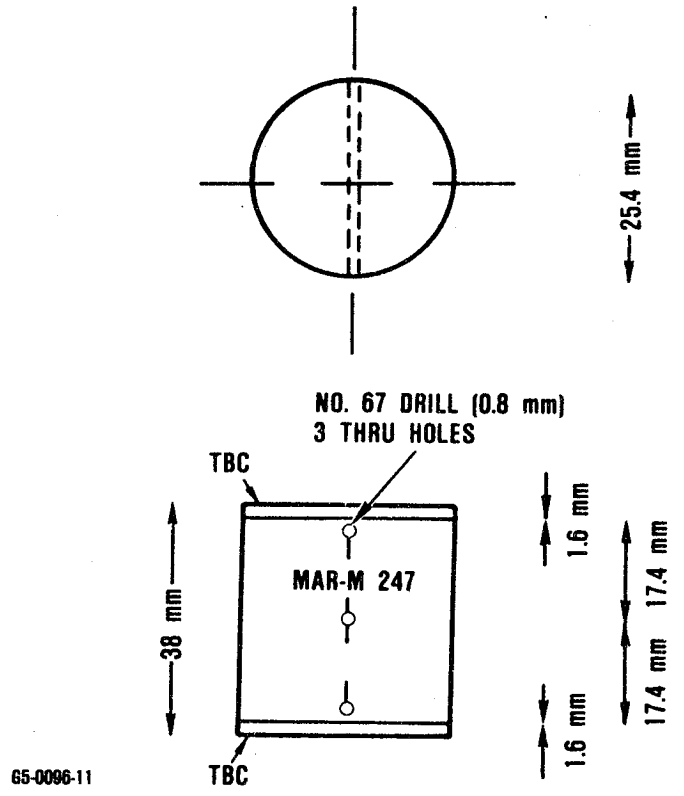

Figure 12. Thermal Conductivity Specimens Were Used to Quantify Heat Conductance of TBC System.

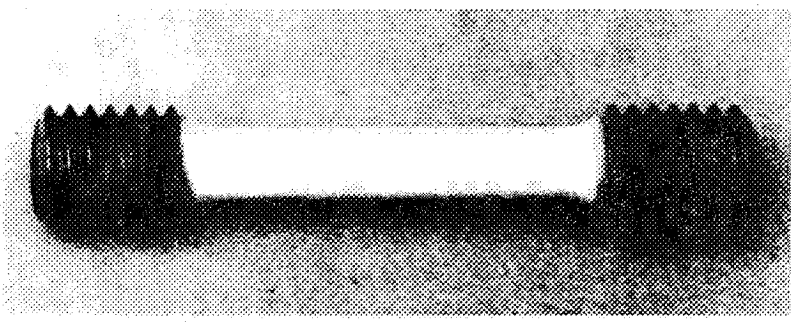

TENSION

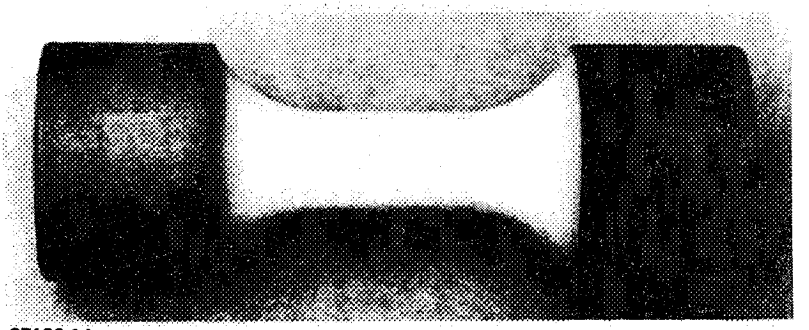

G7106-14

COMPRESSION

Figure 13. Solid Mar-M 247 TBC Coated Samples Were Used to Obtain the Spalling Strain Data for the Chromalloy and Temescal TBC Systems.

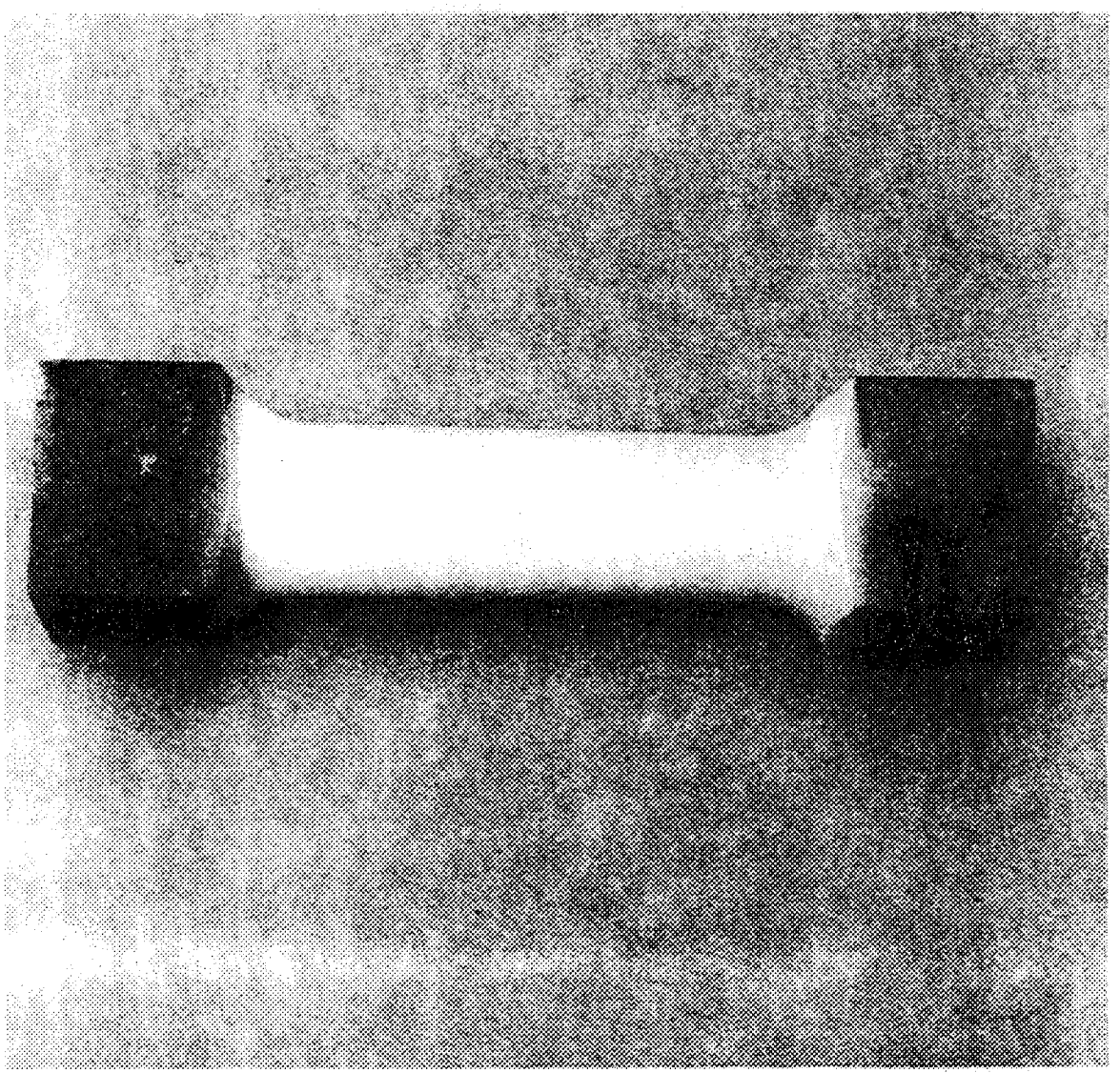

G7106-15

Figure 14. Modulus Data for the ZrO_2 and Bond Coat Were Determined with a Thin Wall Sample Made of Mar-M 247.

4.0 TBC SYSTEM CHARACTERIZATION

In preparation for the development of thermomechanical and thermochemical models for TBC life, the TBC systems were characterized for strength and toughness, tensile and compressive spalling strains, oxidation and molten salt film damage, and thermal conductivity. In addition, feasibility was assessed for NDE methods to quantify TBC thickness and flaw size. The results from these investigations are reviewed in the following paragraphs.

4.1 TBC Strength and Fracture Toughness

Biaxial compressive stresses within the plane of the zirconia coating result in tensile stresses within the zirconia perpendicular to the plane of the ceramic-metal interface. Zirconia layer spalling can occur when these stresses exceed critical values, which are flaw size dependent.

In order to predict the viability of a TBC system, it is necessary to quantify the strength and toughness (flaw size dependence of strength) of the zirconia layer (plasma-sprayed TBCs) or the zirconia-bond coating interface (EB-PVD TBCs). Therefore, a series of bond-strength tests, with and without artificial flaws at or near the interface, were conducted to obtain the required data. Toughnesses of the zirconia or zirconia-bond coating interface were determined in both the as-received condition and after thermal exposures at high temperatures (1100 and 1150C) characteristic of turbine engine applications.

Cohesive strength data for the plasma-sprayed zirconia were obtained by epoxy bonding TBC bond specimens (Figure 15) into threaded pull rods and loading to fracture in a universal tensile test machine. Fracture toughness of the zirconia was obtained by briefly interrupting coating and incorporating an artificial (vacuum grease) flaw of known diameter into the zirconia-coating layer and

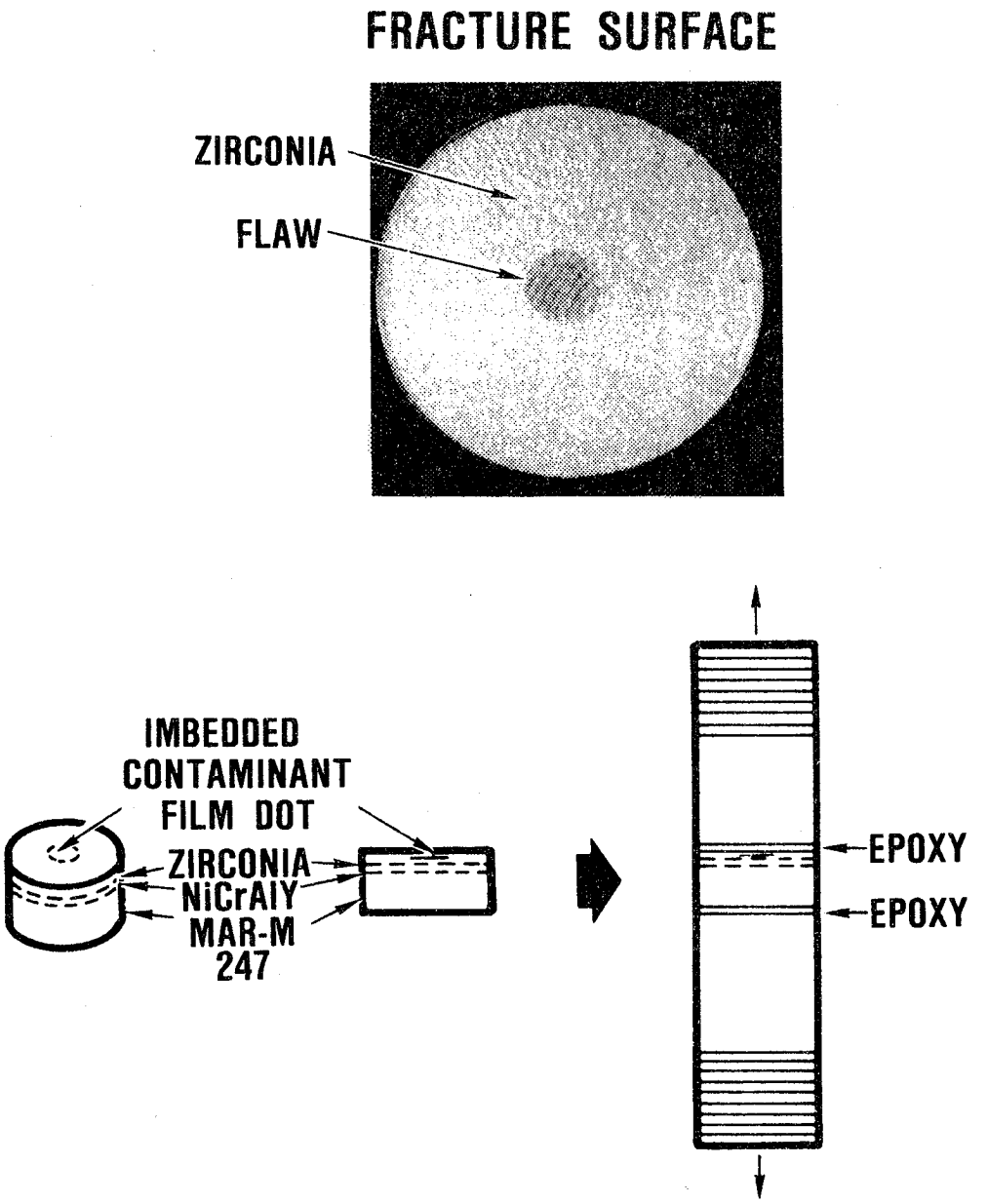

Figure 15. Cohesive and Interfacial Toughness of TBC System Can Be Quantified with Modified Bond Strength Test.

testing in a similar manner. The fracture toughness relationship for a penny-shaped crack in an infinite body subjected to uniform tension,

$$K_{Ic} = 2/\sqrt{\pi}\ \sigma_f \sqrt{c/2} \qquad (1)$$

where σ_f is the fracture strength of the flawed specimen and c is the flaw diameter, was used to estimate the fracture toughness of the yttria partially-stabilized zirconia layer.

Cohesive toughness data were obtained with the Chromalloy and Union Carbide specimens in several "pretest" conditions, which included short post-coating heat treatments and after longer exposures at 1100 and 1150C. Posttest visual examination confirmed that the artificial flaw within the zirconia layer initiated the preliminary crack. As indicated in Figure 16, crack propagation typically remained within the zirconia layer for all of the Chromalloy specimens and for Union Carbide specimens with shorter exposures at 1100 and 1150C. For Union Carbide specimens exposed for longer times (300 hours at 1100C and 30 hours at 1150C), the cracks propagated only a short distance within the zirconia before the crack path changed to the oxidized interface. The change in crack path is illustrated in Figure 17. This result is thought to imply that the toughness of the oxidized interface has become lower than the zirconia layer. In contrast, flaw propagation remained within the Chromalloy zirconia layer for the range of thermal exposures investigated.

An engine mission analysis capable fracture mechanics approach to predicting zirconia spalling stresses requires that the zirconia toughness be quantified as a function of high-temperature exposure time and temperature. It is also desirable that acceptable variations in zirconia processing, composition, and microstructure be included in the toughness data base. Therefore, zirconia-fracture

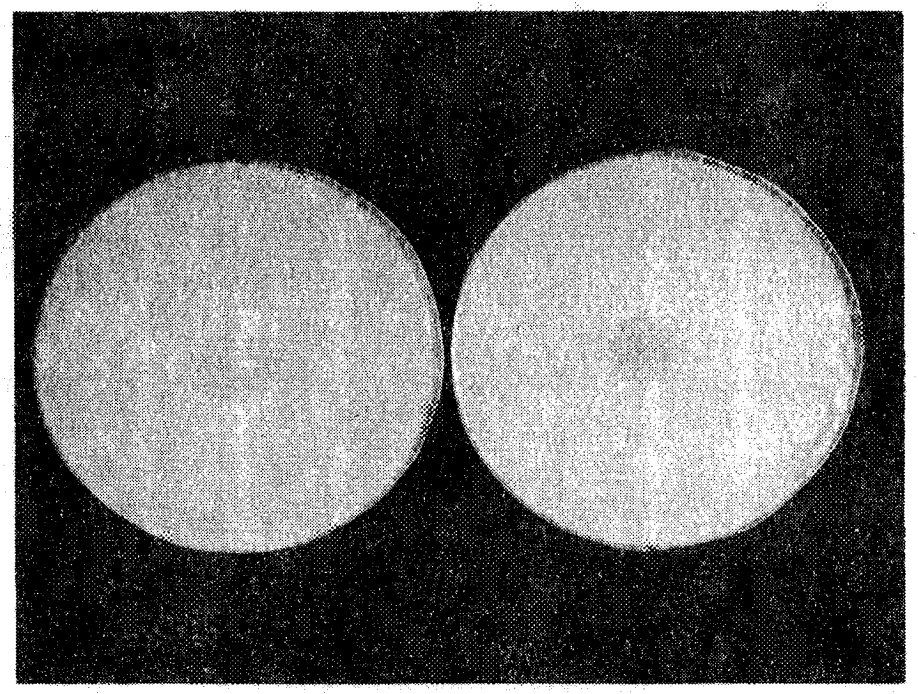

G7106-17

Figure 16. An Artificial 6-mm-Diameter Flaw Initiated Fracture in the Zirconia Layer of a Chromalloy-Coated Cohesive Toughness Specimen.

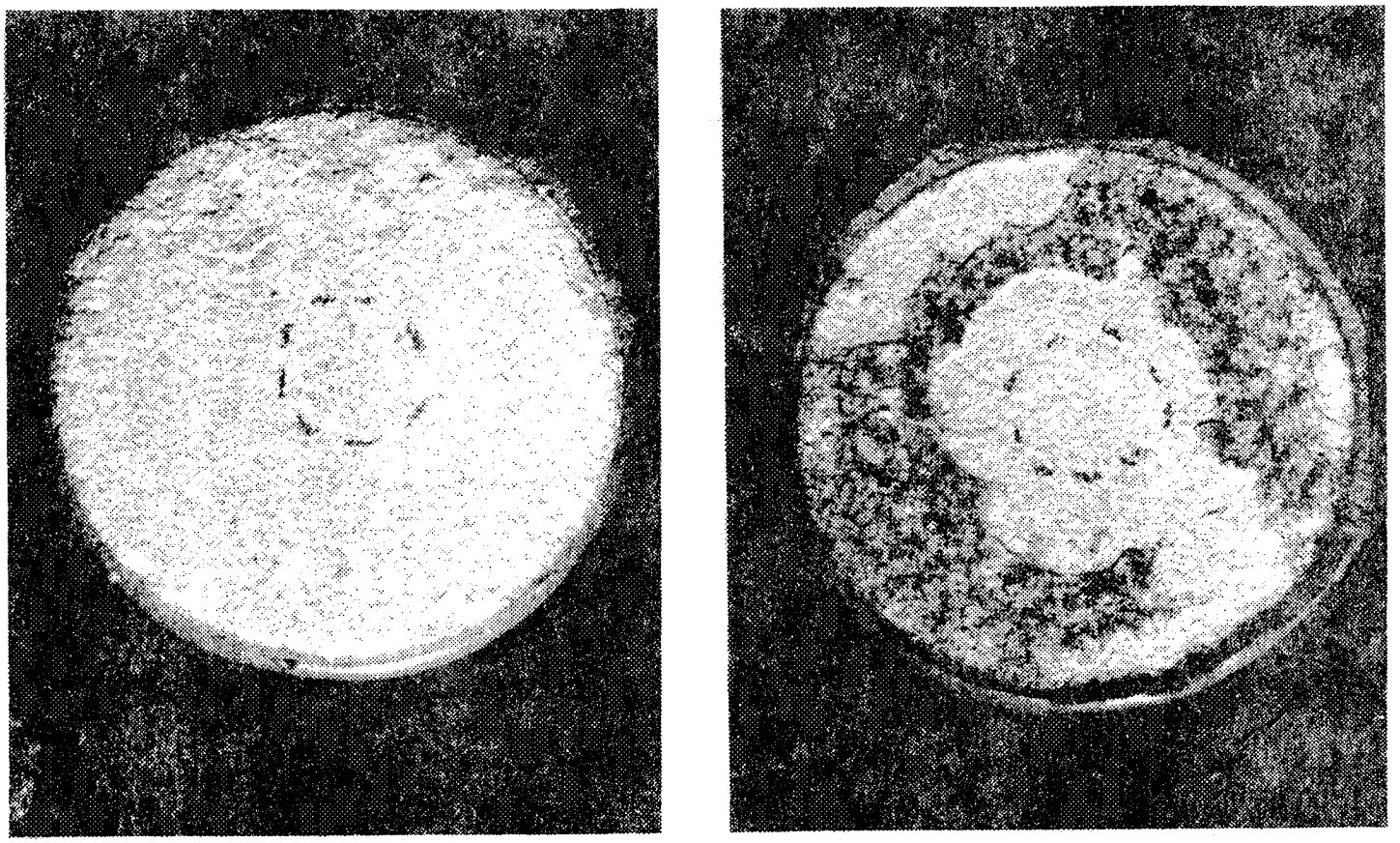

G7106-18

3 Hours at 1100C
K_{IC} = 1.05 MPa $\sqrt{m}$
Specimen: U15K6-18

300 Hours at 1100C
K_{IC} = 0.62 MPa $\sqrt{m}$
Specimen: U15K6-10

Figure 17. Longer Exposure Times Favored Crack Propagation Along the Oxidized CoNiCrAlY/Zirconia Interface.

toughness data for both Union Carbide and Chromalloy TBC systems are shown as a step function of exposure time at 1100C and 1150C in Figures 18 and 19, respectively. Although other functional relationships may be possible to represent these data, the step function is preferred because it facilitates component analysis as a function of exposure time and temperature. Combining the data for Chromalloy and Union Carbide TBC systems also permits effects of production source variations to be assessed from a data scatter standpoint.

Pretest and shorter time exposure data (both 1100 and 1150C), which had relatively high values of toughness, were used to establish the typical and typical minus 2 standard deviations values for the upper shelf. Longer exposure time and lower toughness data were similarly analyzed to estimate the typical and typical minus 2 standard deviations values for the lower shelf. Transition from the upper to lower shelf values of toughness were analyzed as an assumed linear relationship between temperature and the logarithm of transition time. Transition times are currently shown as vertical lines. However, a more gradual transition between the upper and lower shelf values of toughness may be more realistic. The analytical expression for toughness was as follows:

$$K_{Ic} = 0.91 + 0.235 \tanh (\exp [-0.041(T+273)+61.15] - t) \text{ MPa } \sqrt{m} \qquad (2)$$

where T is the temperature in C and t is the time in hours.

No significant differences were observed between the toughness data for the Chromalloy and Union Carbide zirconia after exposures at 1100C. On the other hand, the Union Carbide coatings had higher toughness after exposure at 1150C than the Chromalloy TBCs. (However, if the flaw was placed at the oxidized interface, the ranking would be expected to reverse.)

Constrained sintering shrinkage, as evidenced by miniature "mud-flat" type cracking, was observed in the zirconia coatings on

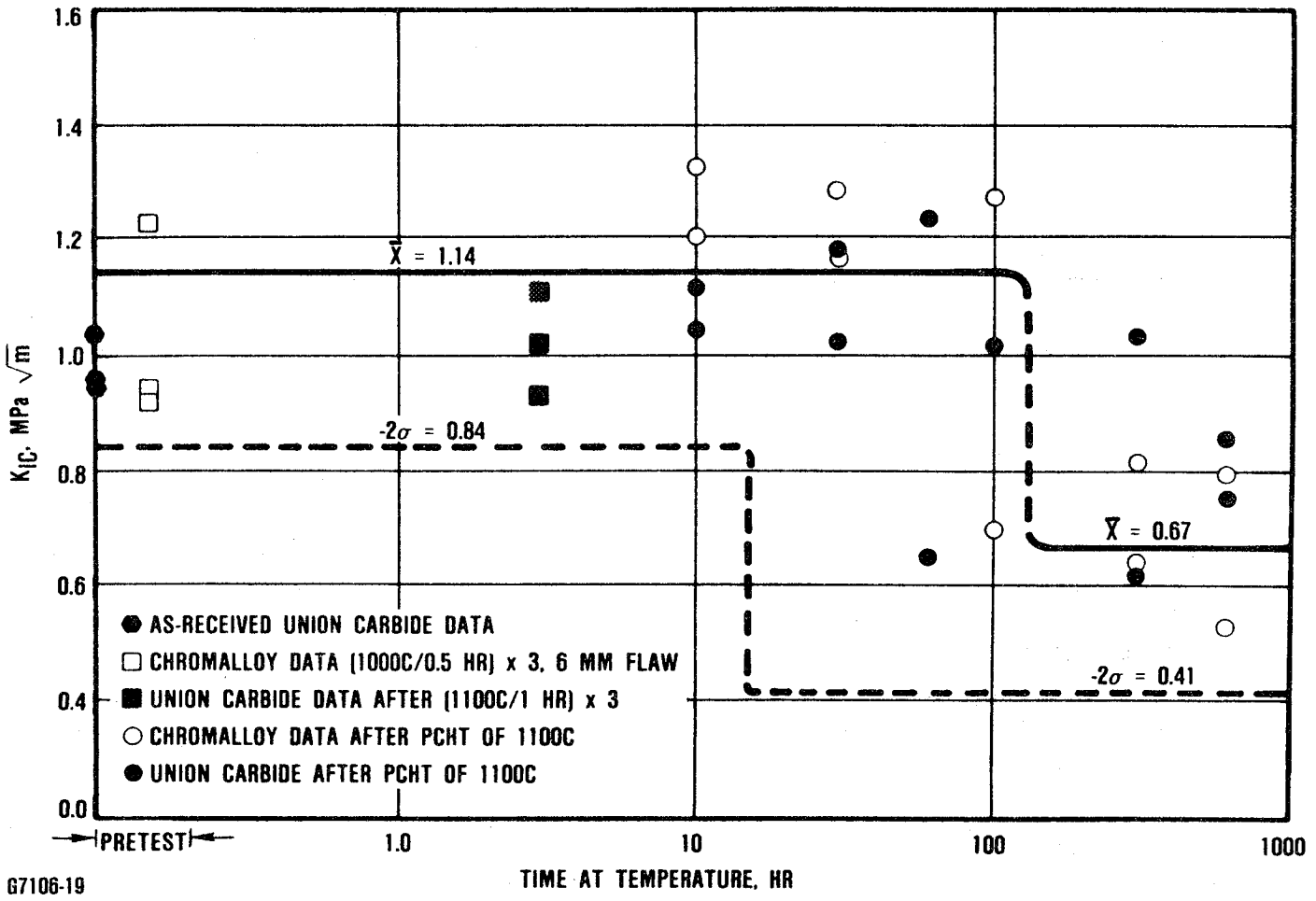

Figure 18. Fracture Toughness of Plasma-Sprayed Yttria (8 Percent) Stabilized Zirconia is Reduced After Long Exposures at 1100C.

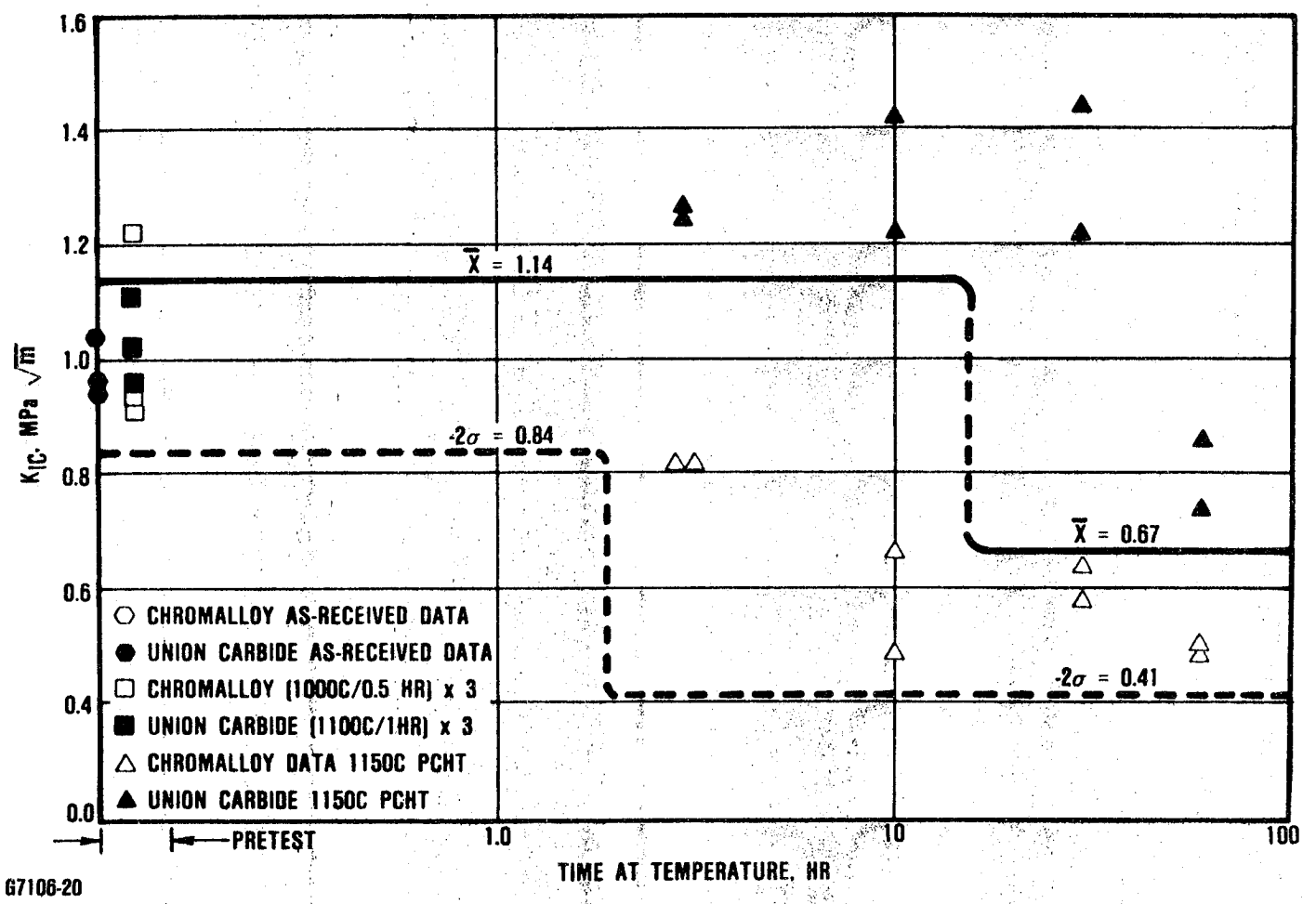

Figure 19. Fracture Toughness of Plasma-Sprayed Yttria (8 Percent) Stabilized Zirconia is Reduced After the Longer Exposures at 1150C.

toughness specimens, which had relatively long static furnace exposures at 1100 and 1150C. It is thought that the constrained sintering shrinkage is associated with the reduction in zirconia toughness.

The observation of sintering shrinkage at these temperatures is consistent with available literature data. It has been determined that microcrystalline plasma-sprayed, yttria-stabilized zirconia coatings can creep at temperatures above 1100C (ref. 2). Sintering shrinkage has also been observed in stabilized zirconia coatings at temperatures above 1100C in thermal expansion tests (ref. 3). Evidence of sintering densification has also been observed in engine-tested components. Significant zirconia densification was observed in plasma-sprayed zirconia coatings tested on high pressure turbine blades. Leading edge temperatures of these TBCed components was reported to be 1153C (ref. 4). More recently, evidence was presented that "mud-flat" cracking is associated with the typical TBC failure mode on airfoils (ref. 5).

Cohesive strength tests were also performed on the Chromalloy and Union Carbide TBC systems using specimens without artificial flaws in order to obtain an estimate of the inherent flaw size present within the TBC system. In most instances, failure occurred within the epoxy rather than the zirconia when artificial flaws were absent. However, in several instances, cracking did initiate within the zirconia layer adjacent to the bond-coating interface (Figure 20). Rearranging the fracture mechanics relationship (equation 1) permitted an effective circular flaw size to be calculated, which was under 2.8 mm in diameter in all cases. (In reality, actual flaws present within the zirconia layer are probably a few closely spaced microcracks that can easily link-up rather than a single circular flaw.)

Cohesive strength and toughness tests conducted with the Klock TBC system were inconclusive because the epoxy wicked completely

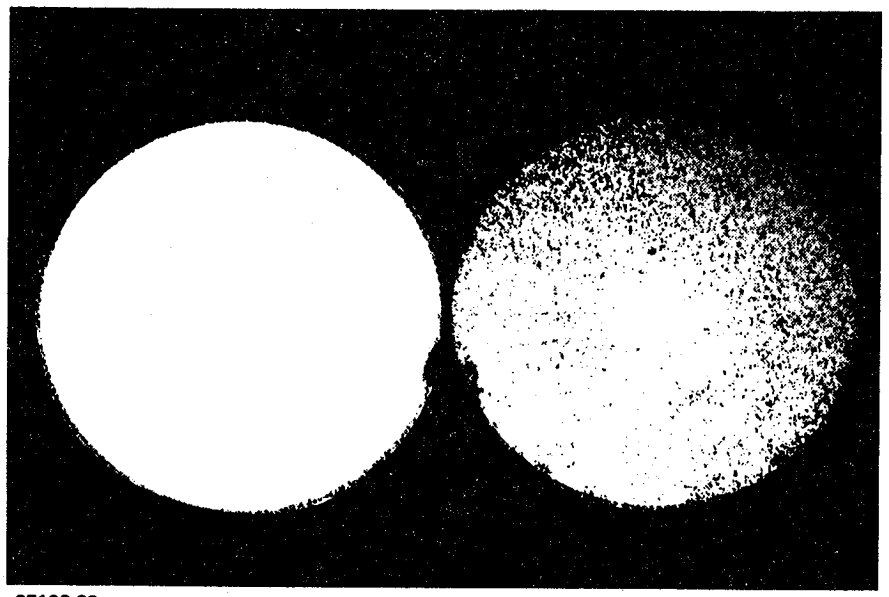

G7106-22

Figure 20. Cohesive Strength Failures of Chromalloy TBC System Occur Adjacent to the NiCrAlY/Zirconia Interface.

through the zirconia to the NiCrAlY/zirconia interface. The epoxy wicking problem was attributed to a greater amount of interconnected porosity in the Klock specimens. In an effort to eliminate epoxy wicking through the Klock zirconia, several specimens were sprayed with an additional 250 μm of zirconia prior to bonding. A small amount of cobalt aluminate (about 0.1 percent) was added to the additional zirconia layer to provide a sufficient color difference to distinguish between the Klock zirconia and the added layer. Unfortunately, visual examination of the specimens indicated that the vacuum grease flaws within the Klock specimens did not initiate the crack that led to specimen failure. Instead, the primary crack seemed to initiate at the edge of the specimen in the doped zirconia coating or at the interface between the doped zirconia/Klock zirconia layer. None of the unflawed specimens failed within the Klock zirconia layer.

Failure of the Temescal EB-PVD TBC system typically initiates within the interfacial zone between the NiCoCrAlY bond coating and columnar zirconia layers. This 1- to 4-micron-thick zone consists of the oxidation resistant alumina scale and a relatively dense, noncolumnar zirconia layer, which is less than 2-microns thick when the coating is properly processed.

In order to characterize the toughness of the EB-PVD TBC system, 1 and 3 mm diameter carbon dots were sputtered onto the NiCoCrAlY layer, which formed an artificial flaw, prior to deposition of the zirconia layer. Specimens were then tested in the as-received and thermally-exposed conditions in an equivalent manner to that of the plasma-sprayed TBC systems.

Unfortunately, the flaw sizes selected were, in most cases, insufficient to initiate interfacial failure before the epoxy failed.

Only two specimens failed at the NiCoCrAlY/zirconia interface. Calculated interfacial toughnesses were 1.9 and 1.6 MPa $\sqrt{m}$ after 1 and 30 hour exposures at 1150C. All other tested specimens failed at locations other then the interface, which is consistent with high toughness. In a GTEC R&D study in which 4 mm diameter flaws were used, about 75 percent of the specimens produced useful toughness data. Values were similar to those obtained in this program. Six mm diameter flaws have been successfully used in an Air Force-sponsored program (F33615-85-C-5155). As-received toughnesses for the Air Force system were slightly greater than 2 MPa $\sqrt{m}$ in the NASA program.

Six of the specimens exposed at 1150C had the zirconia layer spall during the thermal exposure. The inner half of the zirconia thickness was almost transparent and appeared to be of high density. Microstructural examination of a specimen indicated that the columnar grains were sintering together.

All six of these specimens had been coated concurrently. A review of process records at Temescal indicated that the oxygen flow rate had been only 30 to 50 percent of that normally used to maintain zirconia stoichiometry. It is thought that the slightly oxygen deficient zirconia absorbed oxygen and expanded during the 1150C exposure, which put the columnar zirconia grains into compressive contact, facilitating sintering and subsequent spalling.

4.2 Zirconia Spalling Strain

In service, a TBC system will be exposed to both compressive and tensile strains at different points of a mission cycle. Consequently, the strain capabilities of the plasma-sprayed and EB-PVD TBCs were determined at room temperature and 1000C to establish the strain tolerance of each system.

Spalling strain tests were performed in both tension and compression using the solid Mar-M 247 specimens shown in Figure 13.

Initiation of spalling was determined visually. Data from these tests are discussed in the following paragraphs.

Plasma-sprayed TBCs applied by Chromalloy were tested in the as-received condition and after 10 hour exposures in air at 1100 and 1150C. The zirconia thickness for most of these tests was 125 μm, but in three instances the thickness was increased to 250 μm.

No significant differences in the spalling strains with respect to the post-coating heat treatment and thickness of the ZrO_2 layer were observed. However, the compressive spalling strain increased substantially with test temperatures, as indicated by the 1000C data (Figure 21). From a design standpoint, low temperature compression spalling strains were the most limiting. The mean value of the nineteen room temperature compression spalling strain data is 1.09 percent and the mean-3 sigma value is 0.5 percent compressive strain. Compression cracking was detected prior to actual spalling; mean and mean-3 sigma values for compression cracking strain were 0.91 percent and 0.48 percent, respectively. Therefore, the safe amount of compression in the Chromalloy TBC system is about 0.5 percent.

Results from the 1000C tension tests indicated that zirconia spalling occurred at a mean strain of 2.97 percent. Delamination of the NiCrAlY bond coating was observed in the tensile tests conducted at room temperature. Low values of zirconia spalling are associated with this unexpected occurrence. In previous room temperature tensile tests of tube specimens, zirconia spalling was not observed when the NiCrAlY remained bonded to the substrate.

Results from the IN 718 tube specimens (ref. 1) were in general agreement with the solid specimen data. The zirconia layer of the Chromalloy and Klock TBC systems did not spall when the specimens were pulled in tension. Numerous parallel tensile cracks were observed in the zirconia prior to specimen failure (Figure 22).

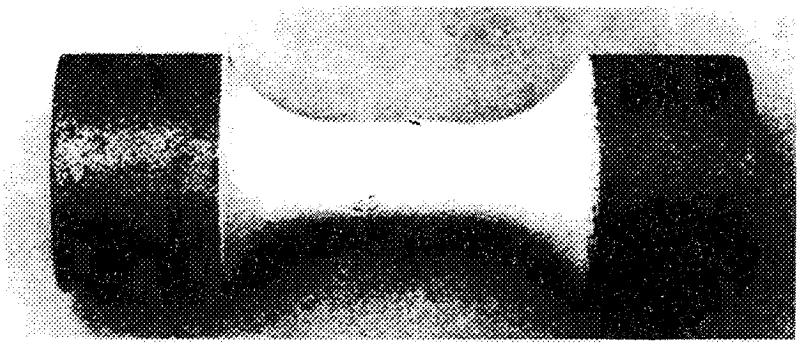

ROOM TEMPERATURE
COMPRESSIVE SPALLING STRAIN > 0.8 PERCENT

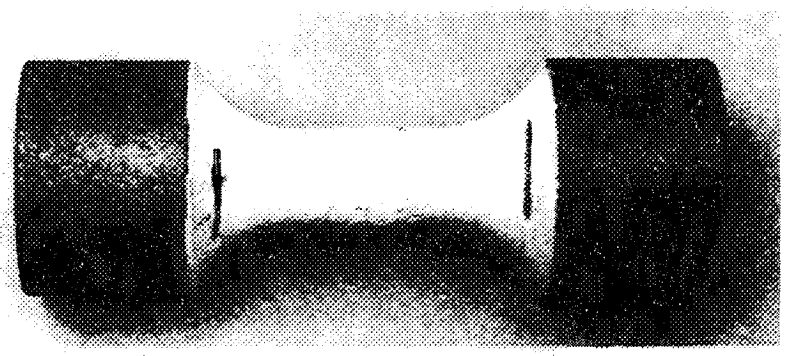

1000C
COMPRESSIVE SPALLING STRAIN >5 PERCENT

G7106-23

Figure 21. The Spalling Strain of Chromalloy TBC System Increased with Test Temperature.

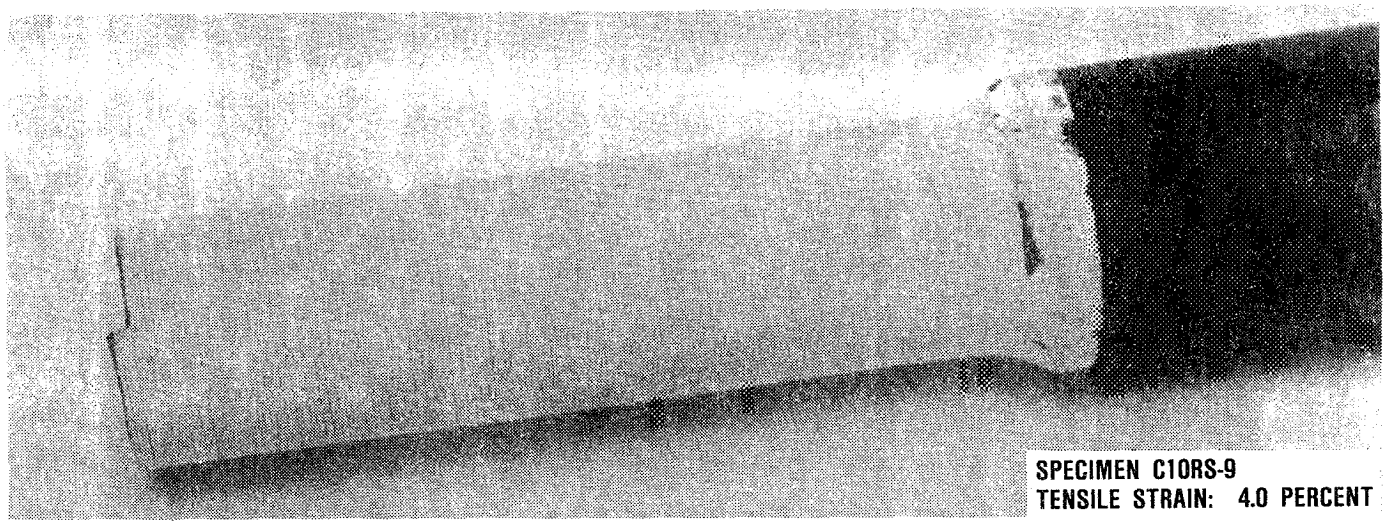

G7106-24

Figure 22. Zirconia Layer of Chromalloy TBC System Did Not Spall When the Specimen Failed. Numerous Parallel Tensile Cracks Were Observed in the Zirconia.

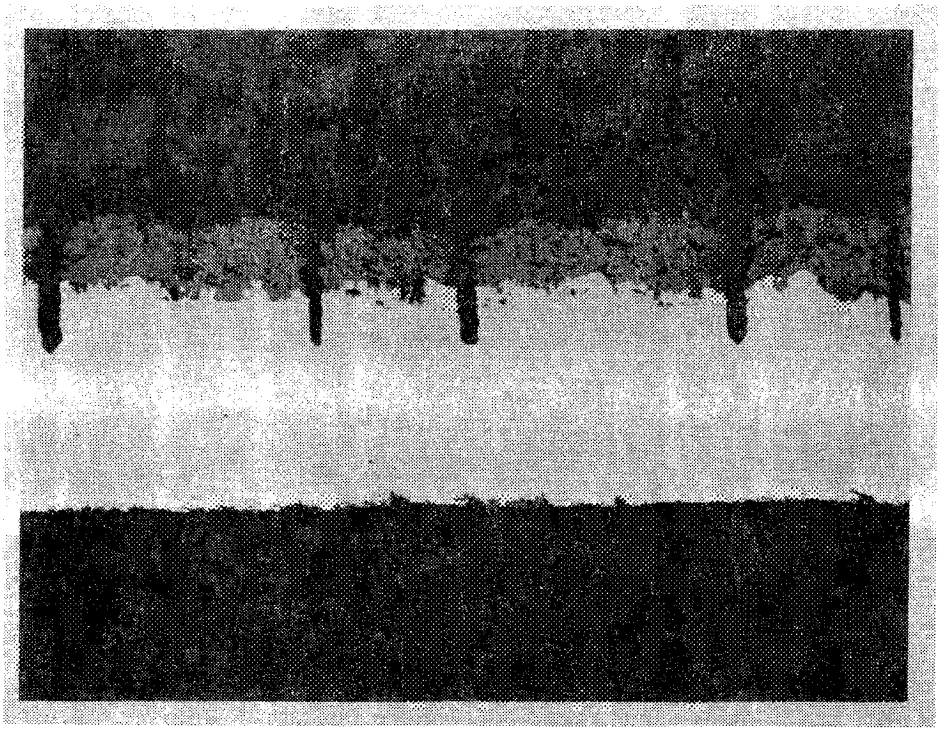

G7106-25

Figure 23. Tensile Cracks in the NiCrAlY and ZrO_2 Layers, 100X Magnification.

These cracks originated in the NiCrAlY bond coat and propagated into the zirconia layer (Figure 23). All of the compression specimens reached a strain of 0.85 or higher (1.5 percent average) prior to specimen buckling and zirconia spalling, which were typically concurrent.

Spalling strain testing was also conducted with Temescal's EB-PVD NiCoCrAlY/yttria stabilized zirconia TBC system. All of the EB-PVD TBCs had zirconia thicknesses of 125 microns. Unexpectedly, the average strain to spall the ZrO_2 layer in the room temperature compression tests was only 0.31 percent. The EB-PVD ZrO_2 did not spall at 5 percent strain in the 1000C compression tests; however, the ZrO_2 subsequently spalled during cool down on two of three samples tested at 1000C. In tension, 1.95 percent was the mean value of the strain required to spall off the zirconia in both the room temperature and 1000C tests.

Based upon previous data for EB-PVD zirconia coatings reported by Sheffler (ref. 6) the low room temperature compression spalling strains were unexpected. Subsequent review of processing records at Temescal indicated that difficulties had been encountered during initial coating of the specimens and that the zirconia had been stripped and then recoated. It is speculated that this processing anomaly may have resulted in a marginally adherent alumina scale.

It has been observed that initially formed alumina scales on NiCoCrAlY coatings are the most adherent. Also, initial oxide scale growth can result in yttrium depletion of the adjacent 50 microns of the NiCoCrAlY. If the initial oxide is stripped from the surface, there may be insufficient yttrium in the coating to promote the required adhesion of the subsequently formed alumina scale.

After reviewing these data, Temescal stripped the compression specimens to the Mar-M 247 substrate and recoated the specimens. The process was slightly modified in that the NiCoCrAlY coating was

lightly vapor honed after glass bead peening to remove any glass bead debris. Testing of these specimens indicated that the room temperature compression spalling strain increased to 1 percent, which is comparable with Sheffler's EB-PVD zirconia data (ref. 6) and the Chromalloy plasma-sprayed zirconia data. A comparison of the zirconia spalling-strain data between Chromalloy's plasma-sprayed and Temescal's EB-PVD TBC systems is provided in Figure 24.

4.3 ZrO_2 Modulus Determination Tests

Elastic moduli for Chromalloy and Temescal systems were obtained to facilitate analysis of TBC stresses. The specimen in Figure 14 was used to determine Young's and shear moduli for the zirconia and bond-coating layers of the TBC system. In order to establish load-carrying capabilities of the constituent layers, specimens were tested without coatings, with thick bond coatings, and with thin bond coatings and thick zirconia coatings. Specimens were loaded in tension, compression, and shear up to 50 percent of the capability of the Mar-M 247.

Elastic moduli for both TBC systems are reported in Table 2. Assuming the elastic moduli are interrelated with the following relationship, $E = 2G\ (1 + \upsilon)$, where υ is Poisson's Ratio, there is an apparent error in either the shear (G) or Young's (E) moduli; i.e., either E should be lower or G should be higher. Estimates of the range of these moduli are indicated in Table 2 assuming $\upsilon = 0.1$ for zirconia and $\upsilon = 0.3$ for the bond coat. Average values of these moduli were used for stress analysis and TBC life prediction. The moduli for plasma-sprayed TBCs are consistent with other published data (refs. 7 and 8).

Microstructures of the plasma-sprayed zirconia coating contained interconnected microporosity and microcracking, which are responsible for the low moduli values. Ink drops placed on the surface of this thick TBC system wicked into the coating and penetrated to the zirconia/NiCrAlY interface (Figure 25).

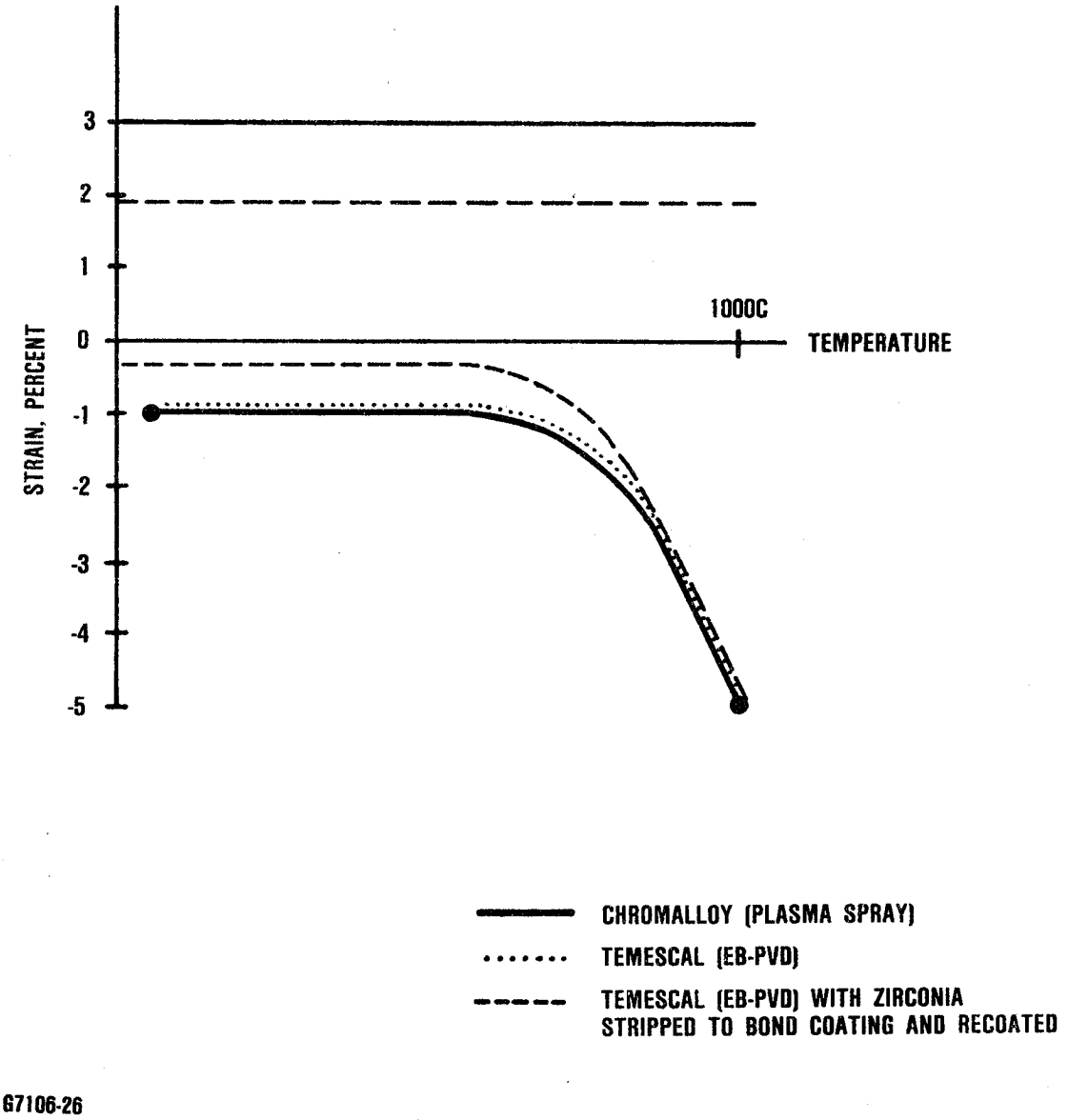

Figure 24. Compressive Strain at Low Temperatures is a Design-Limiting Factor.

Table 2. Elastic Moduli of the Chromalloy and Temescal TBC Systems

	E, MPa		G, MPa	
	Measured	Lower Limit*	Measured	Upper Limit*
Plasma-Sprayed Zirconia	57.5×10^3	17×10^3	7.7×10^3	26.1×10^3
LPPS NiCrAlY	175×10^3	56.2×10^3	21.6×10^3	67.3×10^3
EB-PVD ZrO_2	25.5×10^3	16.9×10^3	7.7×10^3	11.6×10^3
EB-PVD NiCoCrAlY	175×10^3	35.1×10^3	13.5×10^3	67.3×10^3

*Calculated from $E=2G(1+\upsilon)$ assuming $\upsilon=0.1$ for zirconia $\upsilon=0.3$ for NiCrAlY or NiCoCrAlY.

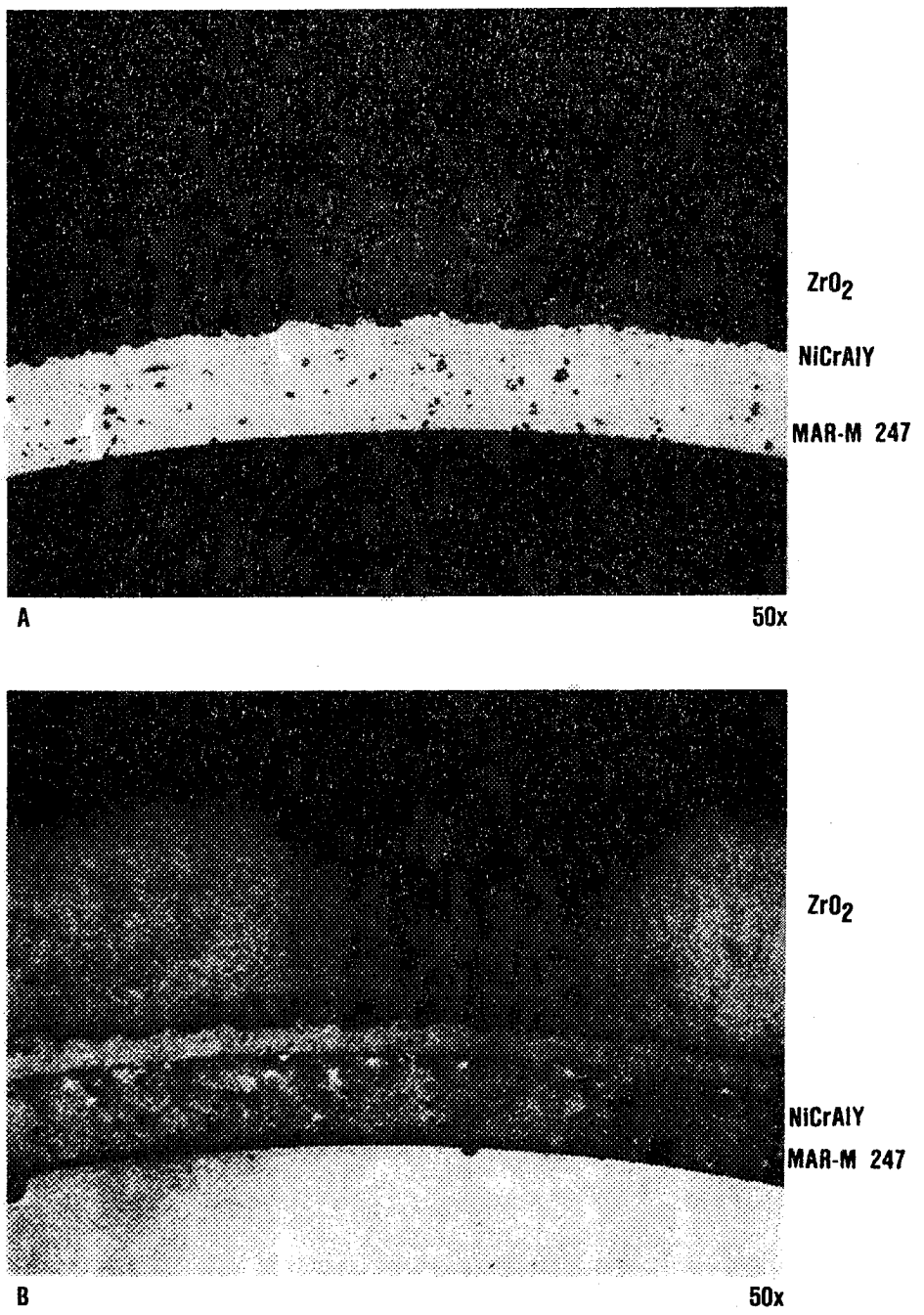

Figure 25. The Degree of Interconnected Microcracks and Porosity is Shown By Ink Wicking into the ZrO_2 Coating: (a) Regular Lighting (b) Polarized Light.

The elastic moduli of the open columnar microstructure of the EB-PVD ZrO_2 are approximately half of the plasma-sprayed ZrO_2. Low values are attributed to the columnar microstructure of the EB-PVD coating. The open columnar microstructure is shown in Figure 26, where ink wicked into the columnar microstructure and penetrated down to the ZrO_2/NiCoCrAlY interface.

4.4 Burner Rig Tests

A preliminary design model for predicting TBC life must be capable of rapid iteration in order to be a viable tool. Therefore, the thermochemical design model was tailored to be driven primarily by the component's thermal analysis, engine cycle data, and the planned flight spectrum for the aircraft. Stress analysis was intentionally limited, during these early design iterations, to verification that the TBC can survive a severe transient snap acceleration-deceleration cycle (i.e., idle to full power to idle with no intermediate power dwells).

Burner rig tests are the primary means for calibrating the preliminary design TBC materials models that quantify the thermally-driven damage modes. Effects of bond-coating oxidation and zirconia densification upon the time required to spall the zirconia layer are quantified with burner rig tests conducted in the 1020 to 1200C temperature range. Condensed molten sulfate salt films can be present upon the surface of a TBC when temperatures are below about 950C for aircraft operating in a predominately marine environment, such as maritime surveillance. Therefore, burner rig tests were conducted in the range of 760 to 925C to assess the significance of molten salt film damage with respect to zirconia-layer spalling.

These tests were conducted in GTEC's Mach 0.3 burner rig facility, which concurrently tests eight to twelve specimens in a carousel. The test cycle was typically 27 minutes in the burner's exhaust followed by 3 minutes of forced air cooling. In one 1020C

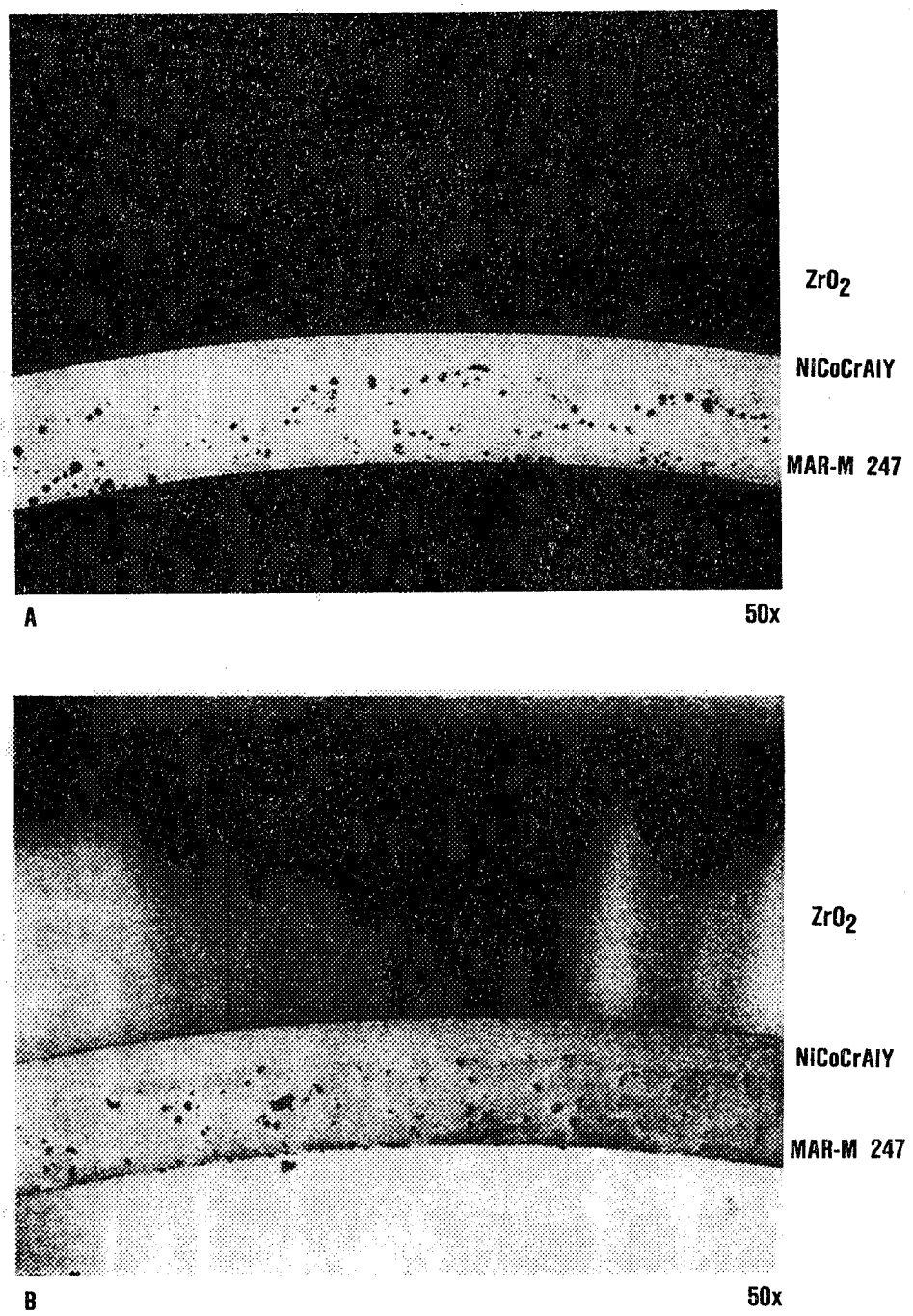

Figure 26. The Open Columnar Microstructure of the EB-PVD ZrO_2 Accounts for the Lower Young's Modulus: (a) Regular Lighting (b) Polarized Light.

test, a shorter test cycle was employed (4-minutes-hot plus 2-minutes-forced air cooling) in order to assess cycle duration effects on TBC life. Coating thicknesses were typically 125 microns of bond coating and 125 microns of yttria stabilized zirconia for all systems. Specimens were examined visually twice daily for zirconia spalling. A TBC was considered to be failed when 0.5 cm^2 of zirconia had spalled in the hot zone of the specimen.

Temperatures of the specimens were controlled by an optical pyrometer. Several times during a test (initially daily), the pyrometer was calibrated into agreement with two centerline thermocouples inserted into the hottest portion of two bars (middle of the heat tint pattern). Calibration of the optical pyrometer was always performed after steady-state metal temperatures and burner conditions were achieved. Due to a hearth effect, a small gradient was present in the bars from the outside of the carousel to the inside, with the inside surface being about 20C hotter than the centerline thermocouple; similar results were reported by Sheffler and DeMasi, who conducted comparable burner rig tests under contract NAS3-23944 (ref. 7).

Burner rig data for the plasma-sprayed Chromalloy and Union Carbide systems are summarized graphically in Figure 27 for tests conducted with the 27-minutes-hot plus 3-minutes-forced air cool cycle. Development of life prediction model curves, which are forced through minimum life points, are described in detail in paragraph 5.2. Klock's plasma-sprayed TBC system exhibited longer lives in the burner rig cyclic oxidation tests (Figure 28). Also, in contrast with the other plasma-sprayed TBC systems, the Klock TBCs were not failed in any of the lower temperature tests with molten salt ingestion; these tests were terminated at times $\geq$ 500 hours.

Similar burner rig data for concurrently tested Temescal EB-PVD TBCs are provided in Figure 29. These data indicate that this EB-PVD system exhibits superior lives in cyclic oxidation, but

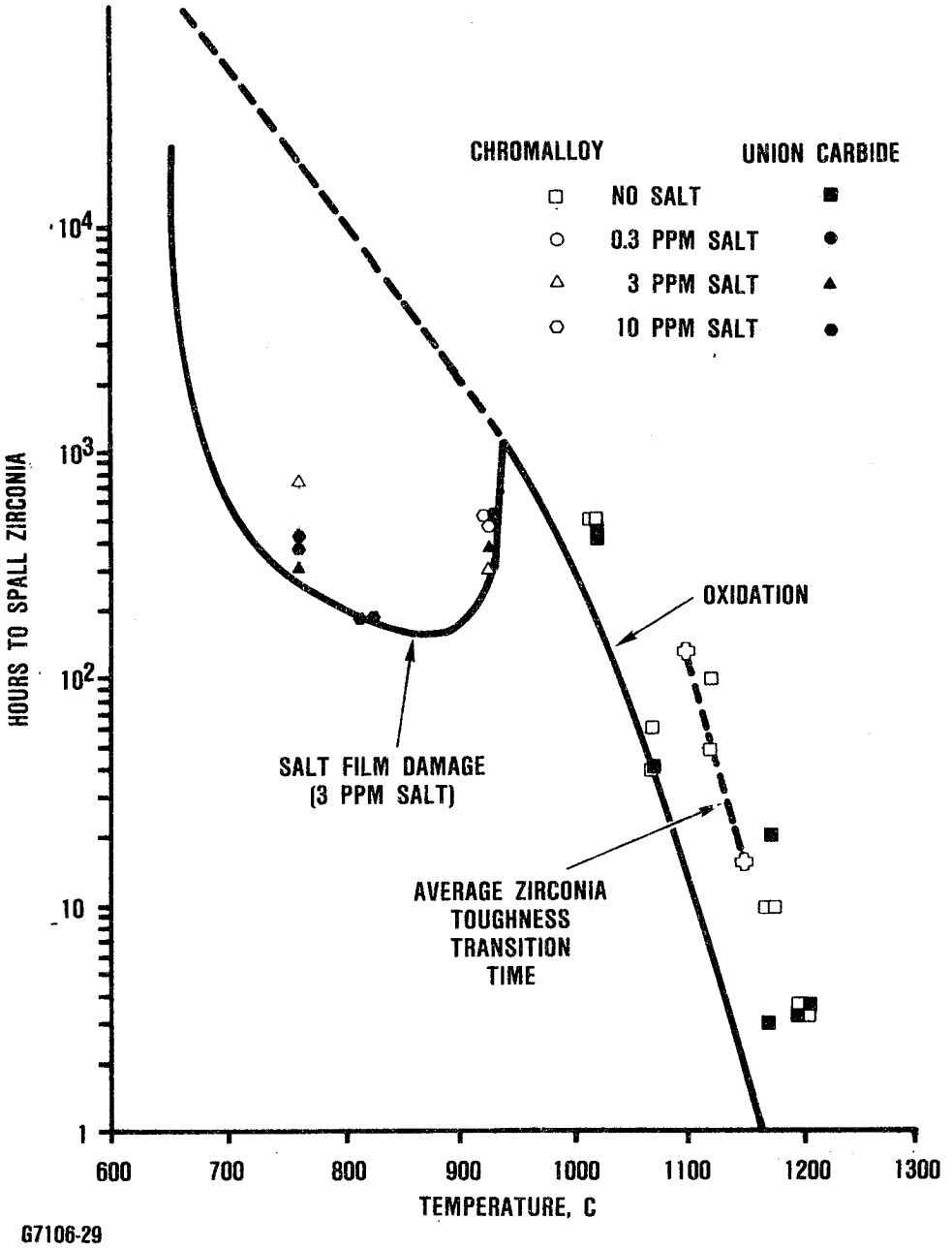

Figure 27. Life Curve for Chromalloy and Union Carbide Plasma-Sprayed TBC Systems is Forced Through Minimum Life Data from Cyclic (27-Minutes-Hot Plus 3-Minutes-Forced Air Cool) Burner Rig Tests.

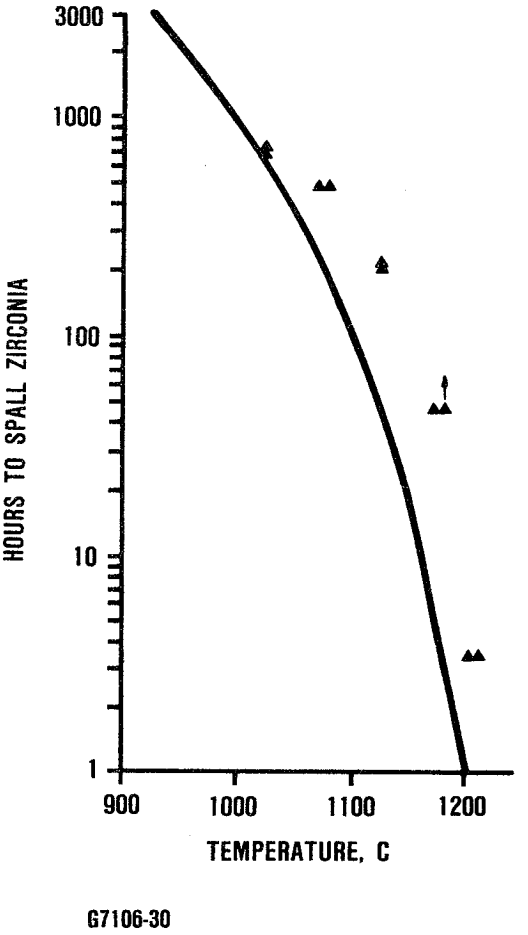

Figure 28. Lives of Klock TBC System Exceeded Those of the Other Plasma-Sprayed TBCs in Cyclic Oxidation Burner Rig Tests.

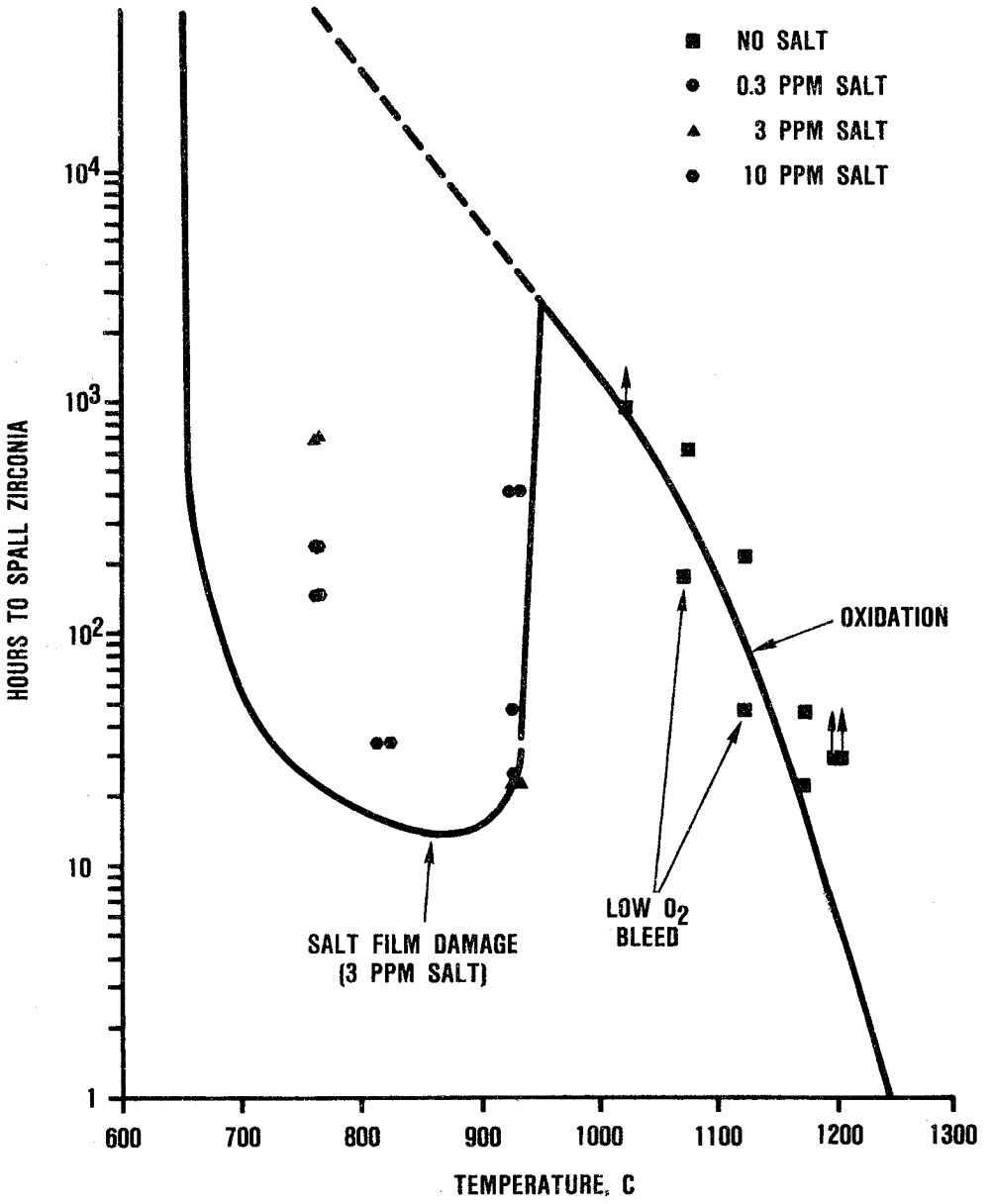

Figure 29. The Life Curve for Temescal EB-PVD TBC System is Forced Through Minimum Life Data From Cyclic (27-Minutes-Hot Plus 3-Minutes-Forced Air Cool) Burner Rig Tests.

greatly reduced lives when molten salt films are present. EB-PVD ceramic coatings with dense outer layers, which are resistant to molten salt penetration, are being developed by GTEC in Air Force-sponsored (Contract F33615-85-C-5155) and Navy-sponsored (Contract N00167-86-C-0097) programs.

Three damage modes were observed during these tests. In the lowest temperature (760 to 945C) tests, the presence of salt deposits reduced the spalling life of the TBC systems. Oxidation of the bond coating was associated with TBC spalling at temperatures above 1000C. At still higher temperatures, zirconia densification (sintering) further accelerated TBC degradation.

Data were also obtained for a rapid (4-minutes-hot plus 2-minutes-forced air cool) burner rig cycle at 1020C to assess the effect of cycle length on TBC life. Data from the 1020C tests with 4 and 27 minutes of hot time per cycle are shown graphically in Figure 30 and compared with 1100C data reported by Miller (ref. 9). These data indicate that the shorter cycles result in a slightly reduced life over the temperature range of 1020 to 1100C. Sheffler and DeMasi (ref. 10) reported similar trends were observed over the interval of about 1100 to 1170C.

A typical aircraft engine mission cycle will have dwell periods of varying durations at several different temperatures; for example, a few minutes at take-off power, perhaps 10 minutes at climb power, and 0.5 to 5 hours at cruise power. Therefore, in order to analyze burner rig data obtained at different cycle periods as well as predict TBC spalling for engine mission cycles of various lengths, the following cycle length correction factor was developed:

$$\text{Coating life}_{t_i} = (\text{Burner rig test life})\ (t_i^{0.25} + 0.181), \quad (3)$$

where t_i is the increment of hot time in hours and the burner rig test life is for the 27-minutes-hot and 3-minutes-forced air cool

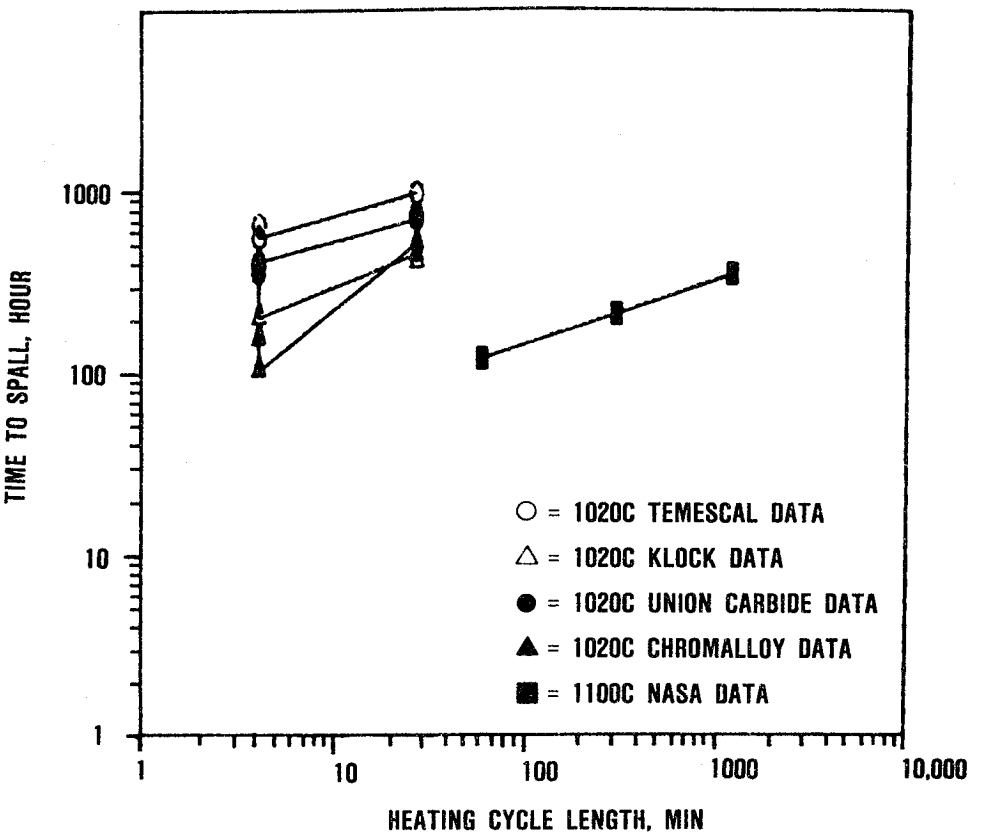

G7106-32

Figure 30. TBC Life Decreases with a Shorter Heating Cycle.

cycle. The cycle period correction term equals one when there is 27 minutes of hot time per cycle.

In order to be viable, TBC life models must be capable of accurately predicting TBC durability for complex, multitemperature engine missions. With this objective in mind, a 1000-hour multitemperature burner rig test was conducted to verify the capability to predict TBC lives under simulated engine mission conditions.

The miltitemperature cyclic (1050C) 7 minutes plus 925C/20 minutes plus 3 minutes forced-air cooling) burner rig testing was conducted to validate the predictive capability. Test data for the plasma spray and EB-PVD systems are provided in Table 3 and compared with model predictions, based on Miner's law cumulative damage; i.e.,

$$\text{Life} = \frac{1}{\dfrac{f_{1050C}}{\text{Life}_{1050C,\ 7\ \text{min.}}} + \dfrac{f_{925C}}{\text{Life}_{925C,\ 20\ \text{min.}}}}$$

where, f is the fraction of the burner rig cycle at the indicated temperature and the life is calculated as a function of temperature and heating cycle length. Comparison of the predicted and actual multitemperature test lives indicates excellent agreement for the Temescal and Klock TBC systems. Agreement is also good for the Chromalloy TBC system, although one of the data points is slightly underpredicted. In contrast, the model prediction for the life of the Union Carbide TBC was overestimated by a factor of four.

Miner's law appeared to provide satisfactory predictions for three of the four TBC systems. A more conservative cumulative damage model than Miner's law would be required to achieve a satisfactory (conservative) prediction for the Union Carbide TBC system.

Table 3. Comparison Between Predicted and Actual TBC Lives in Multitemperature Burner Rig Test*

Specimen	Vendor	TBC System	Time to Spalling, hr	Predicted Life, hr
T5B-10	Temescal	EB-PVD ZrO_2 on NiCoCrALY	1000+	1202
T5B-11	Temescal	EB-PVD ZrO_2 on NiCoCrAlY	1000+	
C5B-8	Chromalloy	Plasma-Sprayed ZrO_2 on NiCrAlY	400	203
C5B-10	Chromalloy	Plasma-Sprayed ZrO_2 on NiCrAlY	135	
K5B-16	Klock	Plasma-Sprayed ZrO_2 on NiCrAlY	896	820
K5B-17	Klock	Plasma-Sprayed ZrO_2 on NiCrAlY	1000	
U5B-22	Union Carbide	Plasma-Sprayed ZrO_2 on CoNiCrAlY	59	203
U5B-23	Union Carbide	Plasma-Sprayed ZrO_2 on CoNiCrAlY	54	

+: Unfailed, test terminated

* Burner Rig Test Cycle: 1050C/7 minutes +925C/20 minutes + Forced Air Cool/3 minutes

To facilitate conservative predictions of TBC life in a multi-temperature engine mission environment, a multitemperature burner rig experience factor (MTBREF), which forces predicted lives into agreement with the lowest burner rig test data, was applied to the oxidation life prediction relationship described in paragraph 5.2; i.e.,

TBC System	MTBREF
Klock	1.00
Chromalloy	0.67
Union Carbide	0.27
Temescal	0.83

Examination of the Chromalloy and Klock plasma-sprayed coatings, which had lives greater than about 100 hours at the higher temperatures, confirmed the presence of significant bond coating oxidation at both the zirconia-bond coating interface and at internal porosity within the bond-coating (Figure 31). This figure also indicates that the lower aluminum content Union Carbide bond coating exhibited significant oxidation degradation at shorter times and lower temperatures. In contrast, TBCs that spalled after only a few hours of testing typically exhibited minimal oxidation degradation of the bond coating (Figure 32). This figure also indicates that propagation of delamination cracks typically occurred within the zirconia adjacent to the bond coating interface.

Densification of the zirconia by sintering shrinkage (Figure 31) was also observed. "Mud flat" type cracking was also observed in the zirconia coating layer during post-test visual examination, which is consistent with constrained sintering shrinkage. As noted in paragraph 4.1, zirconia sintering densification was associated with a reduction in the zirconia toughness. This type of damage was

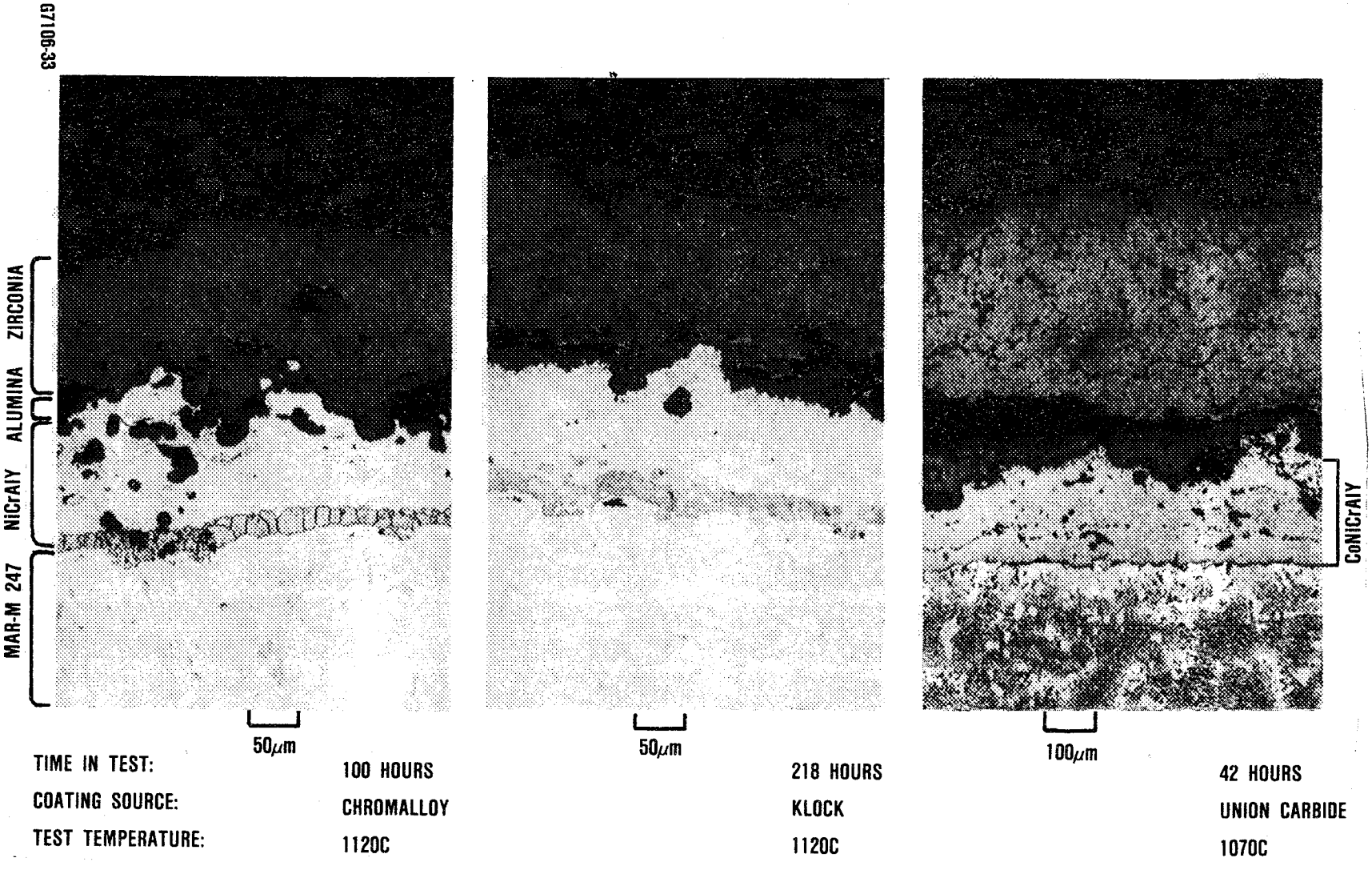

Figure 31. Bond Coating Oxidation and Zirconia Densification Contribute to Plasma-Sprayed TBC System Degradation During Burner Rig Tests.

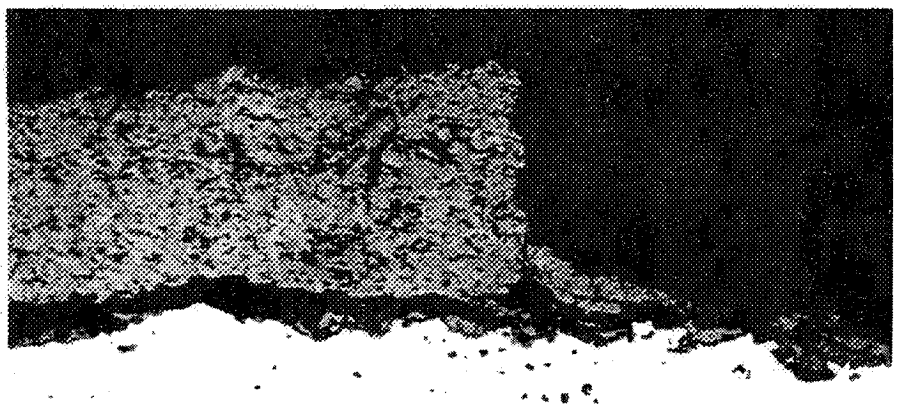

G7106-34

Figure 32. Zirconia Delamination from the Bond Coat is Caused by Crack Running Parallel to the ZrO_2/ Bond Coat Interface, 100X. This Chromalloy Sample Spalled After 59.7 Hours in the 1070C Burner Rig Testing.

observed in both short-time and longer-time tests conducted above about 1050C.

It was thought that a correlation should exist between the time to transition to the lower level of zirconia toughness and the burner rig data. Therefore, the burner rig data obtained above 1000C are compared in Figure 27 with the step transition times obtained from an analysis of toughness data in Figures 18 and 19. The correlation between average zirconia toughness transition times and the average burner rig data is good for the short-life burner rig data points, where zirconia densification (mud flat cracking) was observed.

Failure mechanisms were similar for the NiCoCrAlY + 20 percent yttria stabilized zirconia EB-PVD TBC systems. As indicated in Figure 33, significant bond coating oxidation occurred in the longer tests. When significant oxidation occurred, the cracks associated with zirconia layer spalling propagated along the alumina scale or in the adjacent, relatively dense, noncolumnar zirconia layer. Short-time tests at 1170C indicated that the inner portion of the columnar zirconia had densified, which would increase stresses within the zirconia and the interface (Figure 34). This figure also illustrates that bond-coating oxidation was minimal for the short-time failures.

In two instances, short-time failures occurred at lower temperatures. A review of process records at Temescal indicated that these specimens had been coated at reduced oxygen bleed levels. It is thought that subsequent exposure of the oxygen deficient zirconia microstructure to high temperature air resulted in some volumetric expansion of the columnar grains, which reduced or eliminated the strain accommodating intercolumnar gaps and resulted in significantly increased coating stresses. This processing deficiency was subsequently eliminated. The two questionable data points are indicated in Figure 29.

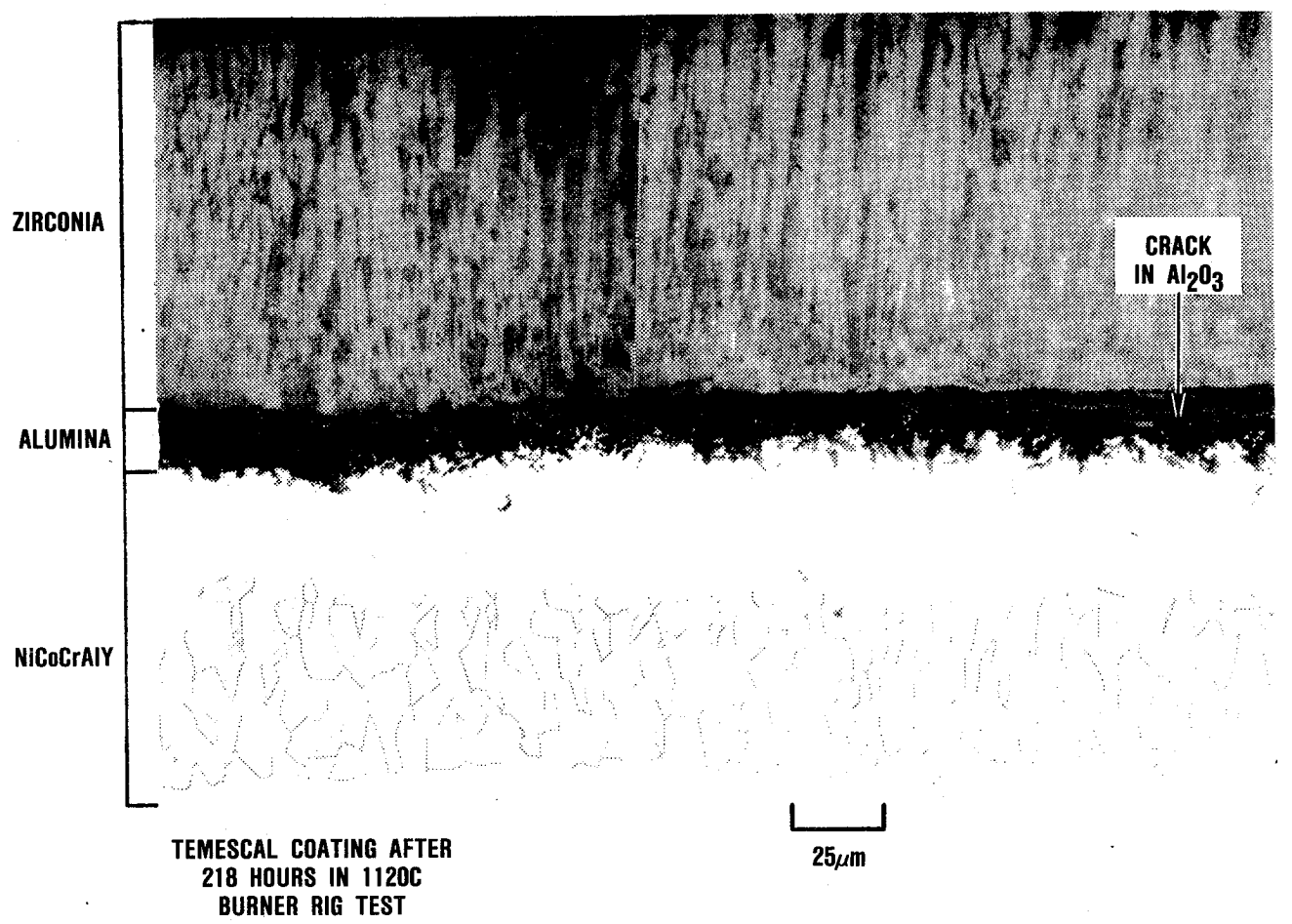

Figure 33. Oxide Scale Growth Contributes to EB-PVD TBC Degradation.

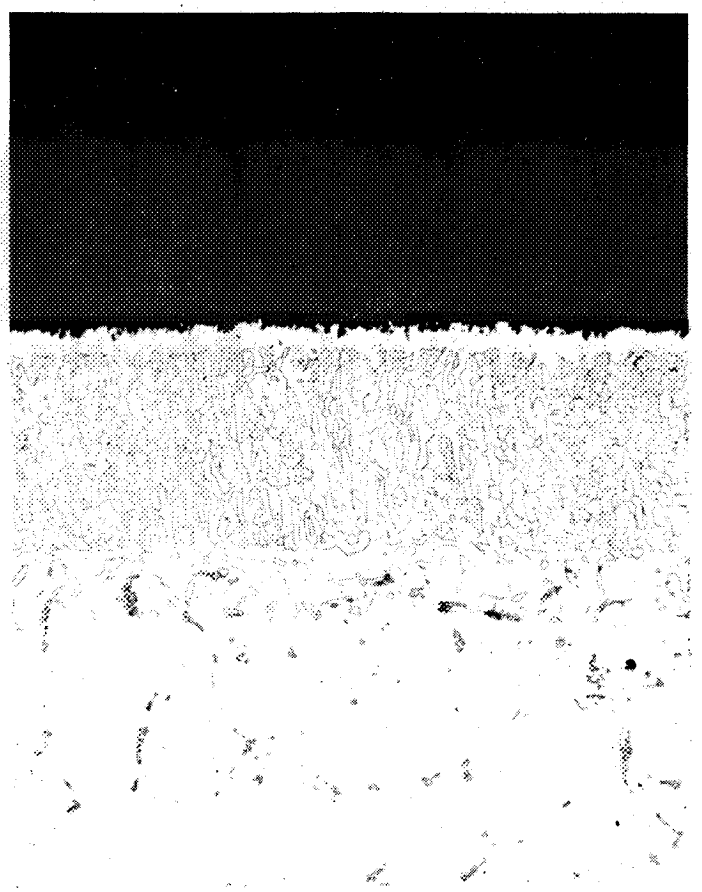

Figure 34. Inner Portion of EB-PVD Zirconia was Densified After 47 Hours in the 1150C Oxidation Test, 200X Magnification.

In the technology review (Appendix A), it was indicated that data from NASA and engine manufacturers' burner rig tests, which simulated industrial, marine, and maritime surveillance engine mission environments, demonstrated that molten salt deposits can wick into porous zirconia coatings and significantly reduce the spalling resistance of TBCs. Accelerated burner rig tests conducted in this program (Figures 27 and 29) conducted with sea salt ingestion in the range of 760 to 925C also resulted in significantly reduced lives for the Temescal EB-PVD and Union Carbide and Chromalloy plasma-sprayed TBC systems. Only the Klock TBC system was not failed in these tests, which were generally terminated in the range of 500 to 1000 hours.

Accelerated testing was primarily achieved by increasing ingested sea salt levels well above the 0.012 ppm that is typically present in sea level air. Synthetic sea salt was asperated into the combustion air of the burner at levels ranging from 0.3 to 10 ppm. The composition of the sea salt used in these tests is provided in Table 4.

The sulfur content of the JP-4 fuel used in these one atmosphere burner rig tests was about 0.03 weight percent. In order to better simulate the SO_2 partial pressure conditions in a 10 atmosphere turbine, the sulfur content of the fuel would need to be increased by a factor of 10 to 0.3 percent. Consequently, SO_2 was added to the combustion air at a level equivalent to 0.3 percent sulfur in the fuel for some of the burner rig tests. Other tests were conducted without sulfur enrichment. No clear trend on TBC spalling lives were observed for tests conducted with or without sulfur enrichment.

The visual appearance of typical spalling associated with salt film damage is shown in Figure 35 for plasma-sprayed (Union Carbide and Chromalloy) TBCs. Failure occurred near the ceramic-metal interface with some zirconia remaining attached to the bond coating.

Table 4. Composition of the Sea Salt Used in the Burner Rig Tests

Element	Weight, %
Na	25.25
Mg	7.07
Ca	1.01
K	1.01
Cl	58.59
SO_4	7.07

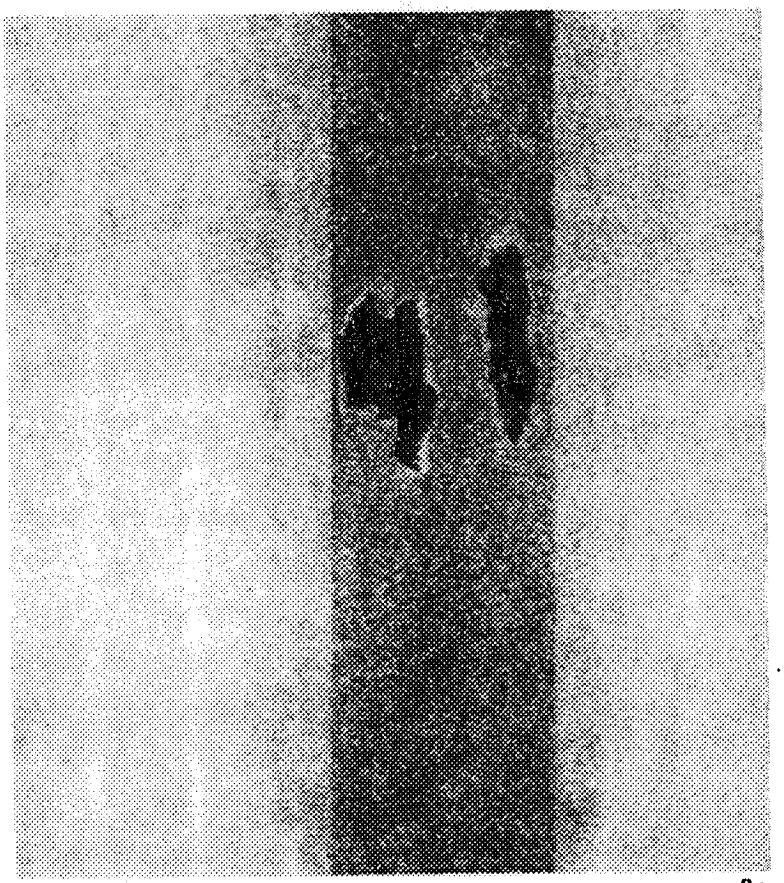

Figure 35. A Typical Union Carbide Molten Salt Film Test Specimen Showing the Spalled Area. This Sample Was Run for 400 Hours in the 760C +10 ppm Sea Salt + 0.3 Weight Percent S Burner Rig Test.

A typical failure of the Temescal EB-PVD TBC was more complex and is shown in 36. Failure in this system occurred throughout the zirconia layer as well as near the interface. A cross-section microstructure of the salt-film-damaged EB-PVD TBC is shown in Figure 37.

A wavelength dispersive X-ray (WDX) analysis of a sea salt deposit on the surface of a plasma-sprayed TBC indicated the presence of sodium, calcium, magnesium, sulfur, as well as aluminum, nickel, cobalt, and chromium. Chlorine was not detected on the surface. This element is thought to have evaporated (as NaCl) or reacted with sulfur oxides to form sodium sulfate. Ni, Co, and Cr are probably deposits from the burner. The aluminum is thought to be a dust contaminant. Subsequent metallographic and WDX analysis confirmed that the Ni, Co, Cr, and Al were surface deposits.

Wavelength dispersive X-ray analyses were conducted on polished cross sections of selected plasma-sprayed and EB-PVD TBC specimens. These specimens were polished with oil-base slurry to preclude leaching of any water-soluble salts from the microstructure. As shown in Figure 38 for a Chromalloy TBC specimen, which survived a 500-hour exposure in a 760C burner rig tests with 10 ppm salt and an effective fuel sulfur content of 0.3 percent, sodium, magnesium, calcium, and sulfur, were detected throughout the zirconia layer. Also the outer surface of the predominately alumina scale at the bond coating-zirconia interface is significantly enriched in magnesium, but not sulfur. Presumably, the magnesium is present as an oxide. High magnesium levels at the interface were also reported by DeMasi and Sheffler (ref. 10), who proposed that the magnesium was reacting with the interfacial alumina scale to form a $MgAl_2O_4$ spinel. Similar analyses were obtained for the Union Carbide and Klock TBC systems tested at 760 and 925C.

WDX analysis of the EB-PVD TBC system showed similar results. S, Ca, Na, and Mg were again detected within the zirconia micro-

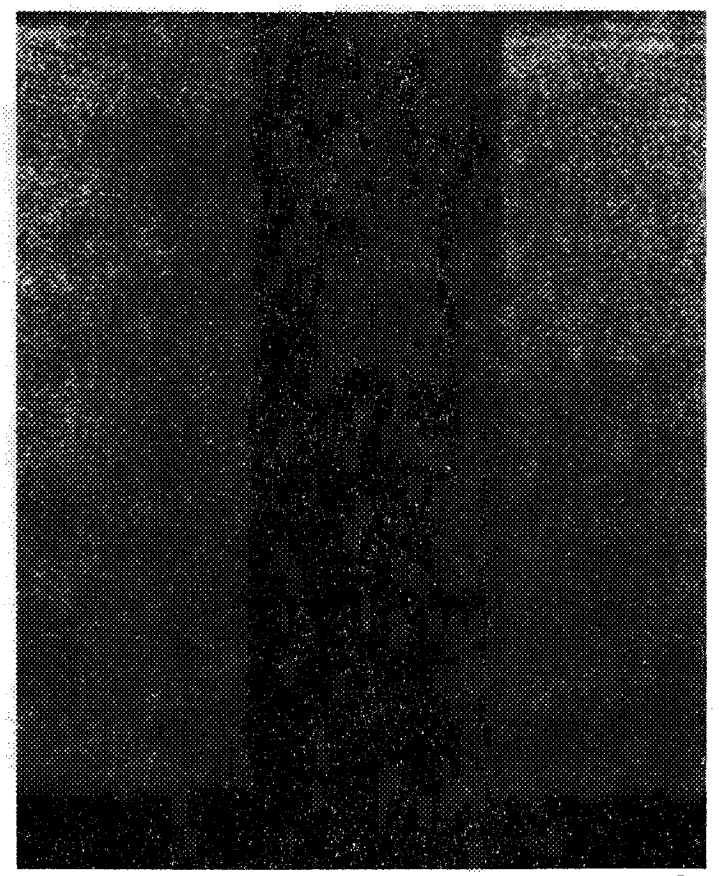

Figure 36. A Typical Temescal Molten Salt Film Test Specimen Showing the Spalled Area. This Sample Was Run for 220 Hours in the 760C +10 ppm Sea Salt + 0.3 Weight Percent S Burner Rig Test.

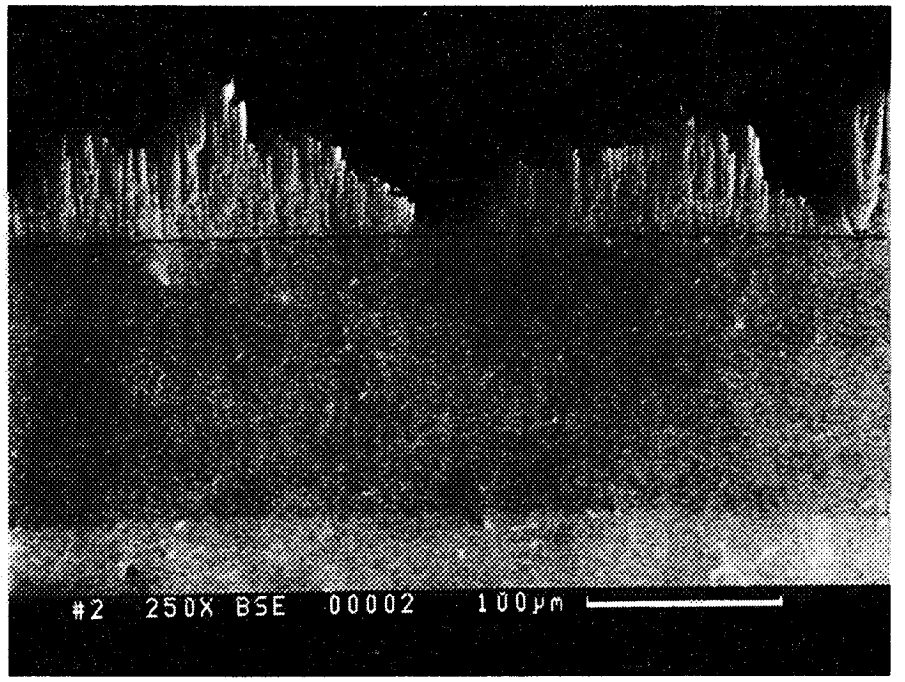

G7106-39

Figure 37. A Cross Section of the Spalled Area on the Temescal Sample from the 760C +10 ppm Sea Salt + 0.3 Weight Percent S Burner Rig Test.

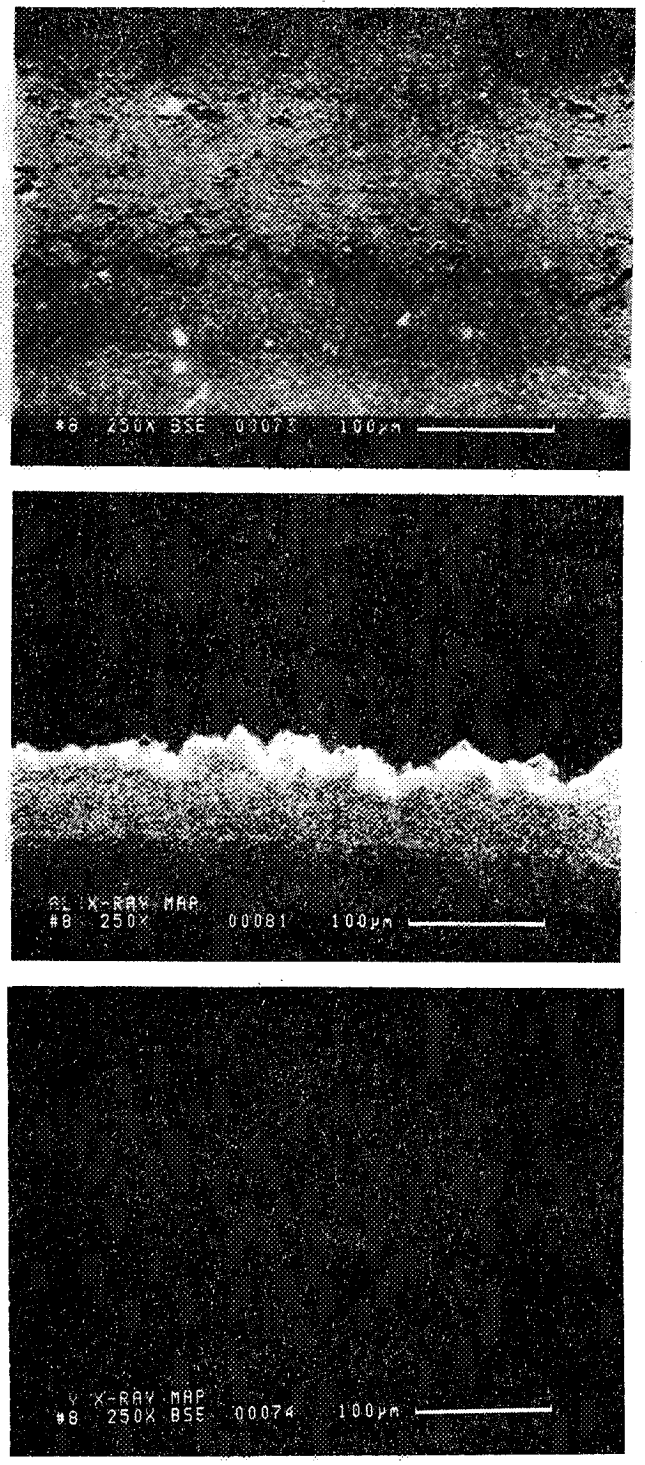

G7106-40A

Figure 38. WDX Analysis Indicates That Molten Salt Wicked Through The Chromalloy TBC System During a 500-Hour, 760C Cyclic (27 Minutes-Hot Plus-3 Minutes-Forced-Air-Cool) Burner Rig Test (10 ppm Salt and 0.3 Percent Surfur).

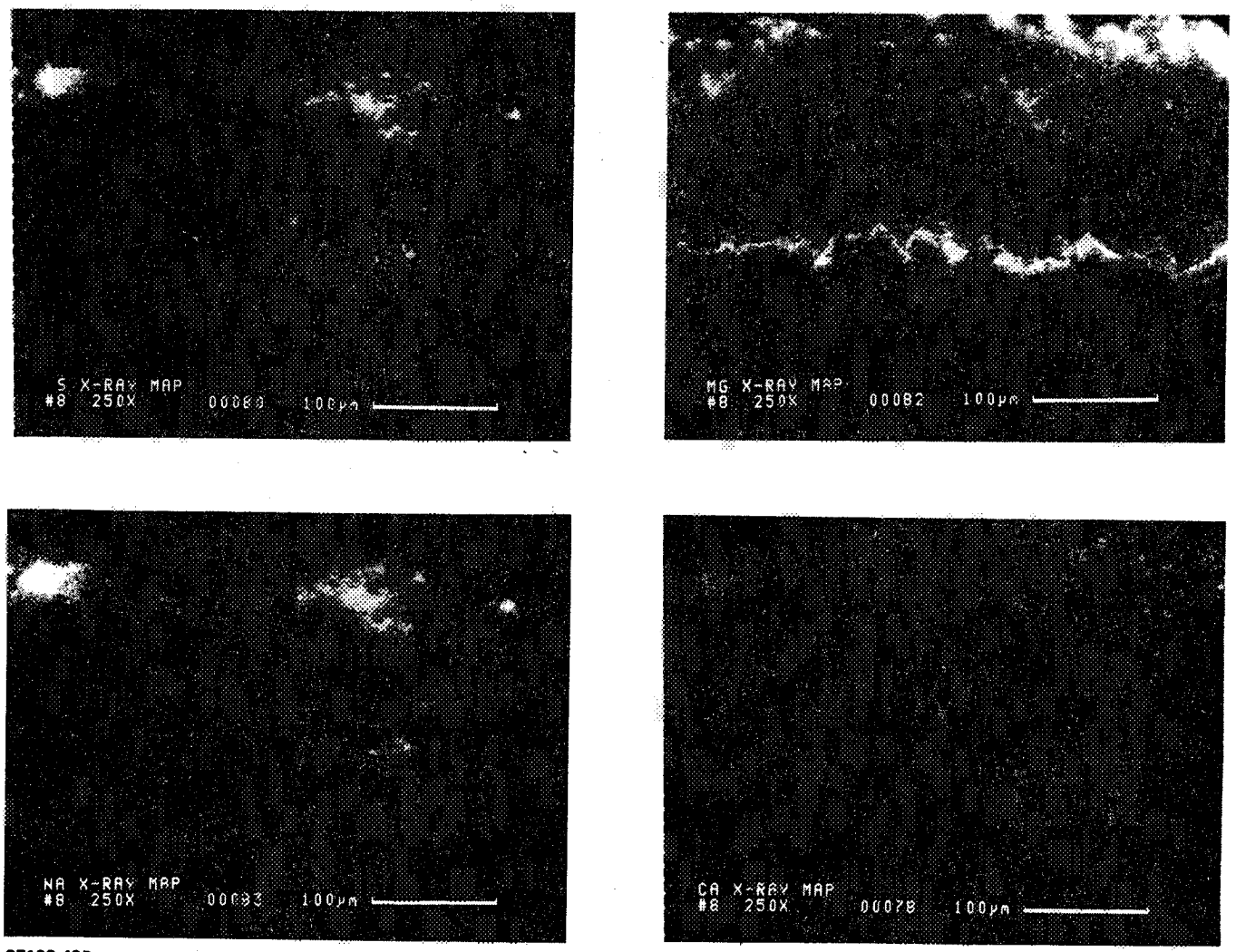

G7106-40B

Figure 38. WDX Analysis Indicates That Molten Salt Wicked Through The Chromalloy TBC System During a 500-Hour, 760C Cyclic (27 Minutes-Hot Plus 3-Minutes-Forced-Air-Cool) Burner Rig Test (10 ppm Salt and 0.3 Percent Surfur) (Contd).

structure. However, in this case, both Mg and Na exhibited enrichment at the alumina scale-zirconia interface (Figure 39).

From these analyses it is apparent that the salt readily penetrates all of the TBC systems evaluated in this program. This is expected because the molten sulfate salt films can be at least partially molten down to the 650C freezing temperature of the sodium sulfate - magnesium sulfate eutectic.

The columnar EB-PVD zirconia microstructure can be thought of as a highly effective wick and was most affected by the molten salt penetration. Salt also wicked into the porosity and microcracks of the plasma-sprayed zirconia coatings. It is thought that the salt penetrated the plasma-sprayed coatings at a slower rate; it may have been more difficult to completely fill the strain accomodating porosity of the plasma-sprayed zirconia systems. The Union Carbide TBC, which had the most-dense zirconia microstructure and, consequently, less porosity to fill, had the most failures of the plasma-sprayed coatings.

At this point, cyclic freezing and melting of the salt within the zirconia layer, and its associated effect on the compressive modulus and stresses are regarded as the most significent aspects of salt film damage. Magnesium enrichment of the alumina scale at the bond coating-zirconia interface is also of concern and may weaken the interface.

4.5 Thermal Conductivity

Thermal conductivity is a critical design property of TBCs and governs heat transfer into air-cooled turbine components. Component metal temperatures and thermal strains are dependent upon the thermal conductivity of the zirconia layer. Therefore, to facilitate thermal and stress analyses of engine components, thermal conductivity of plasma-sprayed and EB-PVD coatings was quantified in this program.

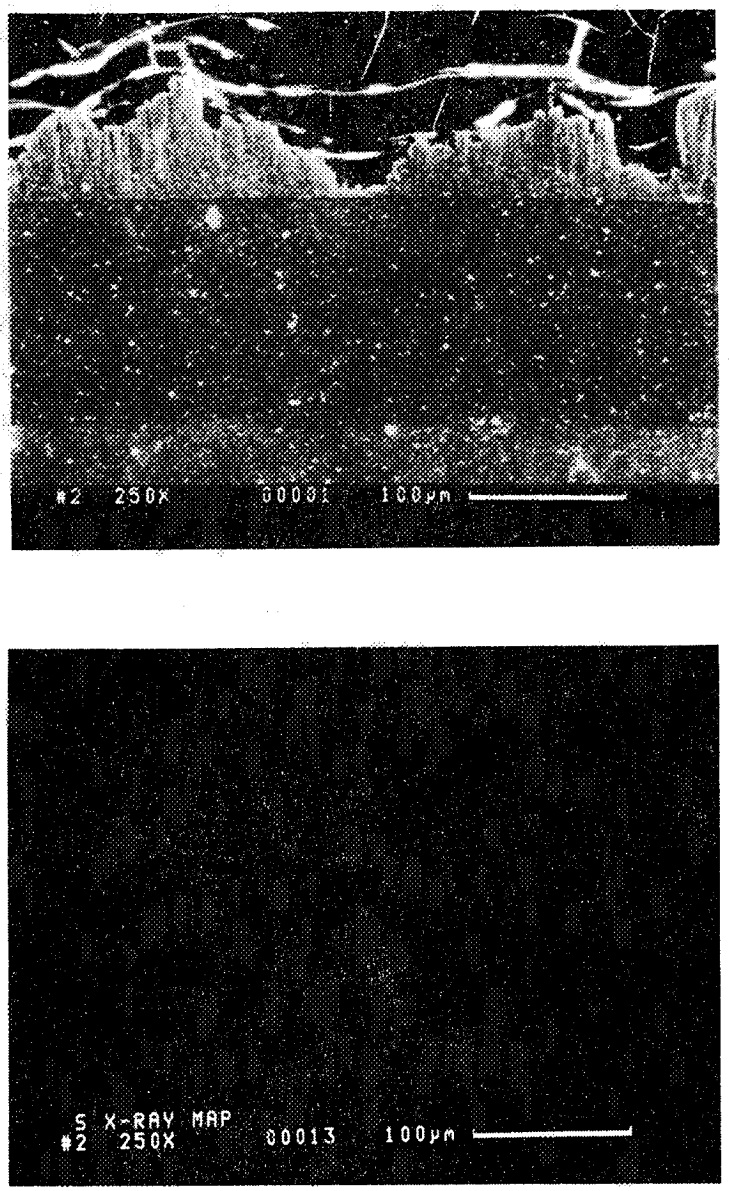

Figure 39. WDX Analysis Indicates That Molten Salt Wicked Through the Temescal TBC System During a 150-Hour, 760C Cyclic (27-Minutes-Hot Plus 3-Minutes Forced Air Cool) Burner Rig Test (10 ppm Salt and 0.3 Percent Sulfur).

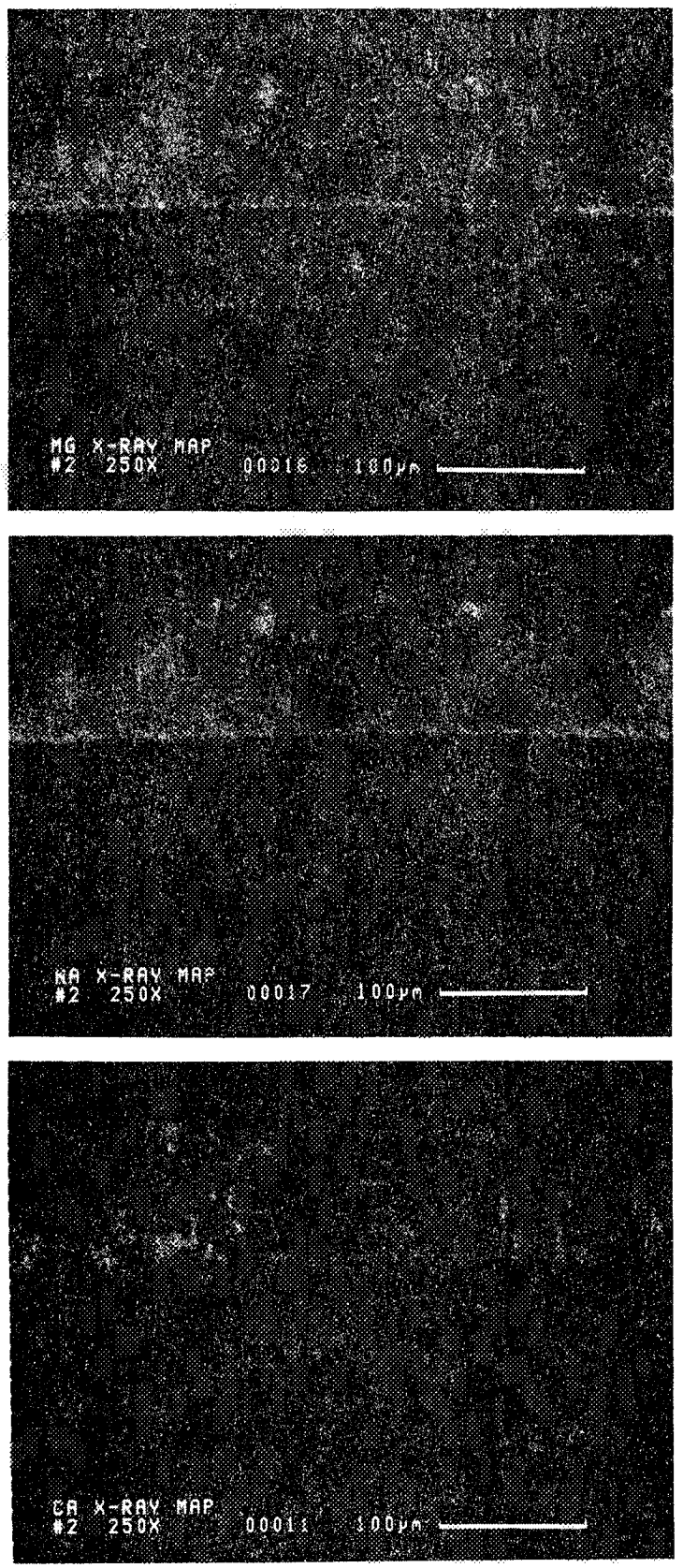

67106-41B

Figure 39. WDX Analysis Indicates That Molten Salt Wicked Through the Temescal TBC System During a 150-Hour, 760C Cyclic (27-Minutes-Hot Plus 3-Minutes Forced Air Cool) Burner Rig Test (10 ppm Salt and 0.3 Percent Sulfur) (Contd).

Testing was performed at Dynatech (Cambridge, MA) using the comparative method to determine thermal conductivity at 500, 800, and 1000C. The specimen geometry is shown in Figure 12. The substrate was instrumented with thermocouples and placed between two reference standards of identical geometry Figure 40. Each standard (heat meter) was instrumented with thermocouples at known fixed distances. The composite stack was fitted between an upper heater and lower heater of appropriate geometry and the complete system placed on a liquid-cooled heat sink. A reproducible load was applied to the top of the system to ensure intimate contact between all components. A thermal guard tube that could be heated or cooled was placed around the system and the interspace and surroundings filled with an insulating powder.

The temperature drop across the coatings was obtained by extrapolating internal temperatures of the references and substrate to the surface on either side of the coatings.

By setting the top heater to a temperature higher than the lower heater, a temperature gradient was established in the stack. Radial heat loss was minimized by establishing a similar gradient in the guard tube. The system was allowed to reach equilibrium conditions after which successive readings of temperatures at various points were averaged and evaluated. From this data, heat flux was determined and specimen thermal conductivity calculated.

Thermal conductivity data for the Chromalloy and Klock plasma-sprayed ytrria (8 weight percent) stabilized zirconia coatings and Temescal EB-PVD yttria (20 weight percent) stabilized zirconia coating, provided in Figure 41 and Table 5, are in excellent agreement with published data for this coating from other NASA-sponsored programs. This figure also indicates that the plasma-sprayed and EB-PVD zirconias are about a factor of 30 lower than a typical superalloy, such as Mar-M 247 at about 1000C. Zirconia coatings evaluated in this program are also about a factor of 3 lower in con-

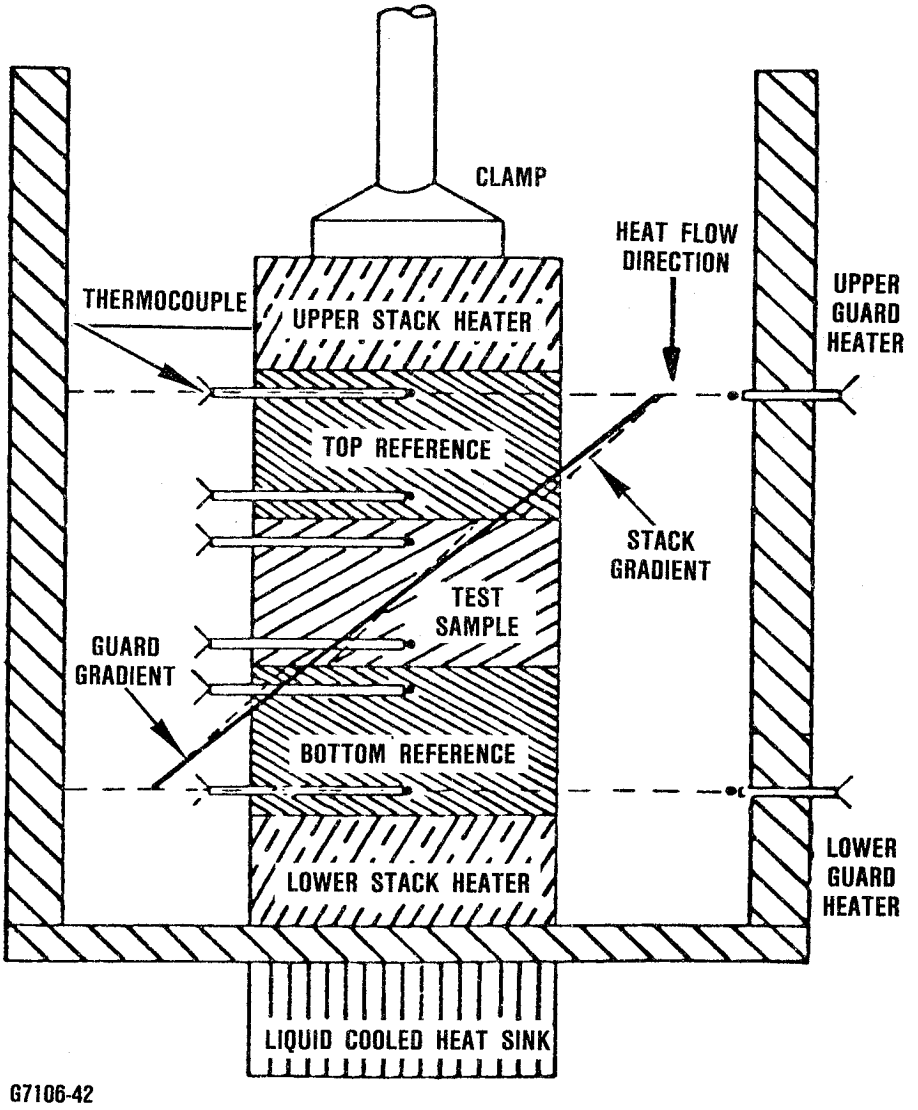

Figure 40. Schematic Diagram of Comparative Thermal Conductivity Test Shack.

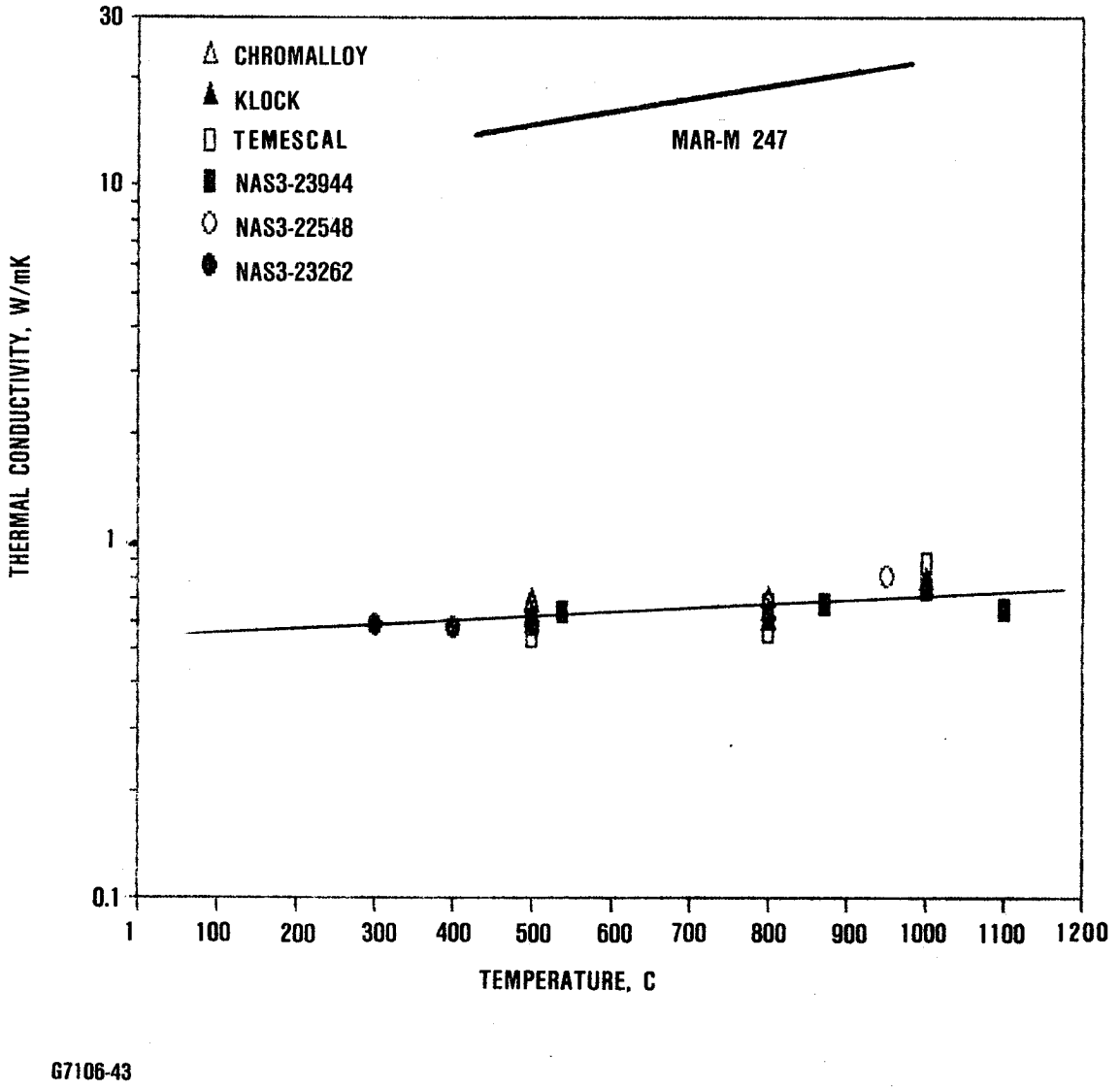

Figure 41. Thermal Conductivity Data for Plasma-Sprayed Yttria (8 Weight Percent) Zirconia and EB-PVD Yttria (20 Weight Percent) Zirconia are in Excellent Agreement with Published Data.

Table 5. Plasma Sprayed and EB-PVD Zirconia Coatings have Comparable Thermal Conductivity

Sample	Thermal Conductivity, W/mK			Comments
	at 500C (930F)	at 800C (1470F)	at 1000C (1832F)	
T30H-1T	0.64	0.68	0.89	EB-PVD ZrO_2 from Temescal
T30H-3T	0.54	0.56	0.75	EB-PVD ZrO_2 from Temescal
K50H-1	0.58	0.59	0.78	Plasma-sprayed ZrO_2 from Klock
K50H-2	0.61	0.63	0.74	Plasma-sprayed ZrO_2 from Klock
C50H-1	0.67	0.69	--	Plasma-sprayed ZrO_2 from Chromally
C50H-2	0.68	0.69	--	Plasma-sprayed ZrO_2 from Chromally

ductivity than dense plasma-sprayed zirconia after sintering at 2000C (ref. 3); this result is attributed to the porosity and sub-critical microcracks within the microstructure.

4.6 Nondestructive Evaluation (NDE) Technologies

Effective exploitation of TBCs requires that critical material properties can be verified. The insulative capability of a TBC is dependent upon zirconia thickness and microstructure. The mechanical integrity of TBCs is dependent upon the microstructure of the coating and the size of critical flaws. Therefore, GTEC assessed conventional and emerging NDE technologies for the potential to verify coating thickness and flaw size. The conventional techniques included eddy current inspection and ultrasonic through-transmission and pulse-echo inspection. Emerging technologies considered included photothermal radiometric imaging, scanning acoustic microscopy, and high-frequency ultrasonic inspection. Of the techniques considered for flaw detection, only the high frequency ultrasonics showed promise. Eddy current inspection was verified as a viable method for measuring the thickness of both plasma-sprayed and EB-PVD zirconia coatings. All of the NDE techniques are reviewed in the following paragraphs.

4.6.1 Eddy Current Evaluation

An eddy current technique was used to successfully measure the thickness of the zirconia layer for Chromalloy and Klock's plasma-sprayed TBC systems and Temescal's EB-PVD TBC system. Variations in the thickness of the ZrO_2 coating on the order of 25 to 50 μm (1 to 2 mils) are detectable. The results of this thickness determination study are shown in Figure 42. Five points were taken for each specimen along with air and the uncoated back of each specimen.

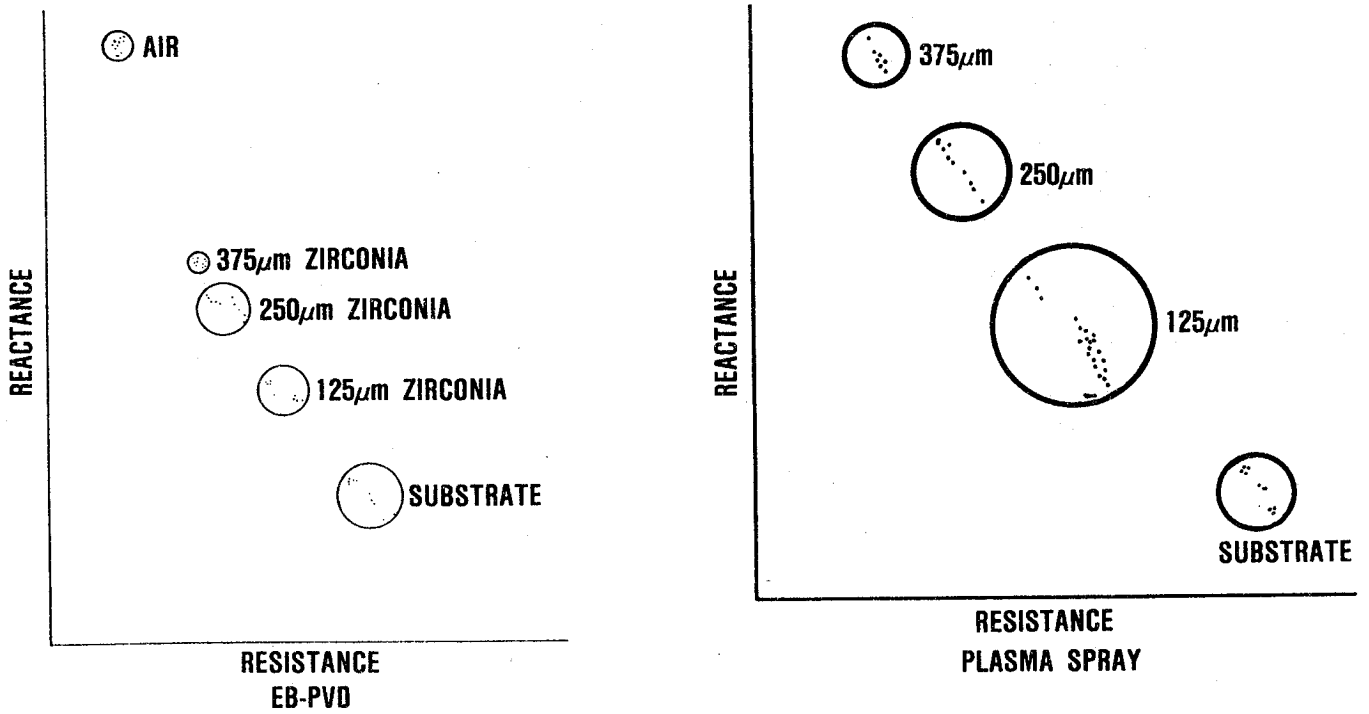

G6-095-29

G7106-44

Figure 42. Eddy-Current Inspections of EB-PVD and Plasma-Sprayed Zirconia Coatings are Comparable.

Insulative capabilities of TBCs on turbine components can, therefore, be established by using Eddy Current technology to verify zirconia thickness and using sample tabs to verify TBC microstructure.

4.6.2 Photothermal Radiometric Imaging

The experimental study of Photothermal Radiometric Imaging NDE technique was conducted by Dr. I. Kaufmann at Arizona State University. Photothermal radiometric imaging is a form of thermal imaging, which detects emitted thermal radiation from surfaces heated by a pulsed scanning laser beam. The experimental apparatus is illustrated schematically in Figure 43. For small temperature variations, the amount of thermal radiation given off by the surface is linearly proportional to the temperature change. If subsurface flaws are to be detected, then the heat must be able to penetrate the top layer so that anomalies in the lower layers are revealed.

Photothermal Radiometric Imaging was not successful in reliably detecting artificial flaws in either plasma-sprayed or EB-PVD TBC systems. The lack of success was attributed to the low thermal diffusivity of the zirconia coating. Limitations of the current technology in photothermal radiometric imaging are a slow scanning rate, which requires a long-inspection time and a low signal-to-noise ratio, which limits reliable detection of a flaw. An improved detector and/or signal processing may enable this technique to detect flaws in TBCs. Results of this investigation are described in detail in a separate report, which has been provided to the NASA program manager.

4.6.3 Scanning Photacoustic Microscopy

The experimental study of the scanning photoacoustic microscopy (SPAM) NDE technique was conducted by Dr. R. Thomas at Wayne State University. SPAM determines thermal variations by measuring dis-

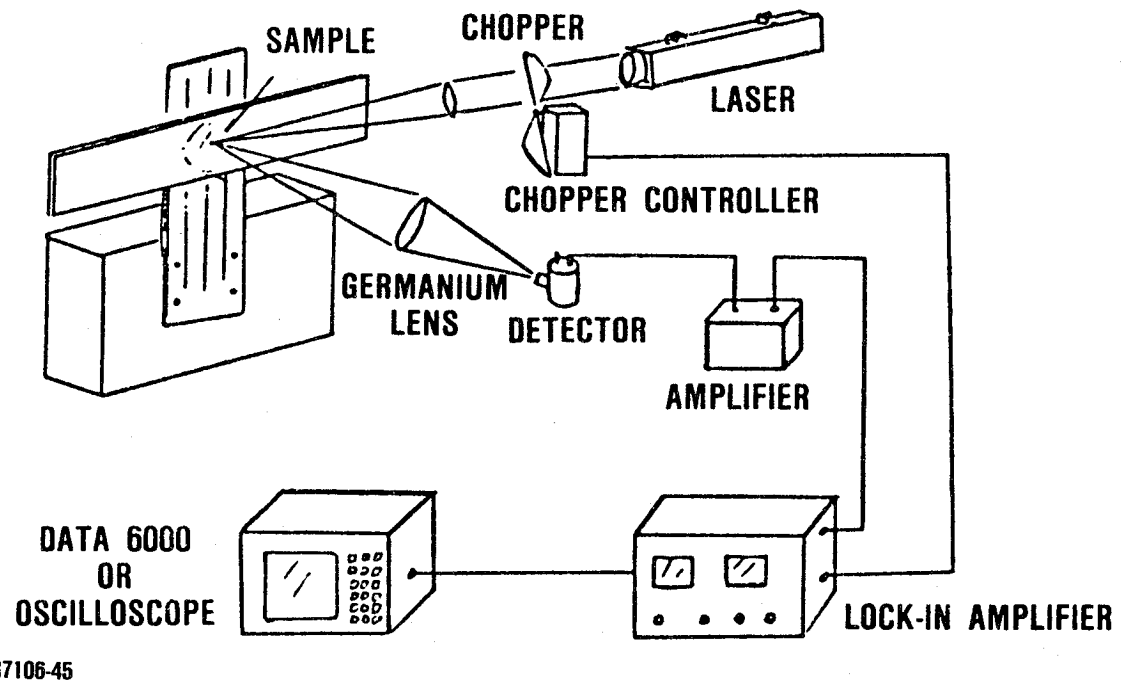

Figure 43. Photothermal Radiometric Imaging NDE Technique was Evaluated at Arizone State University.

placement of a laser beam propagating parallel to the specimen surface. A schematic diagram of the experimental set-up of this technique is shown in Figure 44. The displacement is caused by the index of refraction due to surface heating. There are three ways to measure the laser beam deflection:

- Either by an acoustic gas cell
- An infrared detector
- Piezoelectric detection

In all cases, the measurement is a line integral across the sample surface, rather than a single-point measurement. Defects/disbonds are detected by local variations in the detected thermal wave, while thickness is determined by an analysis of the entire field as compared to specimens of known thickness. Local variations in the detected thermal wave are then processed to determine the presence of a defect.

SPAM was not successful in detecting artificial flaws in either plasma-sprayed or EB-PVD TBC systems. Again, the thermal diffusivity of the zirconia coating probably prevented significant variation in the data for intimate contact disbonds. Full automation and advanced signal processing of the received signals from SPAM may allow the eventual detection of flaws in TBCs. Results of this investigation are described in detail in a separate report, which has been provided to the NASA program manager.

4.6.4 High Frequency Ultrasonics

High Frequency Ultrasonics were investigated as an experimental NDE technique with GTEC funding.

High frequency ultrasonics is a straight-forward, inexpensive technique for evaluation of coating uniformity that is amenable to complex turbine engine components. Ultrasonics are currently used

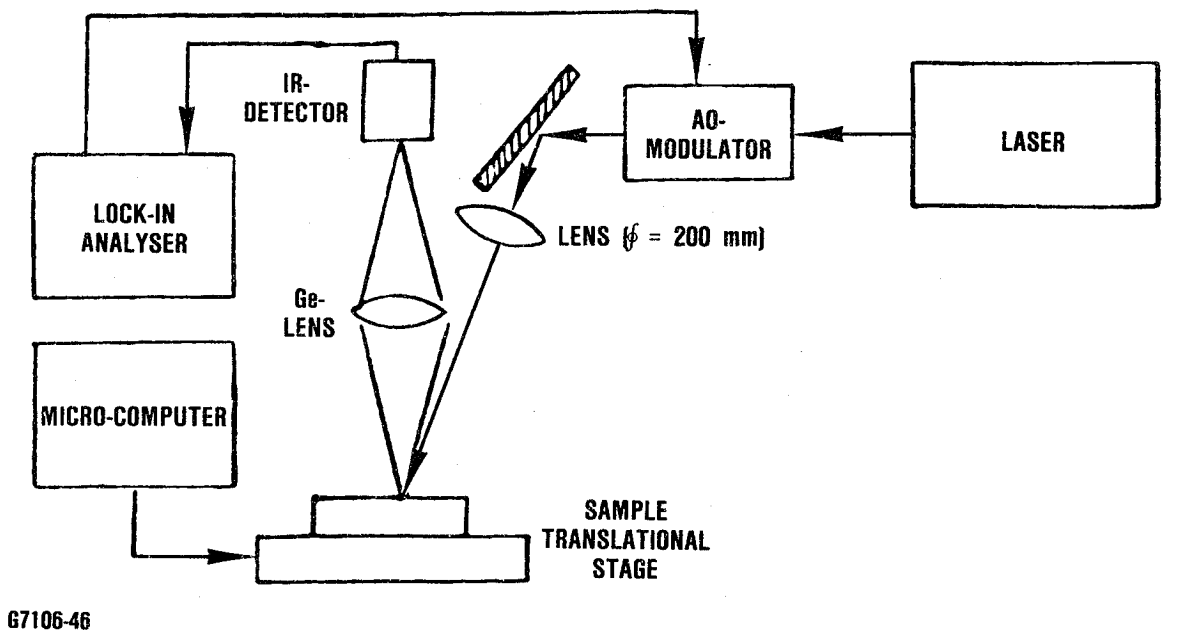

Figure 44. Scanning Photoacoustic Microscropy NDE Technique was Evaluated at Wayne State University.

for component inspection by most turbine engine manufacturers. High frequency ultrasonics use the principles of conventional ultrasonic inspection, except the frequencies used to probe the specimen are much higher, ranging between 30 and 100 MHz. Pulse-echo ultrasonic inspection was used to detect both thickness variations and disbonds in the TBCs. An ultrasonic wave is coupled into the specimen using water or other suitable ultrasonic couplant. Each time the ultrasonic wave encounters an impedance mismatch, some of the ultrasonic beam is reflected back to the transducer. The portion of the ultrasonic beam reflected back to the transducer is proportional to the acoustic impedance mismatch at the interface. For a disbond, the amount of acoustic impedance is greater than for a good bond. The C-scan Figure 45 shows the higher acoustic impedance region in the center of the specimen where an artificial interfacial flaw was present. For thickness measurement, the time between the interface signals is measured and used to determine thickness. This technique requires the probing ultrasonic frequency be high enough to resolve the thicknesses of interest. Frequencies between 75 to 100 MHz were used to determine thickness measurement capability.

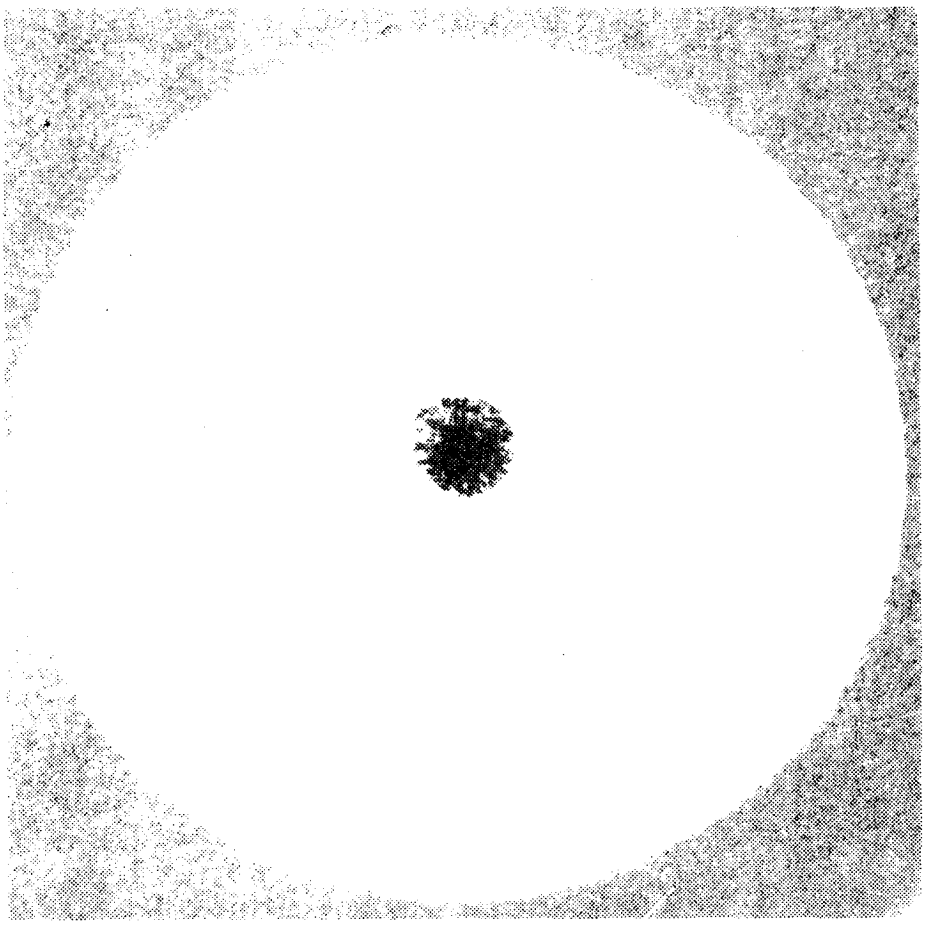

G7106-47

Figure 45. Interfacial Flaw In EB-PVD TBC Detected By Panametrics Ultrasonic Inspection.

5.0 TBC LIFE PREDICTION MODEL DEVELOPMENT

5.1 Analysis Strategy

The primary objective for this program was the development of mechanistic mission-analysis-capable preliminary design life prediction models for plasma-sprayed and EB-PVD TBC systems. Operative TBC damage modes, which contribute to zirconia spalling and, consequently, must be included into a viable life model, are bond-coating oxidation, zirconia toughness reduction (which appears to be associated with sintering densification of the zirconia), and molten salt film damage. These thermochemical damage modes are functions of time, temperature, and engine-mission environment, and they contribute to thermomechanial stresses associated with spalling of the insulative zirconia layer.

Because a TBC must be considered early in the component design process in order to fully incorporate and exploit its benefits, a thermochemical TBC life model was developed to use the relatively inexpensive component thermal analysis and engine mission analysis data that become available early during the component design cycle. This thermochemical model was fully developed, calibrated, and demonstrated during this program.

TBC life calculations may be further refined by a more detailed understanding of the stresses within the coating. Therefore, development of a detailed thermomechanical micromodel was also pursued in this program. When fully developed, this model will be driven by thermomechanical stress analyses of the component for specified engine cycles and include time- and temperature-dependent material system properties. Because thermomechanical stress analyses are expensive and available late in the component design cycle, the thermomechanical TBC life model is projected to be useful for the final design analysis.

GTEC's comprehensive strategy for TBC life analysis is illustrated in Figure 46. Development of the thermochemical and thermomechanical life prediction models are described in the following paragraphs.

5.2 Thermochemical TBC Life Model

A preliminary design model for predicting TBC life must be capable of rapid iteration in order to be a viable tool. In order to facilitate a low-cost, iterative capability for TBC life analysis, the preliminary design model is tailored to be driven primarily by thermal analyses of the component, engine cycle data, and the planned flight spectrum for the aircraft. Stress analysis is intentionally limited, during these early design iterations, to verification that the TBC system can survive a severe transient snap acceleration/deceleration strain cycle (i.e., idle to full power to idle with no intermediate power dwells).

Burner rig tests are the primary means for calibrating the preliminary design TBC materials models that quantify the thermally-driven damage modes. Effects of bond-coating oxidation and zirconia densification on the time required to spall the zirconia layer are quantified with burner rig tests conducted above 1000C.

Condensed, molten sulfate salt films can be present on the surface of a TBC when zirconia temperatures are below about 950C for aircraft operating in a predominately marine environment, such as maritime surveillance. Wicking the salt deposit into the strain accommodating porosity and subcritical microcracks can result in an increase in the apparent compressive modulus, higher stresses, and spalling of both plasma-sprayed and EB-PVD zirconia coatings. Therefore, burner rig tests conducted in the range of 760 to 925C were conducted to calibrate the molten salt film damage model.

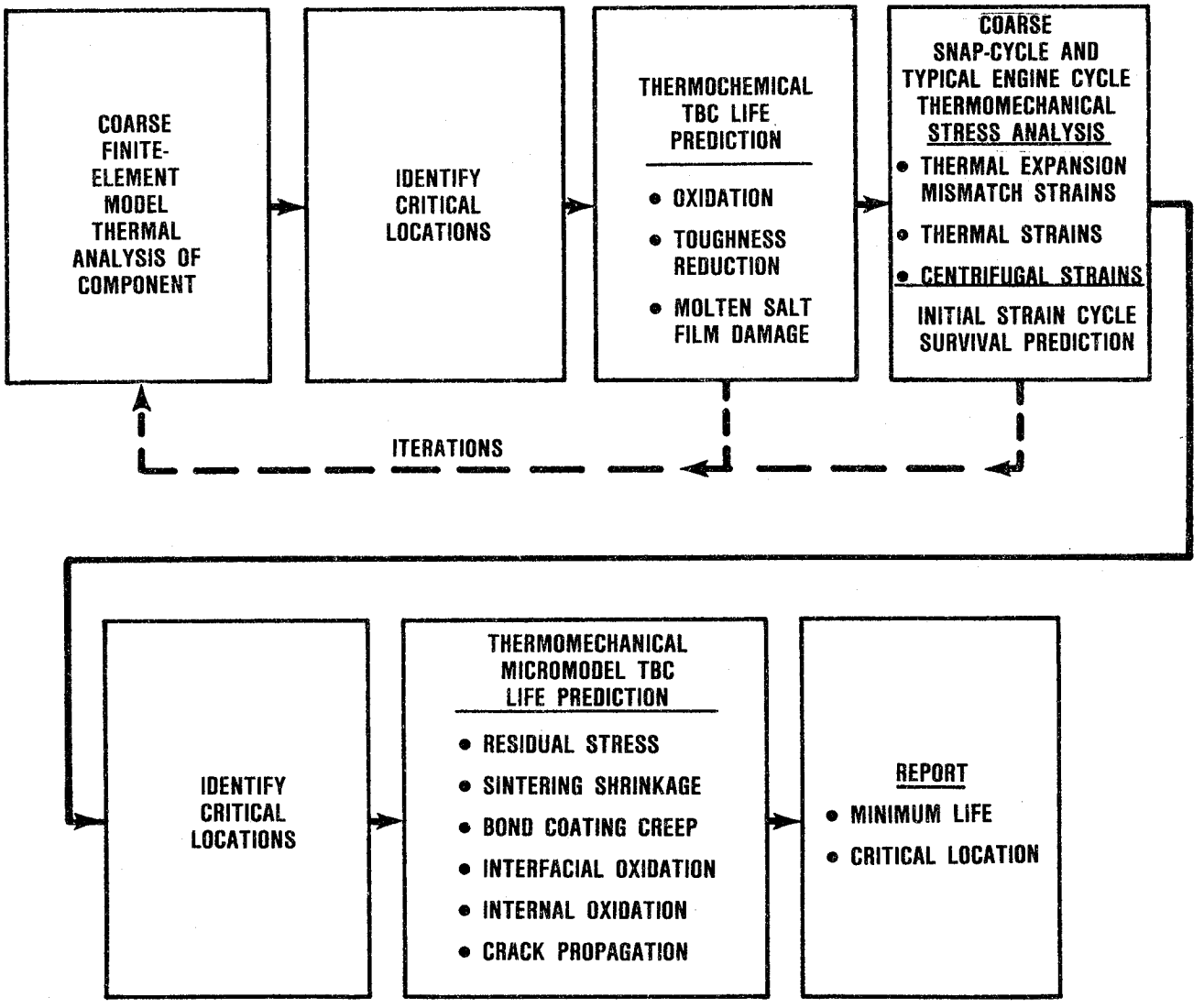

Figure 46. A Comprehensive Strategy Has Been Developed for TBC Life Analysis.

Oxidation Life Damage Modes

In the oxidation damage regime of the burner rig data (above 1000C), the burner rig data has been analyzed as a two-line Miner's law function of the temperature and the logarithm of the burner rig hot time required to spall the zirconia coating; i.e.,

$$\text{Oxidation Life} = \frac{\text{Heating cycle length factor}}{\frac{1}{\text{oxidation life}} + \frac{1}{\text{zirconia densification plus oxidation life}}}$$

In equation form, this life model looks as follows:

$$\text{Oxidation Life} = \frac{(t_i^{0.25} + 0.181) \cdot \text{MTBREF}}{\frac{1}{e^{-0.015(T+273)+C_1}} + \frac{1}{e^{-0.041(T+273)+C_2}}}$$

where T is the bond-coating temperature in degrees C, t_i is the increment of hot time at a specified mission point in hours, and C_1 and C_2 are constants experimentally determined for each particular fixed process TBC system. MTBREF is a multitemperature burner rig experience factor, which forces predicted life into agreement with the lowest life data from multitemperature burner rig tests. MTBREF's and values of C_1 and C_2 for plasma-sprayed and EB-PVD TBC systems, representative of curves forced through the lowest of the burner rig life data for each TBC system, are indicated below:

Plasma-Sprayed TBCs	C_1	C_2	MTBREF
Klock	26.0	61.5	1.00
Chromalloy	25.3	59.0	0.67
Union Carbide	25.3	59.0	0.27
EB-PVD TBC			
Temescal	26.3	62.3	0.83

A typical aircraft engine mission cycle will have dwell periods of varying durations at several different temperatures; for example, a few minutes at take-off power, perhaps 10 minutes at climb power, and 0.5 to 5 hours at cruise power. Therefore, in order to analyze burner rig data obtained at different cycle periods as well as predict TBC spalling for engine mission cycles of various lengths, the following heating cycle length factor was developed:

$$(\text{Coating life})_{ti} = (\text{Burner rig test life})(t_i^{0.25} + 0.181),$$

where, t_i is the increment of hot time in hours and the burner rig test life is for the 27 minutes hot and 3 minutes forced air cool cycle. The cycle period correction term equals one when there is 27 minutes of hot time per cycle.

The slope, -0.015, of the natural logarithm of life-versus-temperature line for the "oxidation" damage mode was determined from an analysis of the longer life (greater than about 100 hours to spall the zirconia) burner rig data. This slope is also consistent with short cycle (4 minutes hot plus 2 minutes forced air cool) burner rig data in the 1100 to 1170 C temperature range, that was reported by Pratt & Whitney Aircraft (ref. 2).

The slope, -0.041, of the natural logarithm of life-versus-temperature line for the "oxidation plus zirconia densification" degradation mode was determined by an analysis of the short life (less than about 100 hours) burner rig data. This slope is also equal to that obtained for the natural logarithm of the high-to-low fracture toughness transition time versus temperature (in the range of 1100 to 1150C) obtained for the Chromalloy and Union Carbine plasma-sprayed TBC systems (Figure 27). It should also be noted that the Pratt & Whitney Aircraft short-cycle burner rig data at the highest temperatures also exhibits a steeper slope (ref. 2), which is similar to that obtained in this program.

Preliminary data obtained by Miller (ref. 11) characterized the oxide scale growth rates on a NiCoCrAlY coating in the temperature range of 1100 to 1200C. Making the simplifying assumption that the zirconia spalls at a constant oxide scale thickness, as proposed by General Electric (ref. 12), Miller's analysis indicates that oxide scale spalling will be the following function of time and temperature:

$$(e^{52771/T})t = \text{constant},$$

where, T is the bond coating temperature and t is the time required to grow the oxide scale to a thickness required to spall the coating. This relationship is also forced through the lowest burner rig life data and compared with the GTEC oxidation life prediction curves in Figure 47. Although the Miller and GTEC curves in these figures have opposite curvature, very similar predictions are obtained for temperatures above about 1000 to 1050C. The GTEC TBC life model is more conservative below 1000C. Comparison of the two relationships indicates that the GTEC curve does a better job conforming to the burner rig data trends for the Klock data. Minimum data trends would be effectively represented by either model for the other TBC systems in the range where test data exists.

Molten Salt Film Damage Mode

As previously noted, a molten salt film on the surface of the component can wick into a TBC system and accelerate zirconia spalling. In developing a model for this damage mode, it has been assumed that salt film damage is primarily a function of salt deposition, retention, solidification, and evaporation kinetics. Since these factors also affect hot corrosion attack of metallic coatings, the molten salt film damage model has similarities with GTEC's hot corrosion life prediction model (ref. 13).

C-2

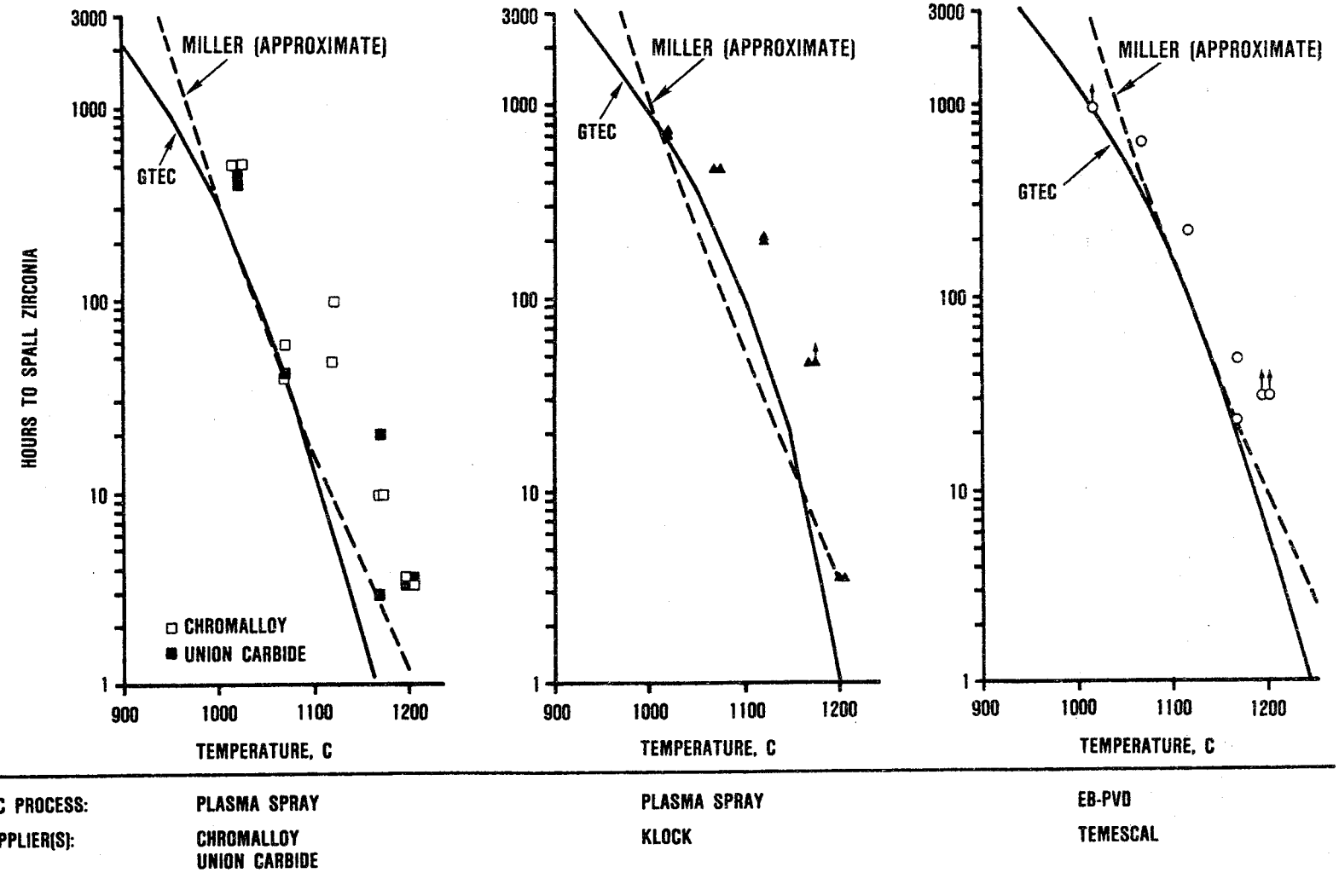

Figure 47. GTEC and Miller's Oxidation Life Prediction Curves are Forced Through Minimum Life Burner Rig Cyclic Oxidation Data.

The salt film damage life model that has been developed is shown below:

$$\text{Salt Film Damage Life} = \frac{\text{Burner Rig Calibration Factor}}{\left(\begin{array}{l}\text{Steady-State}\\ \text{Deposition}\\ \text{Factor}\end{array} + \begin{array}{l}\text{Salt}\\ \text{Shedding}\\ \text{Factor}\end{array} + \begin{array}{l}\text{Salt}\\ \text{Retention}\\ \text{Factor}\end{array}\right)\cdot\left(\begin{array}{l}\text{Location}\\ \text{Factor}\end{array}\right)\cdot\left(\begin{array}{l}\text{Fraction}\\ \text{of Salt}\\ \text{Molten}\end{array}\right)}$$

$$\text{Salt Deposition Factor} \geq 0$$

where,

Steady-State Deposition Factor = $SS = (1-X)\{P\cdot[0.012-0.007Alt]/10-Vap\}$

Salt Shedding Factor = $Shed = X\{0.2P - Vap\}$

Alt = Aircraft altitude in kilometers

P = Turbine pressure in atmospheres at component

$$X = \frac{9(0.012 - 0.007Alt)}{2.0 - (0.012 - 0.007Alt)}$$ = Fraction of mission for salt shedding

$Vap = 4.0\cdot10^5\cdot e^{(0.0276[T+273] - 45.54)}$ ppm

T = Zirconia temperature in degrees C

Location Factor = (0.25 + 0.75 Coast), where Coast is the fraction of coastal takeoffs.

Fraction of the Salt Molten = FM
= 1 for T > 884C
= [T-650]/234 for $650 \leq T \leq 884$C
= 0 for $T \leq 650$C

Salt Retention Factor = SRF = SRF' + F' · (SS' + SHED') - F · VAP
where ' indicates the prior mission point conditions.

$SS' = (1-X') \cdot \{P'[0.012-0.007Alt']/10 - Vap'\}$

$Shed' = X'[0.2P' - Vap']$

F = Fraction of total mission for current mission point

Each of these factors is discussed in the following paragraphs.

U.S. Navy literature indicates that the amount of salt ingested into a gas turbine engine will decrease as the altitude is increased (refs. 14 and 15). Available data indicates that the amount of salt in the air at sea level can vary greatly depending upon weather conditions (refs. 16 and 17). Sea-level salt concentrations in the air ranging from 0.001 to 0.1 ppm have been reported. For the development of this model, an intermediate sea-level salt content of 0.012 ppm has been used. Based on the study by Woodcock (ref. 14), the amount of salt is reduced by 0.007 ppm per kilometer of elevation above sea level. This relationship results in no salt ingestion when the aircraft is above an altitude of 1.7 kilometers. It should also be noted that the salt flux is concentrated by the turbine pressure.

Thickness of the salt film deposit on a turbine airfoil is a function of both deposition and evaporation. Consequently, at high temperatures, salt films will evaporate rapidly; when the evaporation rate is sufficiently rapid, no salt film will be present on the component to cause molten salt film damage of the zirconia. For this model, the vapor-pressure-versus-temperature relationship for molten sodium sulfate (ref. 18) was used to describe the evaporation rate of the molten sulfate salt film, Vap. The constant, $4.0 \cdot 10^5$, in the Vap function converts the vapor pressure from atmospheres to ppm and assumes that the evaporation rate of the mixed sulfate salt film proceeds at 40 percent of the rate of pure sodium sulfate.

McCreath has documented that the compressor of a gas turbine engine has two significant effects on the salt flux that enters the turbine (refs. 19 and 20). Most of the time, the compressor collects ingested salts as deposits on the airfoils. This filtration of the salt from the air was reported to reduce the steady-state salt content entering the turbine by one-half to two orders of magnitude. On the other hand, salt deposits cannot build up indefinitely; consequently, the compressor also transiently sheds a high salt flux into the turbine.

For the purpose of the model, the assumption was made that the steady-state salt ingestion was 10 percent of the salt mass that entered the compressor. The other 90 percent of the salt was assumed to be initially deposited on compressor airfoils and then subsequently shed in transient bursts at a flux of 0.2 ppm. The duration of the transient salt-shedding event is calculated to be 5.4 percent of the mission at sea level and considerably less at higher altitudes.

The third portion of the salt deposition factor, which is necessary for engine mission analysis, is the salt retention factor. For example, a salt film deposited onto the surface of the airfoil during engine idle or low altitude operation, may remain on the airfoil when the aircraft reaches higher altitudes. Also, salt deposition can occur during low altitude mission points, while salt evaporation can be more rapid at other mission points. Therefore, the salt retention factor is designed to account for all salt retained on the airfoil from prior mission segments. It is calculated using the steady-state, transient salt deposition and salt retention terms from the preceding mission interval. Because salt deposited during previous mission intervals can be eliminated by evaporation, the vaporized quantity of salt times the fraction of the total mission for the mission segment currently being calculated is subtracted. The salt retention factor for the first mission segment is set equal to zero.

The location factor assumes that the salt content over land is only 25 percent of that over the ocean.

Because only molten salt can wick into the zirconia coating, the Salt Deposition Factor is multiplied by the fraction of the salt that is molten. Above the melting point of sodium sulfate, 884C, the salt is assumed to be molten. Below the 650C eutectic between sodium sulfate and magnesium sulfate, the salt is assumed to be

solid. The salt is assumed to be partially molten between these temperatures.

Burner rig calibration factors (BRCF) are obtained by forcing the equation into agreement with minimum TBC spalling lives in the salted burner rig tests. These factors are as follows for the plasma-sprayed and EB-PVD TBCS:

Plasma-Sprayed TBCs	BRCF
Klock	$\geq$1190
Chromalloy	383
Union Carbide	383
EB-PVD TBCs	
Temescal	34

The molten salt film damage and oxidation life prediction relationships, and associated burner rig data for the 27 minute heating cycle, are provided in Figures 48 and 49 for the plasma-spray and EB-PVD coating systems, respectively.

The computer code for the thermochemical life prediction model is provided in Appendix B.

TBC life is calculated at each mission segment using Miner's law, i.e.;

$$\text{Mission Segment Life} = \text{MSL} = \frac{1}{(\text{oxidation life})^{-1} + (\text{salt film damage life})^{-1}}.$$

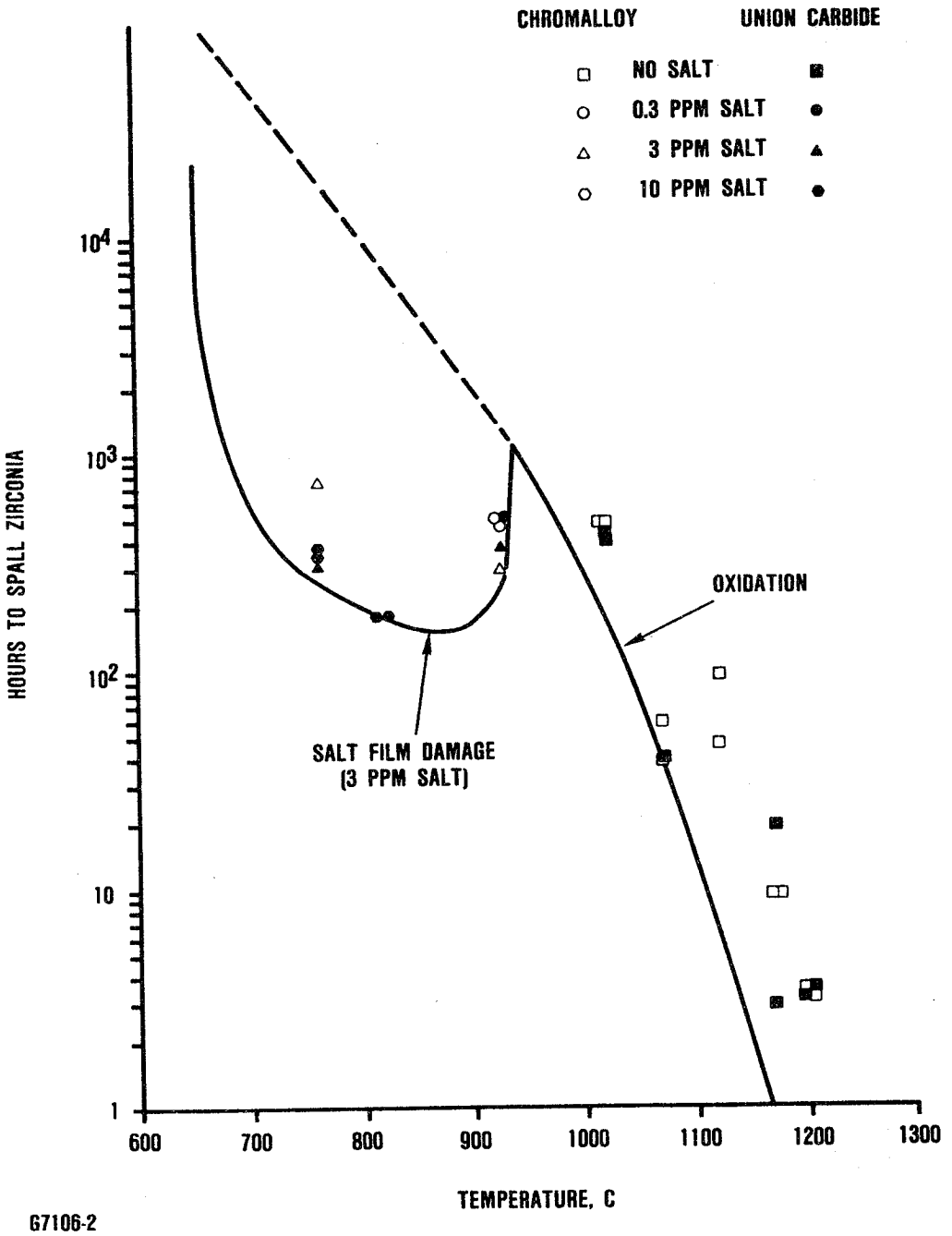

Figure 48. Plasma Spray TBC Life Prediction Model Curves are Forced Through Minimum Life Cyclic Burner Rig Data.

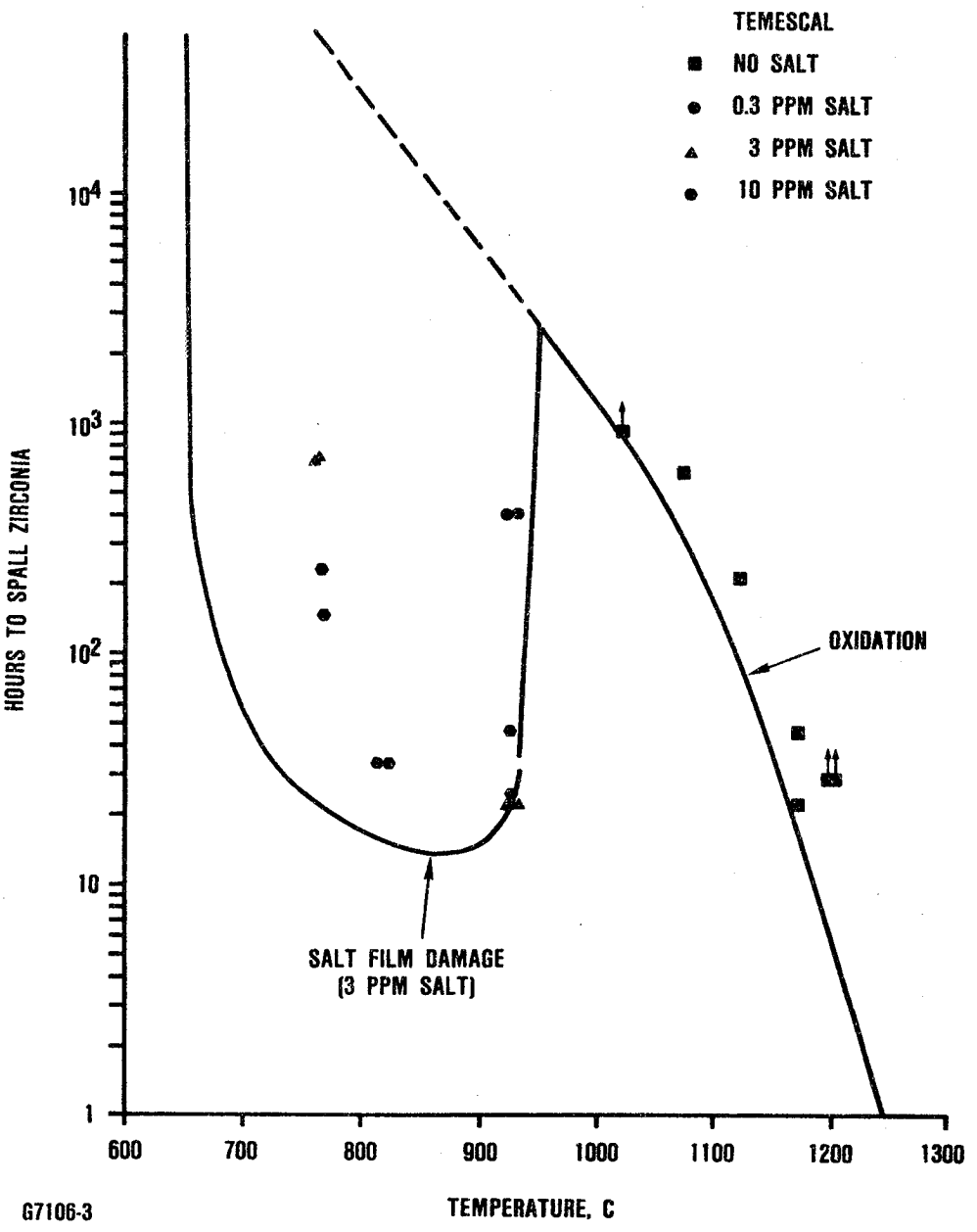

Figure 49. EB-PVD TBC Life Prediction Model Curves are Forced Through Minimum Life Cyclic Burner Rig Data.

Total TBC life is then obtained with the following relationship:

$$\text{TBC life} = \frac{1}{\frac{f1}{MSL_1} + \frac{f2}{MSL_2} + \ldots\ldots + \frac{fn}{MSL_n}},$$

where fi are the time fractions at each mission segment.

In order to evaluate the model's capability to extrapolate the data to turbine engine conditions of interest, parametric studies were conducted to evaluate effects of component temperature, aircraft altitude, and turbine pressure on TBC life. Computer model predictions are provided in Figures 50 and 51, respectively, for the Chromalloy plasma-spray and Temescal EB-PVD TBC systems. Based upon these curves, it is anticipated that TBCs in business aircraft engines, which operate predominately at the higher altitudes, will be dominated by the TBC's oxidation life. In contrast, molten salt film damage of the TBC is expected to be limiting when the aircraft is utilized for maritime surveillance missions.

Component Analyses

The computerized thermochemical life prediction model was used to analyze TBC life on high pressure TFE731 turbine blades for business jet and maritime surveillance mission cycles. These two cycles are identical with the exception that the maritime surveillance aircraft spends 95 minutes of the cruise portion of the mission at an altitude of 0.5 kilometer. These mission cycles and associated TBC life analyses for the Chromalloy plasma-sprayed and Temescal EB-PVD coating systems are provided in Tables 6 and 7. TBC lives are calculated by the computer for each mission point and a total life is calculated using a Miner's Law cumulative damage approach. The following total TBC lives were calculated for the program coatings:

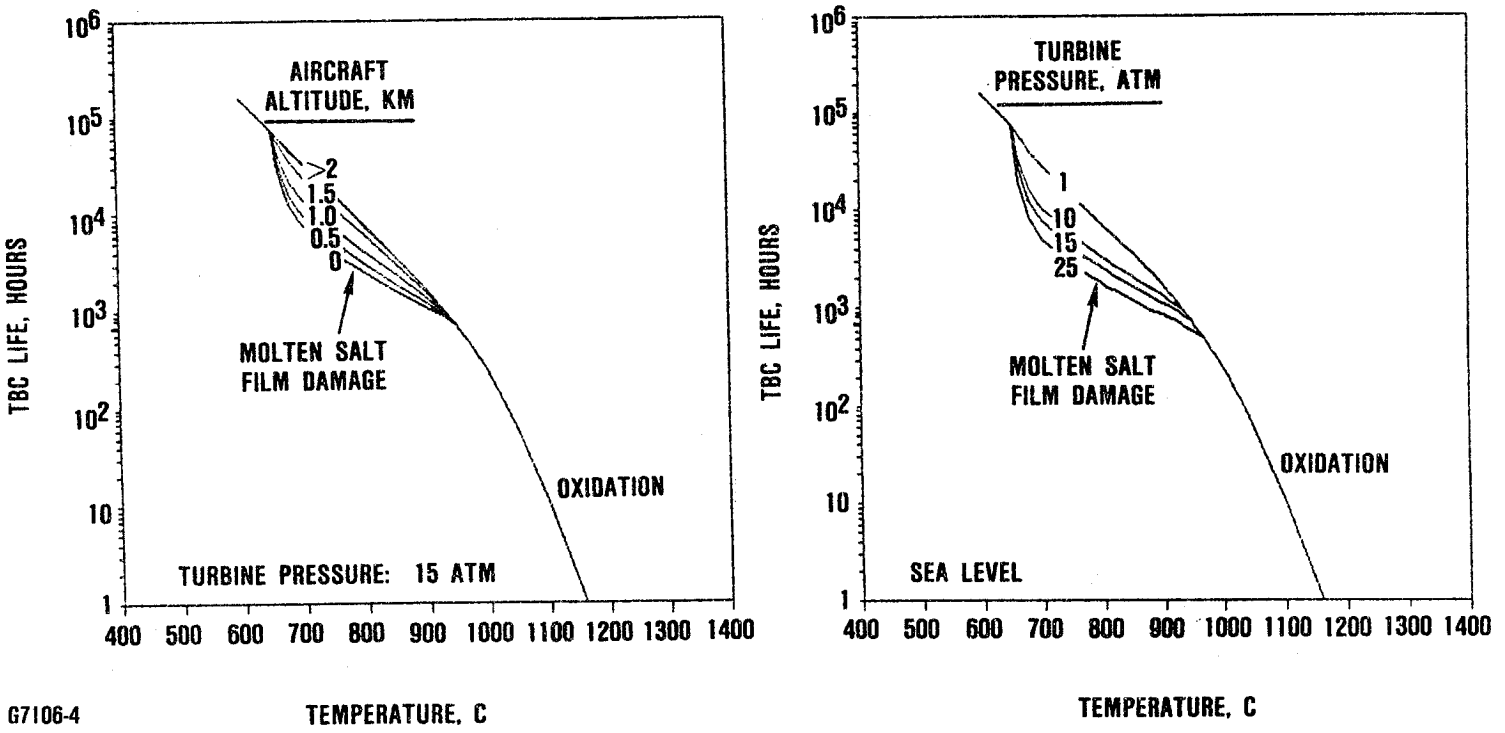

Figure 50. Computer Model Predicts Life of Chromalloy Plasma-Sprayed TBC System as a Function of Engine, Mission, and Materials Parameters.

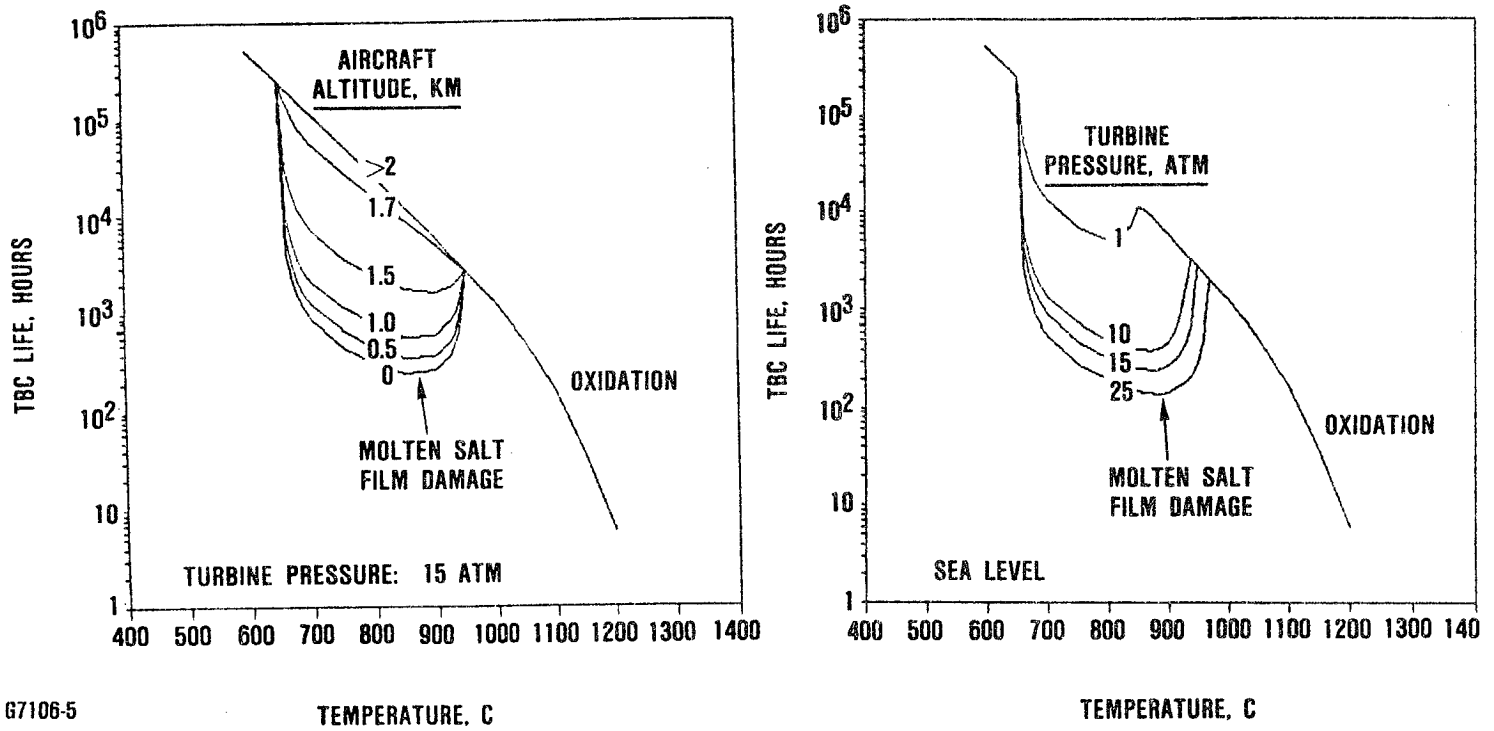

Figure 51. Computer Model Predicts Life of Temescal EB-PVD TBC System as a Function of Engine, Mission, and Materials Parameters.

Table 6. Predicted Lives of the Chromalloy Plasma Spray TBC System Are Dependent on the Engine Mission Cycle.

Business Jet Cycle

Fraction Coastal Takeoffs = 1
Material System = Chromalloy

Mission Segment	Bond Coat Temp., C	Zirconia Temp., C	Pressure, atm	Altitude, km	Time, minutes	*t_i hour	Mission Segment Life, hours
Idle	482	538	1.3	0	5	0.1	564,041
Take-Off	788	871	8.2	6.1	17	0.3	7247
Cruise	760	821	5.4	12.2	135	2.8	17,816
Part Power	760	816	4.4	6.1	30	2.8	17,816
Landing	482	538	1.4	0	5	0.1	564,041

Total Life = 16,517 hours

Maritime Surveillance Mission

Fraction Coastal Takeoffs = 1
Material System = Chromalloy

Mission Segment	Bond Coat Temp., C	Zirconia Temp., C	Pressure, psi	Altitude, km	Time, minutes	t_i, hour	Mission Segment Life, hours
Idle	482	538	1.3	0	5	0.1	564,041
Take-Off	788	871	8.2	6.1	17	0.3	7247
Cruise	760	821	5.4	12.2	20	2.8	17,816
Cruise	760	821	5.4	.5	95	2.8	7720
Cruise	760	821	5.4	12.2	20	2.8	17,816
Part Power	760	821	4.4	6.1	10	2.8	17,816
Landing	482	538	1.4	0	5	0.1	564,041

Total Life = 9843 hours

*The increment of hot time at a specified mission point in hours.

Table 7. Predicted Lives of the Temescal EB-PVD TBC System Are Dependent on the Engine Mission Cycle.

Business Jet Cycle

Fraction Coastal Takeoffs = 1
Material System = Temescal

Mission Segment	Bond Coat Temp., C	Zirconia Temp., C	Pressure, atm	Altitude, km	Time, minutes	t_i hour	Mission Segment Life, hours
Idle	482	538	1.3	0	5	0.1	999,999
Take-Off	788	871	8.2	6.1	17	0.3	24,453
Cruise	760	821	5.4	12.2	135	2.8	60,052
Part Power	760	816	4.4	6.1	30	2.8	60,052
Landing	482	538	1.4	0	5	0.1	999,999

Total Life = 55,607 hours

Maritime Surveillance Mission

Fraction Coastal Takeoffs = 1
Material System = Temescal

Mission Segment	Bond Coat Temp., C	Zirconia Temp., C	Pressure, psi	Altitude, km	Time, minutes	t_i, hour	Mission Segment Life, hours
Idle	482	538	1.3	0	5	0.1	999,999
Take-Off	788	871	8.2	6.1	17	0.3	24,453
Cruise	760	821	5.4	12.2	20	2.8	60,052
Cruise	760	821	5.4	.5	95	2.8	1185
Cruise	760	821	5.4	12.2	20	2.8	60,052
Part Power	760	821	4.4	6.1	30	2.8	60,052
Landing	482	538	1.4	0	5	0.1	999,999

Total Life = 2106 hours

TBC System	Business Jet	Maritime Surveillance
Plasma Spray		
Chromalloy	16,517 hours	9843 hours
Union Carbide	6656 hours	5207 hours
Klock	49,644 hours	29,973 hours
EB-PVD		
Temescal	55,607 hours	2106 hours

Examination of these predicted TBC lives indicates that they are strongly mission-cycle dependent, and that molten salt film damage of the TBC can be significant for aircraft that spend significant time at low altitudes. Fortunately, the majority of business and commercial aircraft spend very little time at low altitudes and long lives are expected.

Lives of EB-PVD coatings are predicted to be very low for the maritime surveillance mission. Based upon research with sputtered zirconia coatings by Prater (ref. 21), it is anticipated that sealing the outer surface of the coating will inhibit this damage mode and permit much longer lives to be achieved. EB-PVD ceramic coatings with dense outer layers, which are resistant to molten salt penetration, are being developed by GTEC in Air Force- (Contract F33615-85-C-5155) and Navy- (Contract N00167-86-C-0097) sponsored programs.

Subsequently, TBC lives on TFE731 HP turbine blades have been computed for the 6-hour factory engine test cycle used for 150-hour endurance tests (Figure 52). Predicted lives were calculated for an engine altitude of 0.3 kilometers (Phoenix) and 2 kilometers (no salt ingestion).

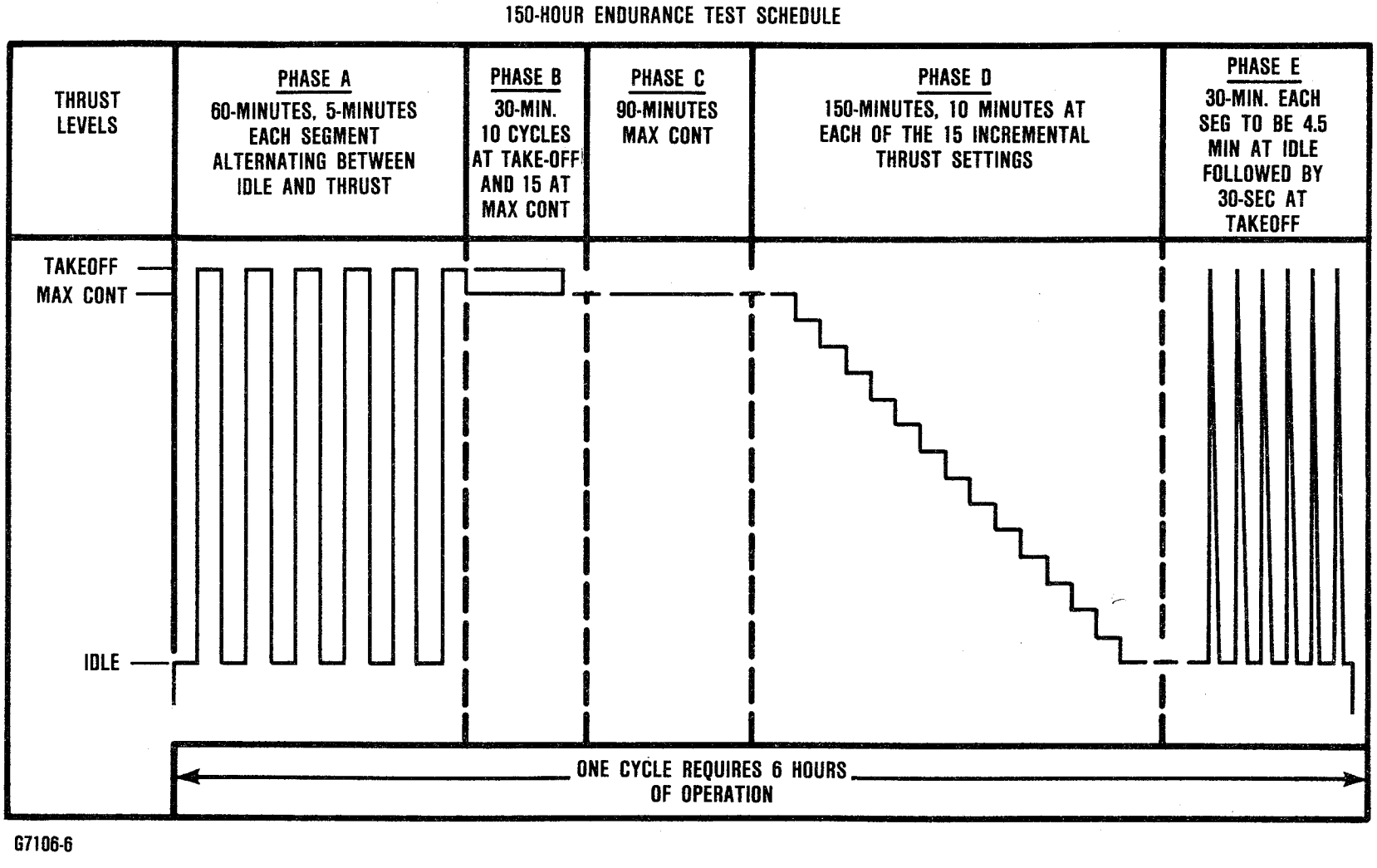

Figure 52. Endurance Test Cycle for TFE731-5 Engine.

TBC System	Predicted TBC Life in Factory Engine Test	
	0.3 km Altitude	2 km Altitude
Plasma Spray		
Chromalloy	1,343 hours	1,429 hours
Union Carbide	561 hours	576 hours
Klock	4,401 hours	4,697 hours
EB-PVD		
Temescal	1,449 hours	5,301 hours

The point-by-point analysis of the life of the Chromalloy and Temescal TBC systems are provided in Tables 8 and 9, respectively. Increased test severity (high temperatures) is associated with reduced TBC lives, relative to those predicted for the business aircraft mission.

5.3 Thermomechanical TBC Life Model

It is thought that more accurate TBC life predictions may result from a finite element-based thermomechanical model designed to provide an accurate description of localized stresses and strains in a TBC system. This model would provide an improved understanding of failure modes interactions and be integrated with appropriate TBC flaw growth data (such as toughness and flaw growth rate) to predict failure. The thermomechanical modeling pursued in this program involved two levels of analysis effort and is illustrated in Figure 3.

In the first level of the analysis effort, a thermomechanical analysis using a design grade coarse 3-D finite element macromodel was performed to achieve the following objectives:

- Identify critical locations for thermochemical and thermomechanical TBC life analyses

Table 8. Predicted Life of Chromalloy Plasma Spray TBC System for TFE731-5 Endurance Test Cycle.

FRACTION COASTAL TAKEOFFS= .000
MATERIAL SYSTEM =CHROMALLOY

Mission Segment	Bond Coat Temp., C	Zirconia Temp., C	Pressure, atm	Altitude, km	Time, minutes	Ti, minutes	Mission Segment Life, hours
IDLE	532.	571.0	1.50	.30	5.0	5.0	266633.6
TAKE-OFF	955.	1040.0	8.06	.30	5.0	5.0	400.1
IDLE	532.	571.0	1.50	.30	5.0	5.0	266633.6
TAKE-OFF	955.	1040.0	8.06	.30	5.0	5.0	400.1
IDLE	532.	571.0	1.50	.30	5.0	5.0	266633.6
TAKE-OFF	955.	1040.0	8.06	.30	5.0	5.0	400.1
IDLE	532.	571.0	1.50	.30	5.0	5.0	266633.6
TAKE-OFF	955.	1040.0	8.06	.30	5.0	5.0	400.1
IDLE	532.	571.0	1.50	.30	5.0	5.0	266633.6
TAKE-OFF	955.	1040.0	8.06	.30	5.0	5.0	400.1
IDLE	532.	571.0	1.50	.30	5.0	5.0	266633.6
TAKE-OFF	955.	1040.0	8.06	.30	5.0	6.5	420.4
TAKE-OFF	955.	1040.0	8.06	.30	1.5	6.5	420.4
MAX. CONT.	921.	1004.0	7.25	.30	1.5	1.5	586.7
TAKE-OFF	955.	1040.0	8.06	.30	1.5	1.5	322.3
MAX. CONT.	921.	1004.0	7.25	.30	1.5	1.5	586.7
TAKE-OFF	955.	1040.0	8.06	.30	1.5	1.5	322.3
MAX. CONT.	921.	1004.0	7.25	.30	1.5	1.5	586.7
TAKE-OFF	955.	1040.0	8.06	.30	1.5	1.5	322.3
MAX. CONT.	921.	1004.0	7.25	.30	1.5	1.5	586.7
TAKE-OFF	955.	1040.0	8.06	.30	1.5	1.5	322.3
MAX. CONT.	921.	1004.0	7.25	.30	1.5	1.5	586.7
TAKE-OFF	955.	1040.0	8.06	.30	1.5	1.5	322.3
MAX. CONT.	921.	1004.0	7.25	.30	1.5	1.5	586.7
TAKE-OFF	955.	1040.0	8.06	.30	1.5	1.5	322.3
MAX. CONT.	921.	1004.0	7.25	.30	1.5	1.5	586.7
TAKE-OFF	955.	1040.0	8.06	.30	1.5	1.5	322.3
MAX. CONT.	921.	1004.0	7.25	.30	1.5	1.5	586.7
TAKE-OFF	955.	1040.0	8.06	.30	1.5	1.5	322.3
MAX. CONT.	921.	1004.0	7.25	.30	1.5	1.5	586.7
TAKE-OFF	955.	1040.0	8.06	.30	1.5	1.5	322.3
MAX. CONT.	921.	1004.0	7.25	.30	1.5	1.5	586.7
TAKE-OFF	955.	1040.0	8.06	.30	1.5	1.5	322.3
MAX. CONT.	921.	1004.0	7.25	.30	1.5	101.5	1339.9
MAX. CONT.	921.	1004.0	7.25	.30	90.0	101.5	1339.9
1	921.	1004.0	7.25	.30	10.0	101.5	1339.9
2	893.	973.0	6.84	.30	10.0	10.0	1309.8
3	865.	942.0	6.43	.30	10.0	10.0	2027.9
4	838.	911.0	6.02	.30	10.0	10.0	2477.2
5	810.	880.0	5.61	.30	10.0	10.0	1900.1
6	782.	849.0	5.20	.30	10.0	10.0	2088.0
7	754.	818.0	4.79	.30	10.0	10.0	2585.9
8	727.	788.0	4.38	.30	10.0	10.0	3410.6
9	699.	757.0	3.96	.30	10.0	10.0	4844.8
10	671.	726.0	3.55	.30	10.0	10.0	7501.7
11	643.	695.0	3.14	.30	10.0	10.0	13435.6
12	615.	664.0	2.73	.30	10.0	10.0	36247.7
13	588.	633.0	2.32	.30	10.0	10.0	131398.5
14	560.	602.0	1.91	.30	10.0	10.0	199984.7
15	532.	571.0	1.50	.30	10.0	14.5	327457.7
IDLE	532.	571.0	1.50	.30	4.5	14.5	327457.7
TAKEOFF	955.	1040.0	7.25	.30	.5	.5	269.1
IDLE	532.	571.0	1.50	.30	4.5	4.5	261448.8
TAKEOFF	955.	1040.0	7.25	.30	.5	.5	269.1
IDLE	532.	571.0	1.50	.30	4.5	4.5	261448.8
TAKEOFF	955.	1040.0	7.25	.30	.5	.5	269.1
IDLE	532.	571.0	1.50	.30	4.5	4.5	261448.8
TAKEOFF	955.	1040.0	7.25	.30	.5	.5	269.1
IDLE	532.	571.0	1.50	.30	4.5	4.5	261448.8
TAKEOFF	955.	1040.0	7.25	.30	.5	.5	269.1
IDLE	532.	571.0	1.50	.30	4.5	4.5	261448.8
TAKEOFF	955.	1040.0	7.25	.30	.5	.5	269.1

TOTAL LIFE = 1343.

Table 9. Predicted Life of Temescal EB-PVD TBC System for TFE731-5 Endurance Test Cycle.

FRACTION COASTAL TAKEOFFS= .000
MATERIAL SYSTEM =TEMESCAL

	Bond Coat Temp., C	Zirconia Temp., C	Pressure, atm	Altitude, km	Time, minutes	Ti, minutes	Mission Segment Life, hours
IDLE	532.	571.0	1.50	.30	5.0	5.0	897870.6
TAKE-OFF	955.	1040.0	8.06	.30	5.0	5.0	1549.8
IDLE	532.	571.0	1.50	.30	5.0	5.0	897870.6
TAKE-OFF	955.	1040.0	8.06	.30	5.0	5.0	1549.8
IDLE	532.	571.0	1.50	.30	5.0	5.0	897870.6
TAKE-OFF	955.	1040.0	8.06	.30	5.0	5.0	1549.8
IDLE	532.	571.0	1.50	.30	5.0	5.0	897870.6
TAKE-OFF	955.	1040.0	8.06	.30	5.0	5.0	1549.8
IDLE	532.	571.0	1.50	.30	5.0	5.0	897870.6
TAKE-OFF	955.	1040.0	8.06	.30	5.0	5.0	1549.8
IDLE	532.	571.0	1.50	.30	5.0	5.0	897870.6
TAKE-OFF	955.	1040.0	8.06	.30	5.0	6.5	1628.4
TAKE-OFF	955.	1040.0	8.06	.30	1.5	6.5	1628.4
MAX. CONT.	921.	1004.0	7.25	.30	1.5	1.5	2099.7
TAKE-OFF	955.	1040.0	8.06	.30	1.5	1.5	1248.5
MAX. CONT.	921.	1004.0	7.25	.30	1.5	1.5	2099.7
TAKE-OFF	955.	1040.0	8.06	.30	1.5	1.5	1248.5
MAX. CONT.	921.	1004.0	7.25	.30	1.5	1.5	2099.7
TAKE-OFF	955.	1040.0	8.06	.30	1.5	1.5	1248.5
MAX. CONT.	921.	1004.0	7.25	.30	1.5	1.5	2099.7
TAKE-OFF	955.	1040.0	8.06	.30	1.5	1.5	1248.5
MAX. CONT.	921.	1004.0	7.25	.30	1.5	1.5	2099.7
TAKE-OFF	955.	1040.0	8.06	.30	1.5	1.5	1248.5
MAX. CONT.	921.	1004.0	7.25	.30	1.5	1.5	2099.7
TAKE-OFF	955.	1040.0	8.06	.30	1.5	1.5	1248.5
MAX. CONT.	921.	1004.0	7.25	.30	1.5	1.5	2099.7
TAKE-OFF	955.	1040.0	8.06	.30	1.5	1.5	1248.5
MAX. CONT.	921.	1004.0	7.25	.30	1.5	1.5	2099.7
TAKE-OFF	955.	1040.0	8.06	.30	1.5	1.5	1248.5
MAX. CONT.	921.	1004.0	7.25	.30	1.5	101.5	4795.3
MAX. CONT.	921.	1004.0	7.25	.30	90.0	101.5	4795.3
1	921.	1004.0	7.25	.30	10.0	101.5	4795.3
2	893.	973.0	6.84	.30	10.0	10.0	4544.9
3	865.	942.0	6.43	.30	10.0	10.0	6929.3
4	838.	911.0	6.02	.30	10.0	10.0	1032.2
5	810.	880.0	5.61	.30	10.0	10.0	278.8
6	782.	849.0	5.20	.30	10.0	10.0	259.1
7	754.	818.0	4.79	.30	10.0	10.0	298.6
8	727.	788.0	4.38	.30	10.0	10.0	380.1
9	699.	757.0	3.96	.30	10.0	10.0	530.8
10	671.	726.0	3.55	.30	10.0	10.0	825.3
11	643.	695.0	3.14	.30	10.0	10.0	1543.3
12	615.	664.0	2.73	.30	10.0	10.0	5387.3
13	588.	633.0	2.32	.30	10.0	10.0	442479.3
14	560.	602.0	1.91	.30	10.0	10.0	673436.8
15	532.	571.0	1.50	.30	10.0	14.5	999999.0
IDLE	532.	571.0	1.50	.30	4.5	14.5	999999.0
TAKEOFF	955.	1040.0	7.25	.30	.5	.5	1042.4
IDLE	532.	571.0	1.50	.30	4.5	4.5	880411.1
TAKEOFF	955.	1040.0	7.25	.30	.5	.5	1042.4
IDLE	532.	571.0	1.50	.30	4.5	4.5	880411.1
TAKEOFF	955.	1040.0	7.25	.30	.5	.5	1042.4
IDLE	532.	571.0	1.50	.30	4.5	4.5	880411.1
TAKEOFF	955.	1040.0	7.25	.30	.5	.5	1042.4
IDLE	532.	571.0	1.50	.30	4.5	4.5	880411.1
TAKEOFF	955.	1040.0	7.25	.30	.5	.5	1042.4
IDLE	532.	571.0	1.50	.30	4.5	4.5	880411.1
TAKEOFF	955.	1040.0	7.25	.30	.5	.5	1042.4

TOTAL LIFE = 1449.

- Verify that the bulk compressive strains in the zirconia layer are within the capability of the TBC system

- Establish boundary conditions for subsequent thermo-mechanical analyses using detailed finite element micro-models for selected critical locations

After the boundary conditions are established for selected critical locations, very detailed finite element micromodels would be constructed to conduct the second level analyses to achieve the remaining objectives:

- Accurately quantify the localized stresses and strains within the TBC system

- Interface the micromodel with appropriate TBC flaw growth data (toughness and flaw growth rate) to predict zirconia spalling

Resources in this program were not sufficient to complete the micromodel development and analysis. Achievements of this task are described in the following paragraphs.

5.3.1 Macromodel Analysis

Steady-state and transient thermal and stress analyses were conducted for TBCed high-pressure turbine blades in Garrett's TFE731-5 turbofan engine using a design grade 3-D macromodel. This model (Figure 3) consisted of a MAR-M 247 metallic blade with internal cooling holes and the TBC system. The TBC system modeled was a plasma-sprayed system consisting of a 0.005 inch-thick bond coating (NiCrAlY) layer and a 0.005 inch-thick zirconia coating

layer, with a smooth interface inbetween. Analyses were carried out via a commercially available general purpose finite element code, ANSYS.

Figure 53 shows a typical temperature distribution over a blade section at the mid-span of the blade at steady-state full power condition of the factory engine test cycle.

Figure 54 shows the temperature and minimum principal stress distributions as a function of time at the leading edge of the mid-span of the blade during the snap acceleration transient period of the factory engine test cycle. The snap acceleration and deceleration transients were analyzed to establish the magnitudes of the in-plane compressive stresses and strains within the zirconia layer. These analyses indicated that the maximum compressive stress, which occurred during the snap acceleration period at 1 second from the beginning of the cycle, was approximately 48 MPa, and the resulting compressive strain was approximately 0.13 percent, which was well within the capability (about 1 percent) of the coating system.

Figure 55 shows a typical TFE731-5 business aircraft engine mission cycle and the maximum bond coating temperatures as a function of the mission time calculated with the finite element macromodel.

Thermal analyses were conducted for business aircraft and factory test engine mission cycles. The resulting temperature distributions were used to predict TBC lives with the thermochemical TBC life model as described in detail in paragraph 5.2.

Although the 3-D finite element macromodel component analysis does not provide an in-depth understanding of the failure mechanisms of the TBC system, it can, when coupled with the preliminary design TBC thermochemical model, give very timely and reasonable estimates of the lives of TBCed engine components.

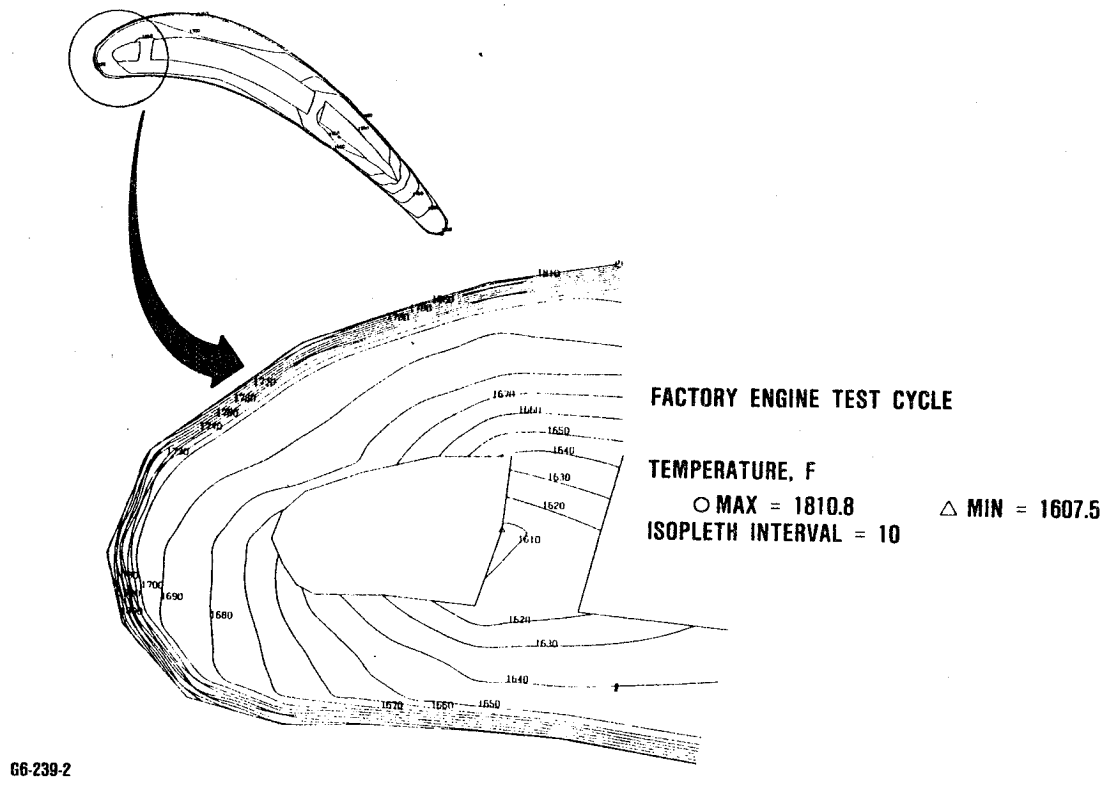

Figure 53. Thermal Analysis of TBC-Coated Blade Has Been Conducted.

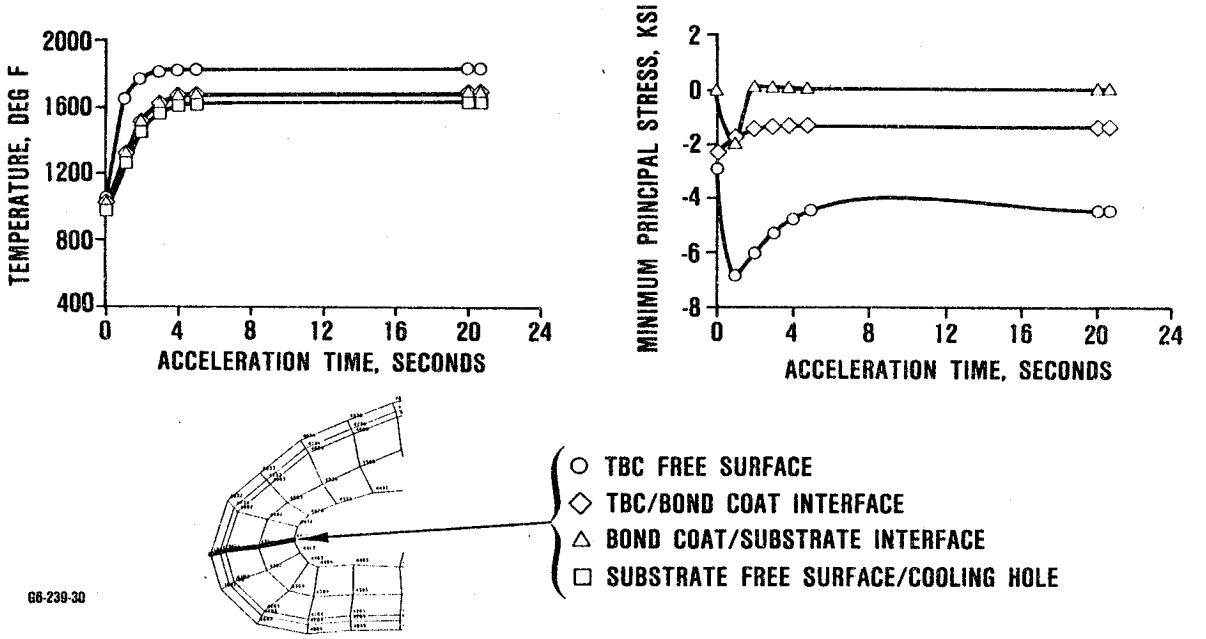

Figure 54. Snap-Cycle Transient Thermal and Stress Analyses Have Been Performed.

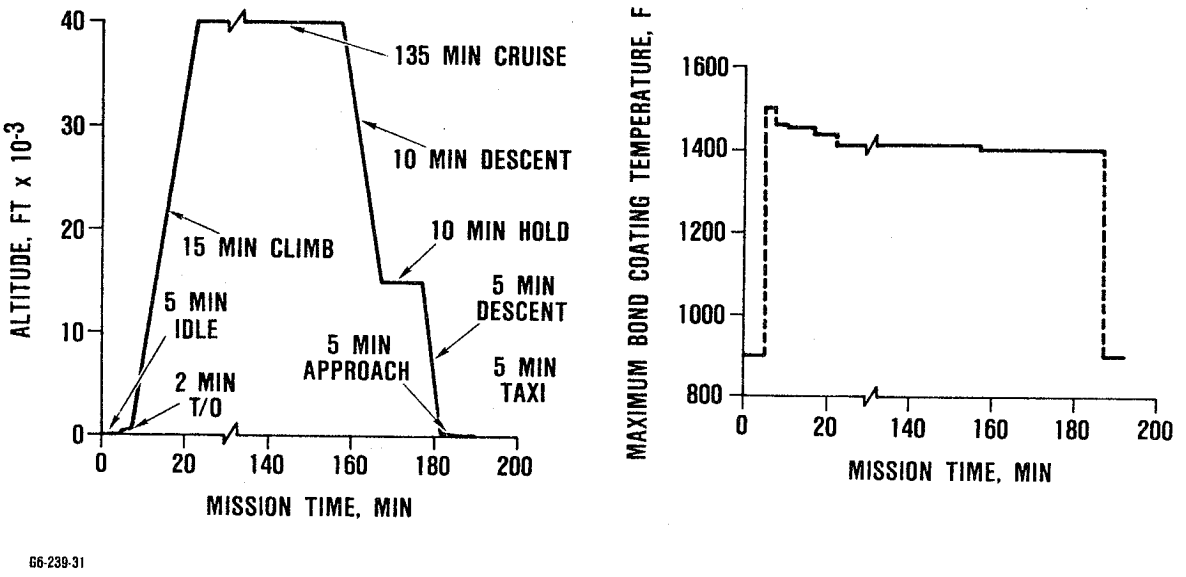

Figure 55. Typical Business Aircraft Mission Cycle Was Used for Bond Coating Oxidation Life Analysis.

5.3.2 Thermomechanical Micromodel Development

The objective of this task was to develop a 3-D finite-element-based micromodel capable of accurately describing the geometries and the material conditions of the TBC system and analyzing the localized stresses and strains in the TBC system. This includes the influences of the rough interfaces between the bond coating and the zirconia coating, internal and interfacial oxidation, and near interfacial flaws.

The interfacial roughness between the bond coating and the zirconia coating was simulated with 3-D repeatable sinusoidal waves evenly spaced at the interface. A thin layer of material was created at the interface to simulate the oxide layer, whose thickness can be changed to simulate its growth. Internal oxidation can be simulated by assigning a group of elements, at the specified locations, the properties of the oxide scale. The oxide growth can be modeled via the oxide kinetics equations developed at NASA. Internal and interfacial flaws can be simulated by disengaging elements or assigning very small density and Young's modulus to the elements at these locations or by inserting crack-tip elements at these locations.

Results from the micromodel can be used to study the influences of the interfacial roughness and the oxide layers on local stresses, strains, and stress intensity factors. This information can be used to calculate the TBC lives using a fracture-mechanics-based flaw growth model. Time and temperature dependent material properties will be required to carry out these analyses.

Figure 3 shows the sequence of the macro- and micro-model development for a TBCed TFE731-5 HPT blade. Figure 56 shows the details of a micromodel.

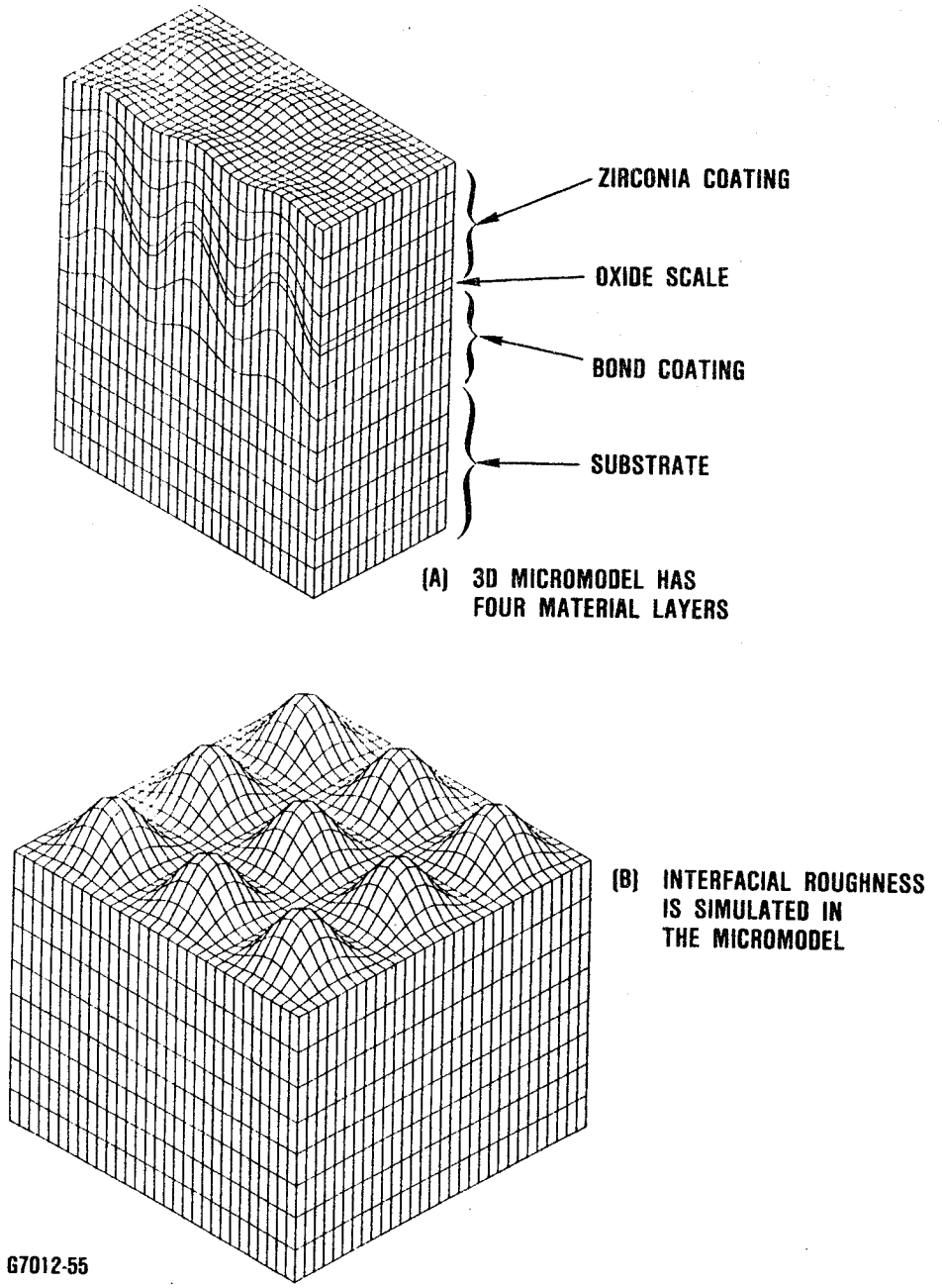

Figure 56. Three-Dimensional Finite-Element Micromodel Incorporates Four Materials and Rough Ceramic-Metal Interface.

At its current state of development the micromodel can be used to calculate local stresses and strains in the TBC system induced by the ceramic/metal thermal expansion mismatch, thermal gradient, residual stresses, centrifugal load, and oxide scale growth. Limited analyses were performed using the micromodel. However, these results are preliminary in nature and are not ready to be reported.

The micromodel is also designed to have sufficient flexibility for planned refinements, such as analysis of:

- Time and temperature dependent changes in local stresses arising from interfacial and internal oxidation of the bond coating
- Stress redistribution associated with bond coating creep
- Zirconia creep and sintering shrinkage
- Cyclic crack propagation in the zirconia layer

A detailed description of the finite element micromodel and the computer program developed to generate the model are provided in Appendix C. With user input of the variables governing the geometry of the TBC system, one can generate the desired local micromodels for the critical locations of the TBCed components. The output from this computer program is in the ANSYS node and element formats, which can be used directly to make ANSYS analysis runs.

It is envisioned that the micromodel development, when completed, will enable one to accurately calculate local stresses, strains and fracture mechanics parameters and gain an in-depth understanding of the failure mechanisms of the TBC system. The logical next step in the TBC life prediction model development would be to develop a fracture mechanics based model utilizing refined local finite element micromodels as the analysis tool. The resulting

thermomechanical model should include the influences of the following parameters on the TBC life:

- Interfacial roughness
- Interfacial and internal oxidation
- Interfacial and internal flaws and porosity
- Residual stresses
- Zirconia sintering shrinkage and creep
- Bond coating creep

6.0 ENGINE TEST

High pressure turbine blades were coated with the program TBC systems applied by Chromalloy, Klock, and Temescal, and were "piggy-back" tested in a TFE731 turbofan test engine (Figure 57). Data from this test was intended to provide data for verification of the TBC life prediction model. The endurance cycle used for most of the 155 hours of this test contained numerous snap-cycles and is shown in Figure 52.

The Chromalloy and Temescal applied TBC systems were in good condition after 155 hours when testing was terminated. In contrast, the Klock-applied TBC system exhibited minor leading edge spalling of the zirconia after 67 hours of testing (Figure 58).

Posttest analysis of the Klock TBC system on the TFE731-5 HP turbine blades revealed that a surface deposit wicked into the strain accommodating porosity and microcracks and densified the zirconia coating (Figure 59). Densification of the zirconia increases both the elastic modulus and stresses within the zirconia layer. This deposit on the blades was rich in silicon, calcium, and aluminum. The chemical composition of the deposit is similar to a sample of cement or dust collected near the test cell (Figure 60). Construction near the test cell was the probable source of cement dust contamination. This indicates that deposits on the TBC are not representative of typical aircraft propulsion engine environments.

ORIGINAL PAGE
BLACK AND WHITE PHOTOGRAPH

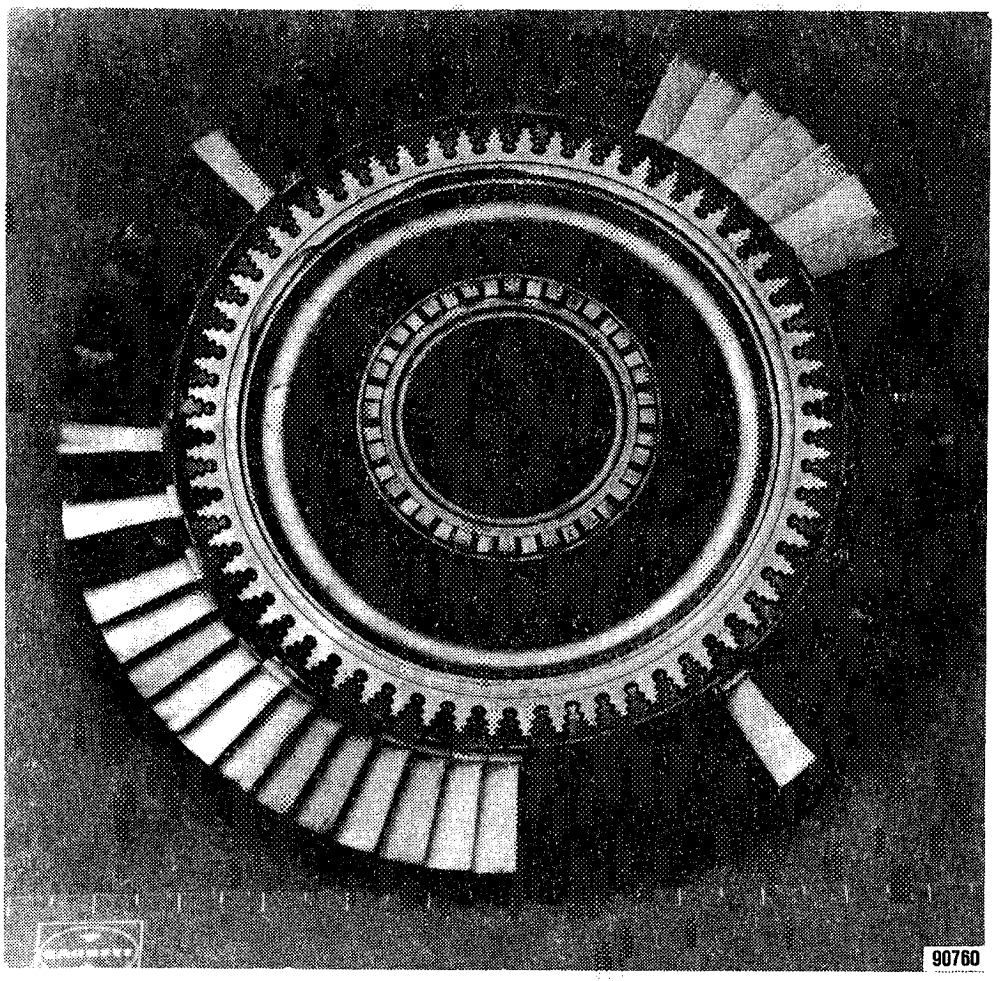

COATING SUPPLIERS

- CHROMALLOY
- KLOCK
- TEMESCAL

G6-239-7

Figure 57. TBC Systems Were Tested in a TFE731-5 Turbofan Engine.

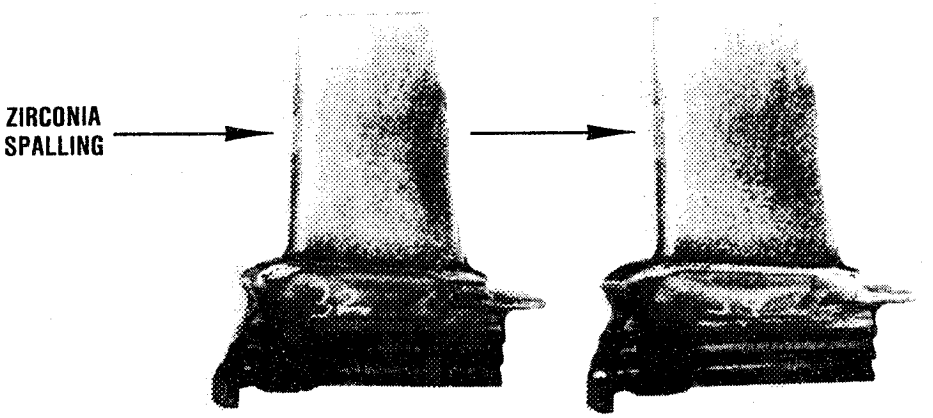

Figure 58. Zirconia Layer of Klock TBC System Spalled In The Center of the Leading Edge of High Pressure Turbine Blades of a TFE731 Engine Test.

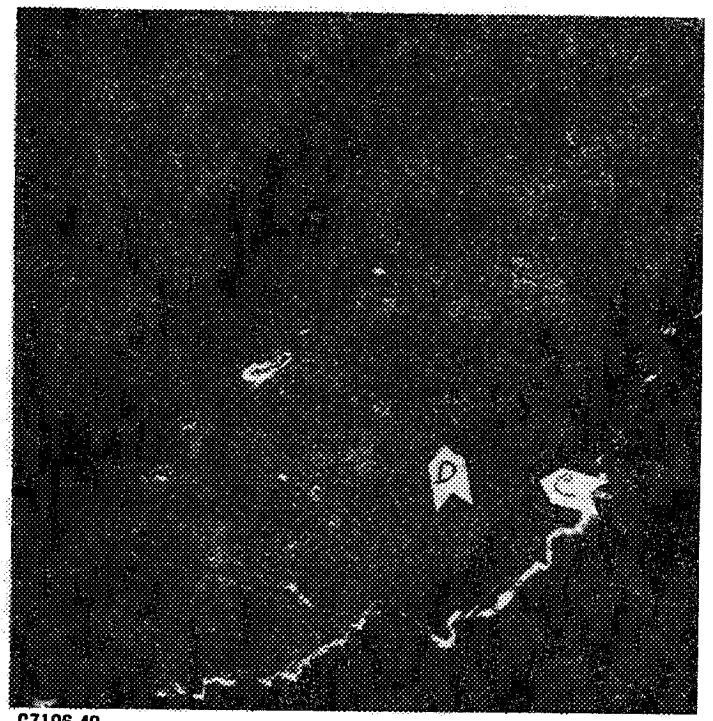

Figure 59. Zirconia Adjacent to the Surface Deposits Was Densified on Klock-Coated TFE731-5 HP Turbine Blades.

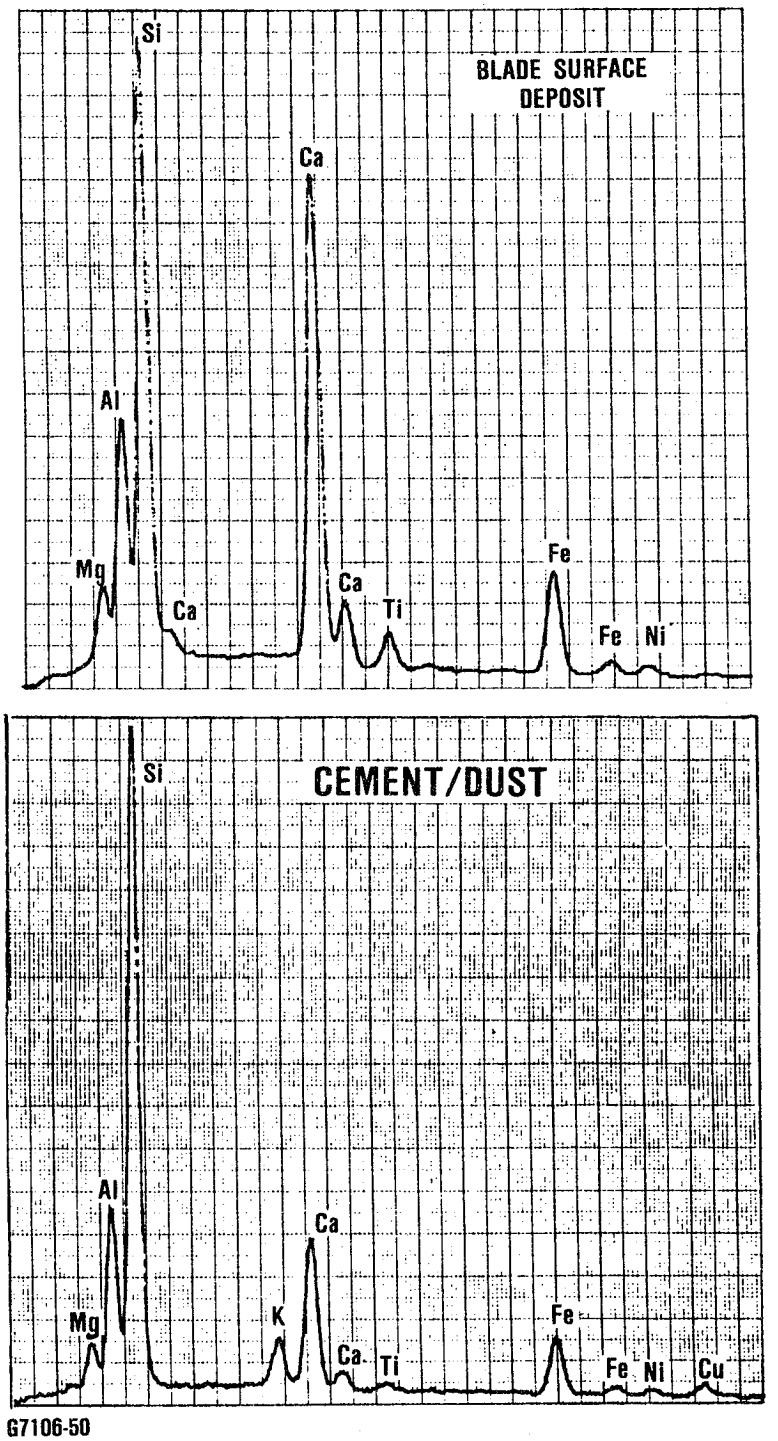

Figure 60. Chemical Composition of Blade Surface Deposit Was Similar to a Sample of Cement or Dust Collected Near GTEC Test Cell.

7.0 SUMMARY AND CONCLUSIONS

GTEC has made signficant contributions to the development of viable prediction methods for TBC life. In particular, this program has resulted in an operational design model, which predicts TBC life as a function of component design, engine mission, and materials system parameters. Major conclusions that may be drawn from this program are indicated below:

- Operative TBC degradation modes include bond coating oxidation, zirconia toughness reduction (associated with sintering densification), and molten salt film damage.

- A thermochemical life model has been developed that predicts TBC durability as a function of component temperature, turbine pressure, and aircraft altitude (salt ingestion). This model has been calibrated with burner rig data obtained for three plasma spray and one EB-PVD TBC systems.

- The thermochemical life model has been interfaced with component design tools and engine mission data to predict plasma-sprayed and EB-PVD TBC lives on TFE731 high-pressure turbine blades for business aircraft, maritime surveillance, and factory endurance test environments.

- A thermomechanical micromodel has been developed to facilitate comprehensive analysis of the stresses within a TBC system. This model can be interfaced with the thermomechanical analysis of a high pressure turbine blade and used to predict local TBC stresses and temperatures.

- The thermomechanical micromodel has been designed to subsequently incorporate time-dependent properties of the TBC system, such as interfacial and internal oxidation and crack propagation.

- Affordable tests have been developed to calibrate thermochemical and thermomechanical TBC life models.

- NDE feasibility was verified for measuring TBC thickness and detecting interfacial flaws.

- Viability of the program TBC systems was confirmed during factory endurance testing of the high pressure turbine blades in a TFE731 turbofan engine.

8.0 RECOMMENDATIONS

While significant progress and success have been achieved in the current program, further improvements in TBCs and life prediction methods are possible. Three areas for further development that merit consideration are:

- Refinement of the thermomechanical micromodel to include computation of time and temperature dependent changes in the TBCs stress state resulting from the following operative mechanisms:
  - Bond-coating stress relaxation
  - Oxidation of the bond coating
  - Constrained sintering shrinkage of the zirconia
  - Cyclic crack growth of near-interface cracks in the zirconia
- Development of less-expensive calibration data requirements for the thermochemical TBC life prediction model should be considered to expedite the development and application of new TBC systems. In particular, zirconia toughness and oxide scale growth data are considerably less expensive to obtain than burner rig data. The possibility of using these alternate tests to calibrate the design model merits consideration.
- Improved TBCs should be developed that emphasize the following characteristics:
  - Dense external surface of the zirconia coating to inhibit salt film penetration
  - Increased bond-coating oxidation resistance
  - Zirconia microstructural stability to inhibit a reduction in toughness

APPENDIX A. TECHNOLOGY ASSESSMENT

1.0 INTRODUCTION

To facilitate development of an experimental plan for TBC life prediction, available literature for coating processing, TBC microstructures composition development, and life prediction were reviewed at the beginning of this program. This review, which was performed in 1984, is presented in the following paragraphs.

1.1 Process-Microstructure Relationships

Two distinct processes have been developed for the application of TBCs to gas turbine components:

- o Plasma Spray
- o EB-PVD

At this stage of development, the plasma-spray process has production status for both combustors and airfoils. In contrast, the EB-PVD process is at an advanced state of development. The following sections review the process-coating microstructure relationships required to achieve viable TBC systems.

1.1.1 Plasma-Sprayed Coatings

The plasma-spray coating process is a form of thermal spray that uses an ionized gas plasma to melt and propel the powdered coating alloy toward the substrate. In this process, a gas mixture is ionized to the plasma state by passing it through a high-intensity electric current. Heat is transferred from the plasma to melt the particles of the injected powdered alloy. Velocity of the plasma can be as high as Mach 2. Powder particles are accelerated by the high velocity plasma and then impacted on the surface of the component to build up the coating.

Plasma-spray factors associated with the degree of particle melting and subsequent particle velocity include the particle size and feed rate, plasma gas composition, electric current strength, and standoff distance to the component. The selection of specific coating parameters depends on the material being sprayed, microstructural requirements, and the equipment design.

The metallic, oxidation-resistant bond coating layer can be applied in either an air environment or a protective atmosphere. The choice is basically dictated by the component metal temperature in service. Application of the oxidation-resistant metallic coating in a low pressure argon environment results in significantly increased oxidation life.

For sheet-metal applications (such as combustors and transition liners), the metal temperature is maintained below about 870C. At these temperatures, air-sprayed NiCrAlY possesses adequate oxidation resistance for long-life applications.

In contrast, turbine airfoils are designed for higher temperature applications above 870C. Consequently, the deposition process should not compromise the oxidation resistance of the bond coating. For this more demanding application, the bond-coating layer is applied using a low pressure plasma spray (LPPS) process in a chamber with a soft vacuum.

The major advantages of LPPS over conventional air plasma spray are better bond strength and oxidation resistance. The better bond strength of LPPS coatings is mainly achieved by the reverse-transfer arc cleaning of the substrate, which removes detrimental base-metal oxides just prior to spraying, and increased substrate temperatures of 870 to 980C, which allow for limited diffusion of the coating into the substrate. In contrast, to avoid excessive oxidation during coating, substrate temperatures in air-plasma spray rarely reach more than 540C.

Ceramic layers of plasma-sprayed TBC systems are typically applied at metal temperatures in the range of 100 to 300C to avoid compressive thermal expansion mismatch stresses, which could buckle the coating (ref. 22). Consequently, mechanical interlocking of the ceramic and metallic layers is the initial adhesion mechanism (Figure 61). Thus, a properly applied TBC system has an (Ni,Co)CrAlY/zirconia interface with a high roughness. This interface provides a tortuous path for cracks to follow, and cracks are forced to propagate within the ceramic layer. On the other hand, if the (Ni,Co)CrAlY layer is improperly applied (relatively smooth), the toughness of the interface is low, and zirconia spalling occurs easily at the interface.

The insulative ceramic layer of thermal barrier coatings is usually applied by air-plasma spray. This is necessary to maintain the chemical balance (stoichiometry) of the zirconia, which can become depleted of oxygen if sprayed in a vacuum chamber.

Strain accommodation has been built into plasma-sprayed TBC systems by incorporating 10 to 15 percent porosity into the coating and by using partially stabilized ZrO_2 compositions that produce a large number of subcritical microcracks (Figures 62 and 63). These modifications reduce the apparent elastic modulus and, therefore, minimize the stress that can develop in the ceramic layer for a given strain level. Both of these strain accommodation mechanisms have contributed to the success of plasma-sprayed TBCs. Porosity can be incorporated into virtually all ceramic-layer compositions of interest. Subcritical microcracking is most readily achieved with zirconia partially stabilized with 6 to 8 percent (by weight) of yttria.

Microcracking is not fully developed, however, in the as-sprayed condition. As indicated in Figure 63, plasma-sprayed yttria partially stabilized zirconia can develop a columnar solidification structure within most of the "splattered" particle layers. Testing

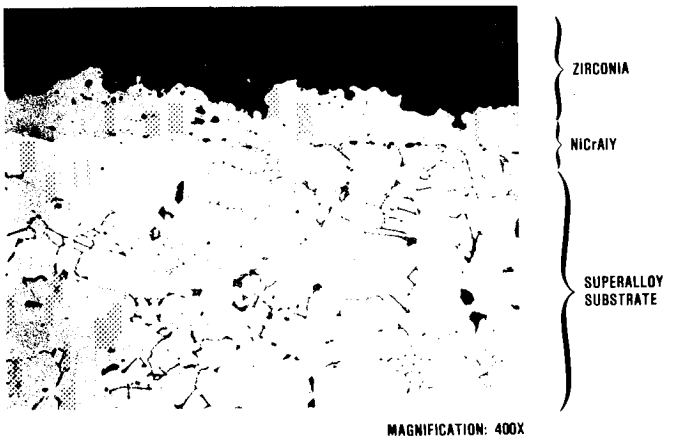

Figure 61. A Ceramic-Metal Interface with High Micro-Roughness Maximizes Ceramic Layer Adhesion in Plasma-Sprayed TBCs.

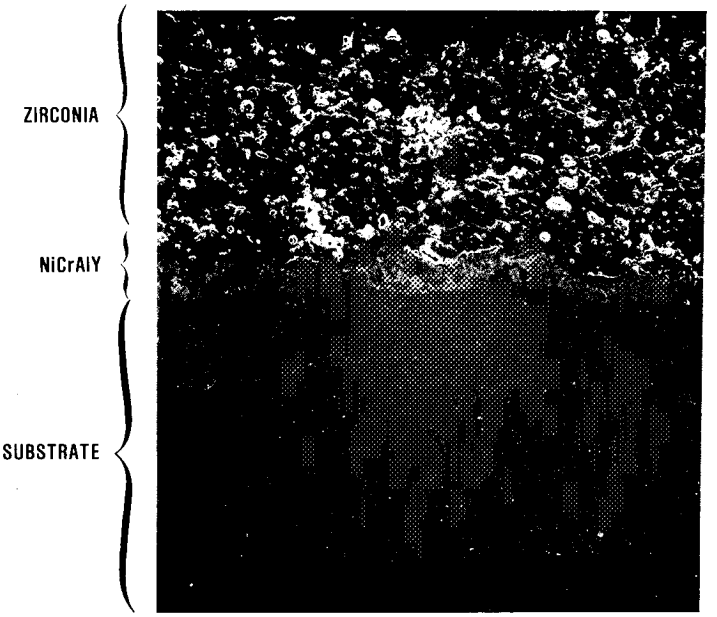

Figure 62. The Zirconia Layer of a Plasma-Sprayed TBC System Contains Microporosity and Subcritical Microcracking to Minimize the Elastic Modulus.

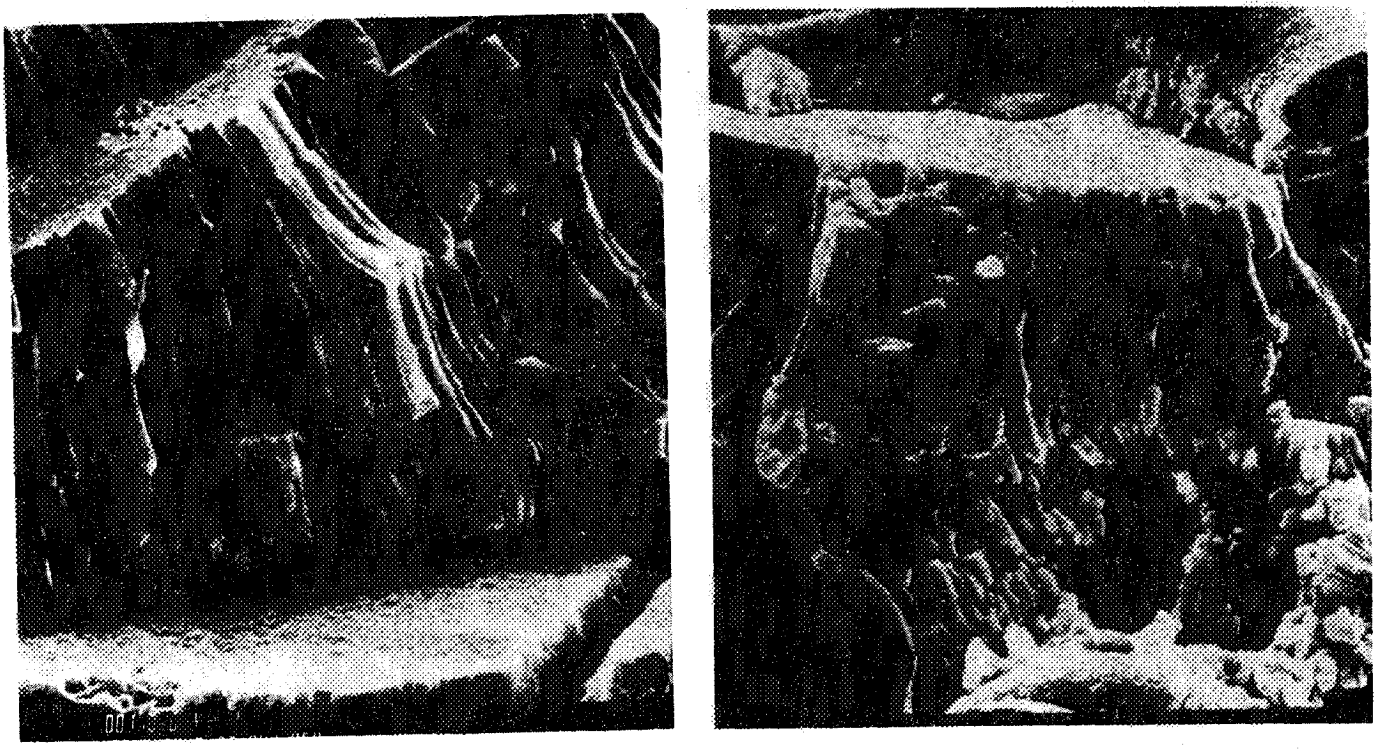

Before Thermal Cycling

After 9000 Oxidation Cycles to 1010°C

Figure 63. Localized Columnar Solidification Microstructure in Plasma-Sprayed Zirconia Coating (Partially Stabilized with Yttria) Becomes Microcracked During Thermal Cycling.

has indicated that thermal cycling is necessary to achieve the majority of the subcritical microcracking of the solidification microstructure. An acoustic emission study indicated that most of the microcracking probably occurs during the initial thermal cycle(s). Once formed, the small intercolumnar gaps in this microstructure are available to accommodate imposed strains by free expansion (or contraction) of the columns into the gaps, which results in minimal stress build-up in the coating.

Published data (ref. 23) indicates that as-sprayed, 8 percent Y_2O_3-stabilized ZrO_2 has tensile and compressive moduli in the 7 to 35 GPa range, which is well below the 154 GPa value for 95 percent dense polycrystalline stabilized zirconia (ref. 24). Following completion of the segmentation of the columnar solidification structure during initial thermal cycling, the elastic modulus of the partially stabilized zirconia may be reduced to well below the levels measured for the as-sprayed coatings.

Acceptable durability of TBCs with strain tolerant microstructures has been thus far limited to relatively mild salt ingestion, mild particulate erosion, and clean fuel environments typical of most aircraft propulsion engine applications. Although zirconia and some other ceramics, such as $ZrSiO_4$, exhibit significant chemical resistance to molten salt attack, thick ceramic coatings will fail mechanically if the salt infiltrates the strain-accommodating porosity and microcracks (refs. 23 and 25). To alleviate this problem for industrial turbine application, NASA has found that laser glazing of the surface of the zirconia can significantly increase durability of TBCs in the presence of molten salt films (ref. 25). Similarly, Westinghouse has reported that thin glass-rich surface layers also inhibit molten salt damage to TBCs (ref. 23).

Finally, it should be noted that the as-sprayed surface of a TBC is substantially rougher [e.g., 6.3μm (250μ inch)] than metallic surfaces. This level of roughness is acceptable on components with

relatively low gas velocities (combustors and transition liners) but adversely affects the aerodynamic performance of turbine blades and vanes. Consequently, airfoils with plasma-sprayed TBCs require some form of media finishing to reduce surface roughness to about 2.5μm (100 μ inch).

1.1.2 EB-PVD Coatings

EB-PVD is the other coating process that has been successfully used to apply TBCs that are viable on gas turbine blades and vanes. Conceptually, this method is a modification of the high-rate vapor deposition process for metallic coatings that has been successfully used to coat millions of turbine airfoils (ref. 26). Power to evaporate the ceramic coating material is provided by a high-energy electron beam gun. Oxygen is also bled into the yttria-stabilized zirconia vapor cloud to minimize any deviations from stoichiometry during coating. This process feature is required since zirconia becomes somewhat oxygen deficient due to partial dissociation during evaporation in a vacuum. Vapor from this cloud condenses onto the turbine airfoil to form the coating.

Unlike the plasma-sprayed TBCs, EB-PVD TBCs achieve maximum durability when applied to a smooth, preferably polished, surface (ref. 27). Consequently, this type of coating depends on a chemical bond for adhesion of the ceramic and metallic layers. Higher deposition temperatures in the 870 to 1090C range and/or postcoating heat-treatments in the 980 to 1090C range are typically used to achieve the required bond quality. Clean surfaces that are free of absorbed gases (e.g., water vapor) and loose oxides are also required to obtain an adequate ceramic-to-metal bond during coating.

Ceramic layer microstructure modification for strain accommodation has been most successful with EB-PVD-applied TBC systems. As shown in Figure 64, the EB-PVD process has the capability of depositing the ceramic layer with a columnar microstructure with

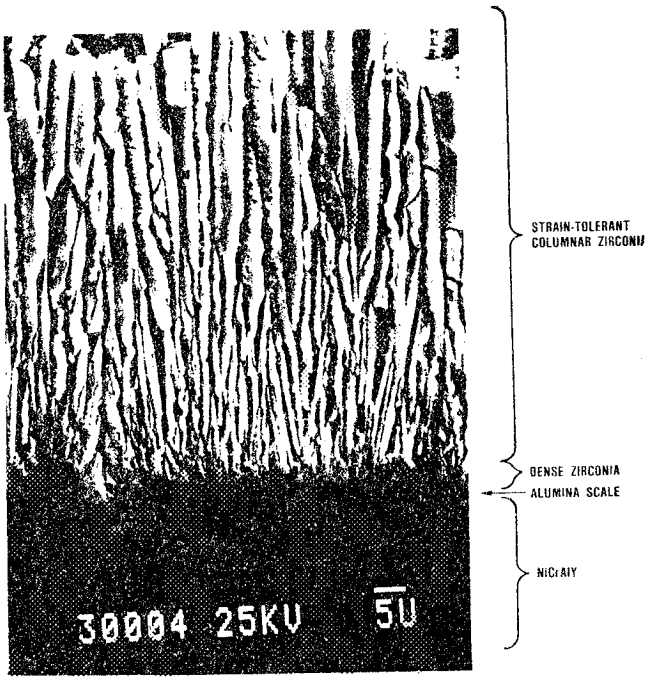

Figure 64. EB-PVD-Applied TBC System Has a Strain-Tolerant Columnar Zirconia Microstructure. (Photograph courtesy of Temescal)

intercolumnar structural discontinuities, which results in negligible stress build-up in the zirconia layer of the coating. To illustrate the success of this approach, NiCoCrAlY + 125μm Y_2O_3 (20 percent weight) stabilized ZrO_2 coatings applied to MAR-M 200+Hf specimens have been burner rig tested to more than 29,000 cycles without failure (cycle: 1010C/4 minutes + forced air-cool/2 minutes) (refs. 27, 28, and 29).

Close inspection of the ceramic-to-metal interface zone of an EB-PVD applied coating (Figure 64) indicates the presence of a thin, dense zirconia layer adjacent to the oxidation inhibiting aluminum oxide scale. This dense layer improves bonding but can develop high compressive stresses during cooling due to the ceramic-metal thermal expansion mismatch. Consequently, thickness of the dense zirconia layer is minimized during deposition to less than about 2 microns to avoid overloading the interface (ref. 26).

The formation of the dense zirconia appears to be associated with the initial deposition of the zirconia in an oxygen-deficient condition, which enhances the development of the bond and the sintering aid effects of transient oxides (e.g., NiO, Cr_2O_3) on the surface of the alumina scale. Once the bond has been established, the oxygen bleed is quickly activated to facilitate the formation of stoichiometric zirconia and the open columnar (low-stress) microstructure.

Erosion resistance of TBC systems is microstructure dependent. A general trend is that denser zirconia coatings are more erosion resistant. Erosion rate data for a medium percent (10 to 15 percent) porosity plasma-sprayed yttria-stabilized zirconia, EB-PVD yttria-stabilized zirconia, and laser-glazed EB-PVD zirconia are illustrated in Figure 65. Inspection of this data indicates TBC erosion rates are strongly dependent on particle impingement angle and surface condition. Some laser-glazed EB-PVD zirconia coatings have exhibited low rates of erosion.

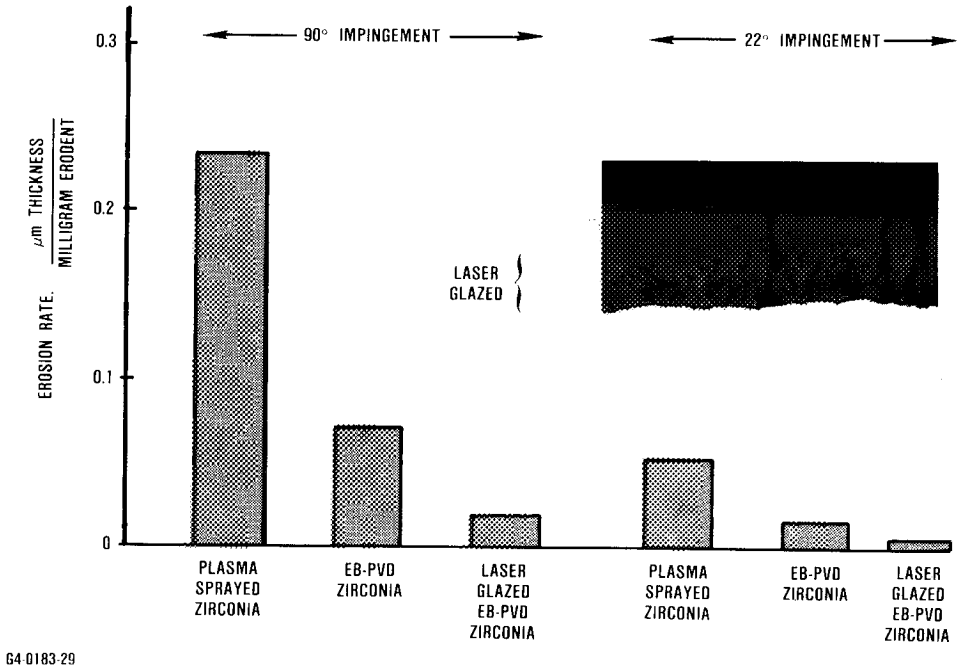

Figure 65. TBC Erosion Rates Are Dependent on Zirconia Microstructure and Impingement Angle.

1.2 TBC Durability and Life Prediction

Durability of a TBC system on gas turbine components in an aircraft engine depends predominantly on the strain tolerance of the ceramic layer, toughness of the ceramic-metal interface, and the oxidation resistance of the metallic bond coating layer.

1.2.1 Thermomechanical Considerations

The effectiveness of the strain-accommodating microstructural features was verified by Sheffler (ref. 6) in spalling strain tests. Both plasma-sprayed and EB-PVD applied TBC systems were reported to have a significant strain-tolerant range (>±1 percent strain) as indicated in Figure 66. Examination of the data indicated that the spalling strains for the plasma-sprayed zirconia were not strongly dependent on thickness or temperature. The strain tolerant range for EB-PVD applied zirconia coatings was also greater than those of the plasma-sprayed system. These data indicate that both plasma-sprayed and EB-PVD yttria-stabilized zirconia coatings can be applied with sufficient strain tolerance for most gas turbine applications.

Fracture toughness of yttria-stabilized zirconia coatings has been estimated using a double cantilever beam (ref. 23), hardness indentation (ref. 30), and modified bond test methods, (ref. 31) (Figure 67). As indicated in Figure 68 for NiCoCrAlY plus EB-PVD yttria-stablized-zirconia coated specimens processed with different conditions, the toughness test provides considerable failure mechanism information in addition to the K_{IC} measurement. The fracture plane, in particular, is clearly identified. Elements present on the fracture surfaces can be quantified by an energy dispersive X-ray (EDX) analysis, and the fractured microstructure can be examined at high magnifications with SEM. Consequently, the weak point(s) in the system can readily be identified, which facilitates the corrective process or composition adjustments. These tests have yielded

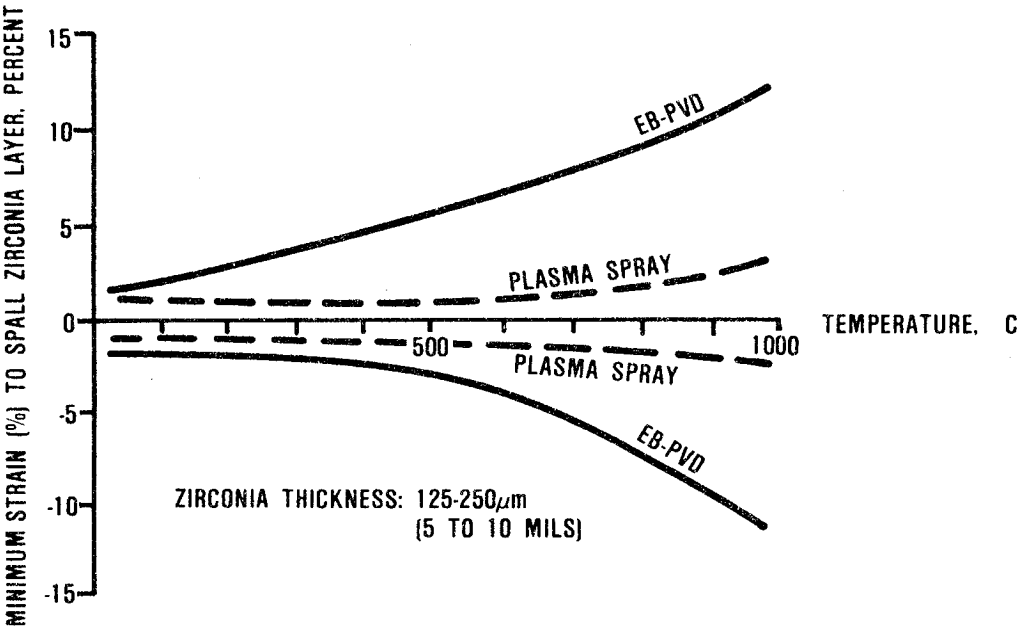

Figure 66. Spalling Strains for Thermal Barrier Coatings Are Dependent on Deposition Process and Zirconia Microstructure.

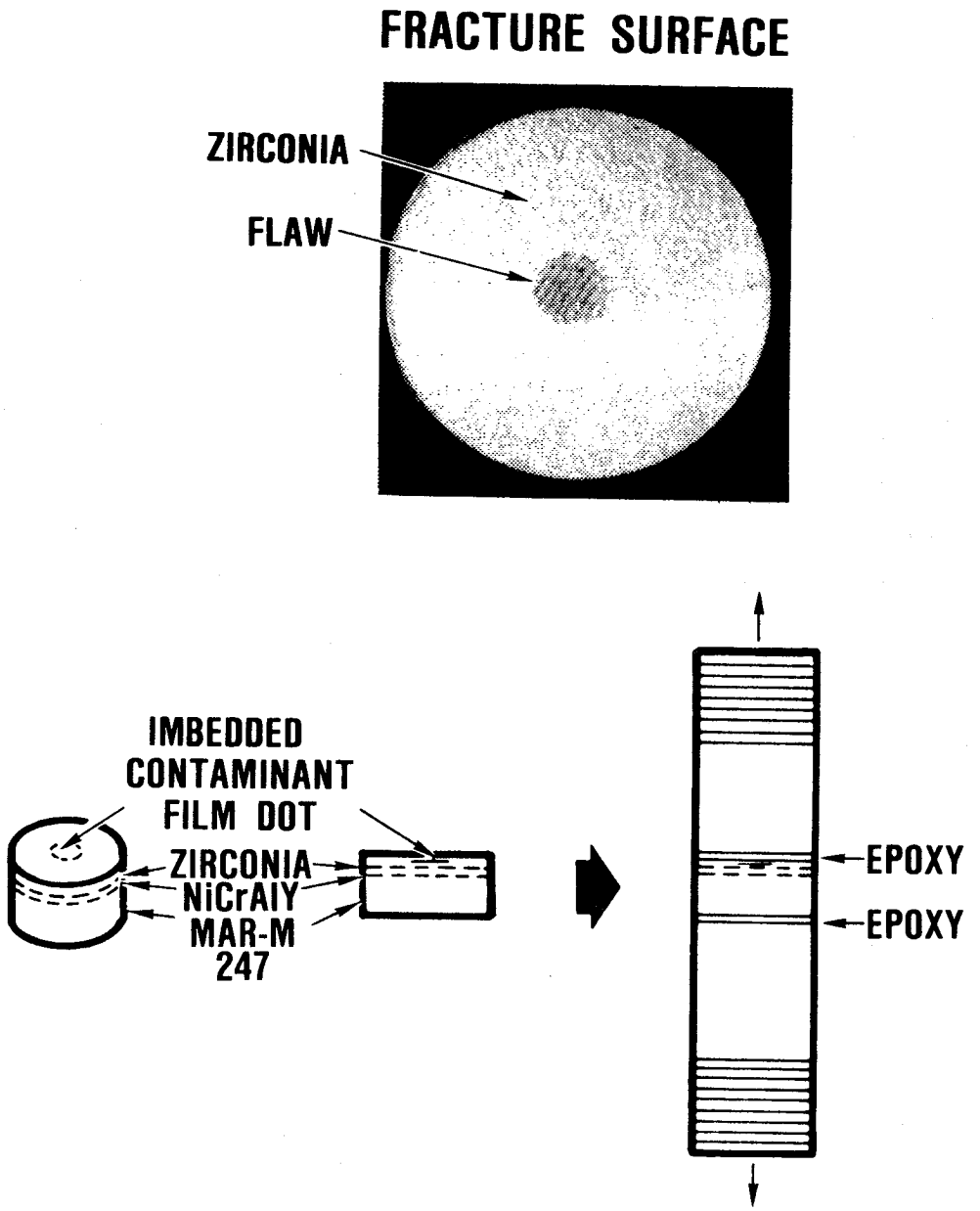

Figure 67. Cohesive and Interfacial Toughness of TBC System Can Be Quantified with Modified Bond Strength Test.

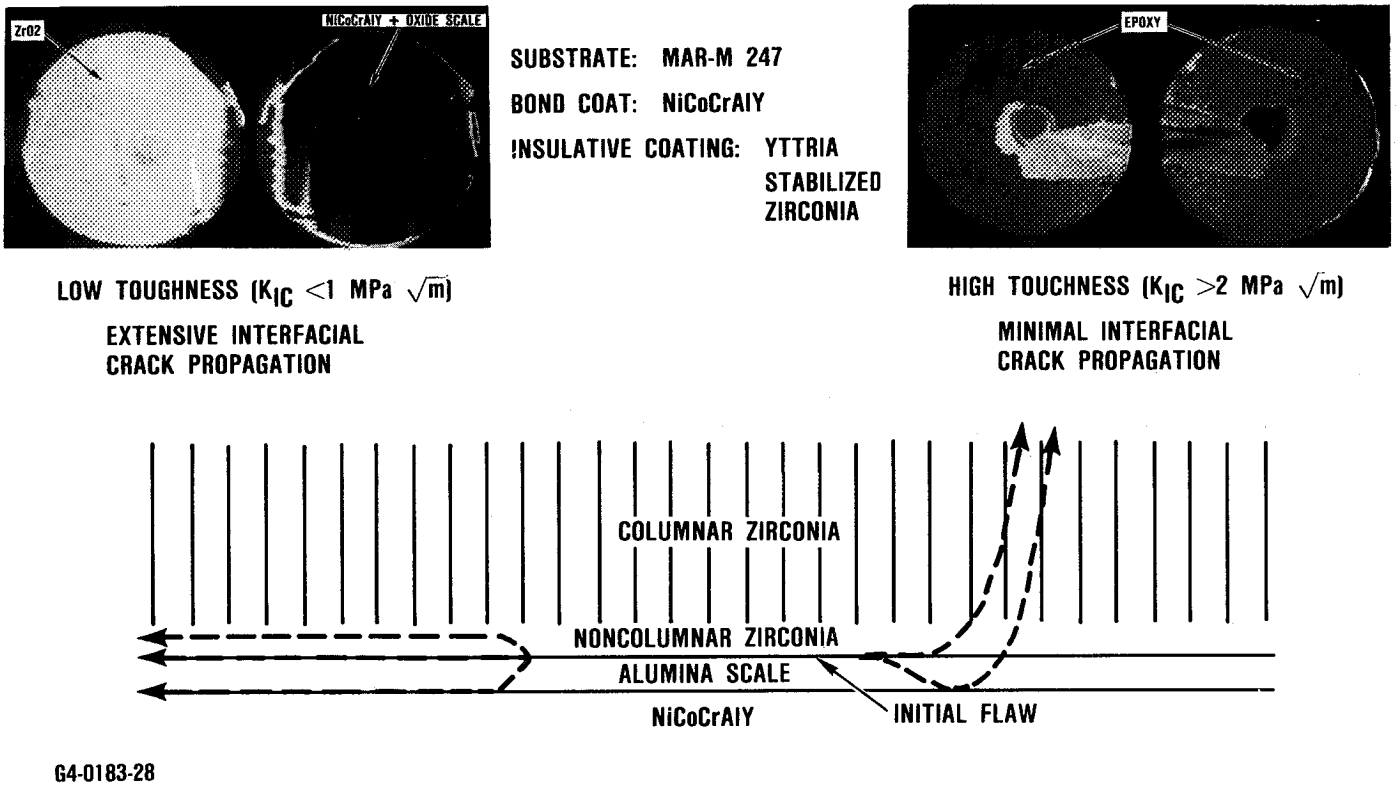

Figure 68. Interfacial Toughness Test Identifies Microstructure Weakness and Quantifies Influence of Process Modifications.

toughness values in the range of 0.5 to 3.2 MPa√m for plasma-sprayed yttria (8 weight percent) stabilized zirconia coatings. Interfacial toughnesses of EB-PVD yttria-stabilized zirconia coatings are also within this range. Toughnesses in this range are sufficient for ceramic coating adhesion (and cohesion) provided that the stresses within the zirconia layer are very low; i.e., achieving the low modulus microstructures is critical to a successful application.

As indicated in Figures 66 and 69, zirconia spalling can be caused by tensile and compressive strains (ref. 6). For TBC-coated components, it has been reported that the most consistent failure mode of the TBC is compressive buckling (refs. 6, 31, and 32).

Zirconia spalling is caused by the complex coating and interface stresses that result from several loading sources. The thermal-mechanical response of the substrate material dominates the coating response. Centrifugal loads and thermal gradients combine to produce a thermal-mechanical response cycle that provides boundary conditions for the zirconia and bond coat response. The coating and interface stresses are further complicated by thermal stresses that develop due to thermal gradients across the coating and the mismatch in thermal expansion between the coating and substrate. The modeling of the coating and interface stresses that drive the failure process requires constitutive data describing the response characteristics of the zirconia, the bond coat, and the substrate. Time-dependent volumetric changes in the coating due to sintering shrinkage and phase transformation can lead to coating-substrate mismatch and additional coating interface stresses.

Andersson, et al., at Westinghouse (ref. 23) have attempted to solve the mechanical problem by developing a fracture mechanics approach to analyze the propagation of interfacial cracks to a critical size. Their analysis indicated that TBCs could be predicted to have satisfactory lives in industrial turbines (operating with clean fuels) with low effective values of the zirconia elastic modulus in the order of 7 to 21 GPa.

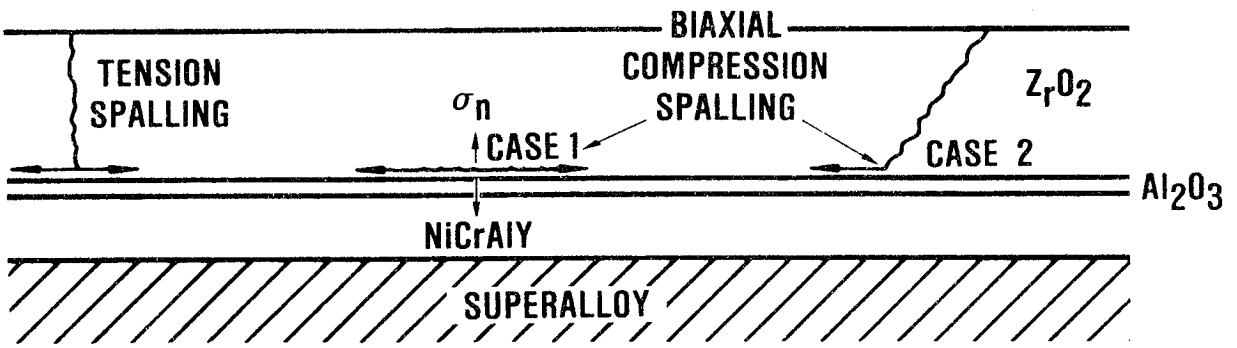

Figure 69. TBCs Have Tensile and Compressive Mechanical Failure Modes.

Measured cyclic crack growth rates parallel to the ceramic-metal interface had a large exponential dependence on the stress intensity factor:

$$\frac{da}{dN} = 153.4\ \Delta K_I^{17.3}$$

where da/dN is the cyclic crack growth rate and ΔK_I is the stress intensity factor in MPa$\sqrt{m}$ for a crack propagating parallel to the interface. For stresses normal to the interface less than 5.5 MPa, lives in excess of 10^4 cycles could be calculated. For slightly higher stresses above 9.0 MPa, one-cycle failures were predicted. (Residual stresses, which can be beneficial (ref. 22) were not considered in this Westinghouse analysis.)

The magnitude of the exponent on the cyclic crack growth rate relationship may preclude reliable fracture mechanics analyses of stable crack growth. If this is the case, the flaw sensitivity of TBCs will require a critical stress intensity factor criterion.

It should be noted that the Andersson analysis is an extension of an earlier TBC life analysis by McDonald and Hendricks (ref. 33). Both of these analytical models assumed that mechanical damage occurred during heat-up in the first few seconds of each cycle. Miller and Lowell (ref. 34) tested that hypothesis and concluded that heat-up stresses in a Mach 0.3 burner rig were insufficient to spall a good coating unless oxidation-induced crack growth occurred during prior thermal cycles. Very high heat flux tests conducted by Miller and Berndt (ref. 35) also showed that a good coating will not fail on heating unless there has been considerable preoxidation. Prior to this program, however, the possibility of reducing the fracture toughness of a good zirconia coating to significantly lower values as a function of exposure time and temperature has not been investigated. An Andersson type analysis is expected to be valid for TBC systems with low fracture toughness.

1.2.2 Thermochemical Considerations

For TBC systems with adequate strain tolerance, oxidation or molten salt film damage becomes the life-limiting factor (refs. 31 and 36). Since the zirconia layer is virtually transparent to oxygen, oxidation resistance is provided by the metallic coating layer. Compositions of these coatings are tailored to form thin, adherent, aluminum oxide scales at the boundary between the metallic and ceramic coating layers. This alumina layer grows very slowly and inhibits additional oxidation.

Spalling failures are induced by the kinetics of the breakdown of the oxidation-resistant metallic coating layer and its protective alumina scale. This should not be interpreted to mean that cracking or crack propagation is absent in strain-tolerant TBCs. Spalling necessarily involves the propagation of cracks. The primary difference between strain-tolerant and nonstrain-tolerant TBCs is that the kinetics of crack propagation are controlled by oxidation (time and temperature) in strain-tolerant TBCs. The following two examples illustrate this conclusion.

For plasma-sprayed TBCs, breakdown of the oxidation-resistant bond coating frequently occurs at the high points. One possibility is that when the alumina scale breaks down, other faster growing metallic oxides (e.g., NiO) are produced with additional oxidation. The volumetric expansion of these oxidation products propagates microcracks in the ceramic layer by a wedge open loading mechanism as indicated in Figure 70. On subsequent heating, the ceramic layer is thermally isolated from the substrate by the crack. Rapid heating of the unbonded ceramic region results in rapid thermal expansion, which further propagates the microcracks until buckling and spalling occur (refs. 31 and 34).

For EB-PVD coatings with open columnar microstructures, the stresses on the ceramic-metal interface are primarily dependent on

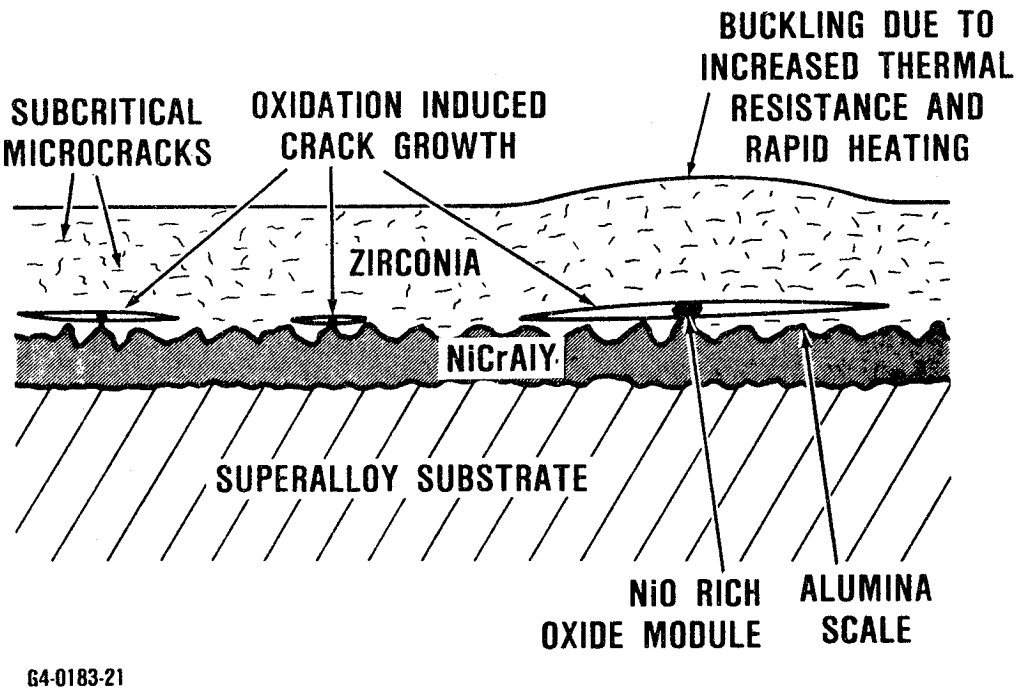

Figure 70. Oxidation-Induced Spalling in Plasma-Sprayed TBC.

the thickness of a thin, dense ceramic layer adjacent to the metallic layer surfaces (ref. 26). The alumina scale, which increases in thickness as a function of time and temperature in an oxidizing environment, is included in the dense ceramic layer thickness that loads the ceramic-metal interface (e.g., by ceramic-metal thermal expansion mismatched stresses). Consequently, alumina scale growth will eventually result in ceramic-layer stresses sufficient to overload the interface or sustain crack propagation in the dense ceramic layer adjacent to the interface.

Although both TBC failure mechanisms described have mechanical attributes, the failure rates are controlled by oxidation and, consequently, are time- and temperature-dependent.

Available data in the literature indicates that the oxidation resistance of TBCs applied by the EB-PVD process can be somewhat better than those applied by plasma-spray processes (refs. 6, 28, 29, and 31). Figure 71 illustrates this conclusion with the best literature data reported to date as a function of bond coating temperature. The slopes extrapolating the temperature dependence are based on experience with metallic coating oxidation. Other variables that affect TBC life are cycle frequency (ref. 36) and bond coating thickness.

One reason for the differences in oxidation resistance is attributable to the plasma-sprayed TBCs requirement for a rough ceramic-metal interface to achieve an adherent, mechanically interlocked TBC system. The very rough ceramic-metal interface significantly increases the surface area requiring protection, compared to the smooth interface of EB-PVD coatings.

Another factor affecting the durability of plasma-sprayed TBCs is the quality of the metallic bond coating layer. In particular, spraying the bond coat in air results in significant oxidation of the aluminum and other reactive elements such as Hf, Y, and Zr,

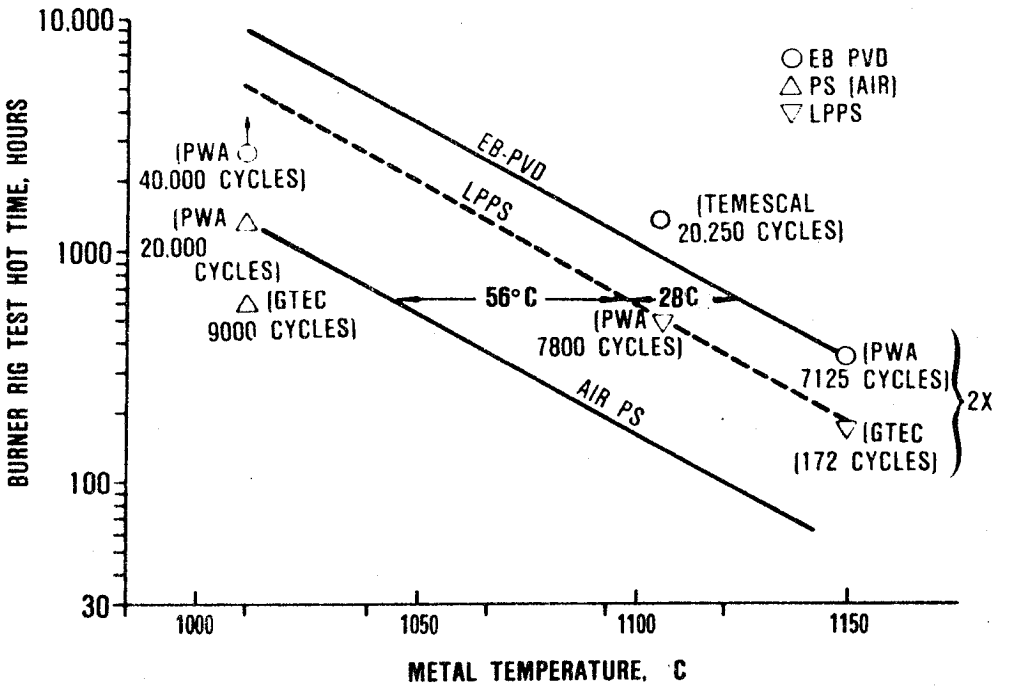

Figure 71. TBC Application Process and Temperature Affect the Oxidation Life of the Bond Coating.

which facilitate adhesion of the alumina scale at the ceramic-metal interface. Consequently, as shown in Figure 71, application of the bond coating layer in the relatively clean low-pressure argon environment of the LPPS process can significantly increase oxidation resistance.

To be a viable mission analysis and design tool, thermochemical life prediction models must predict coating durability as a function of engine, mission and materials system factors. GTEC has developed a mechanistic model (Figure 72) which predicts oxidation and hot corrosion life of metallic coatings in terms of metal temperature, fuel quality, aircraft altitude (salt ingestion), turbine pressure and velocity (ref. 13). Computer-generated coating lives for a diffusion aluminide coating are provided in Figure 73 to illustrate the capability of the model.

A similar approach is anticipated in the development of a thermochemical model for TBC life. In steady-state burner rig tests, simulating industrial turbine conditions, TBC failure conditions have been successfully correlated as a function of condensate melting points and dew points (ref. 37). Although hot corrosion attack of the zirconia is not expected to be significant in an aircraft engine environment, molten salt film induced mechanical damage is of concern for some mission environments. Therefore, a salt-film damage function of temperature, pressure, and altitude (salt ingestion) is expected to be incorporated into a thermochemical life model for TBCs. The anticipated shape of the TBC life model is shown in Figure 74.

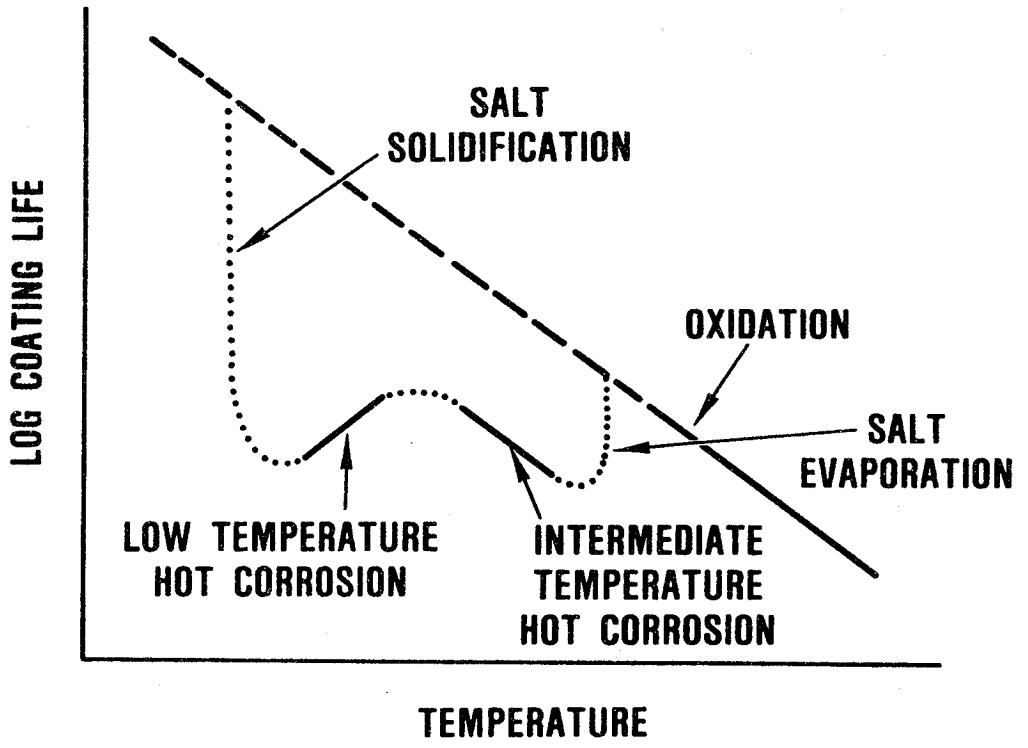

Figure 72. Environmental Life Model Incorporates Two Modes of Hot Corrosion and Oxidation.

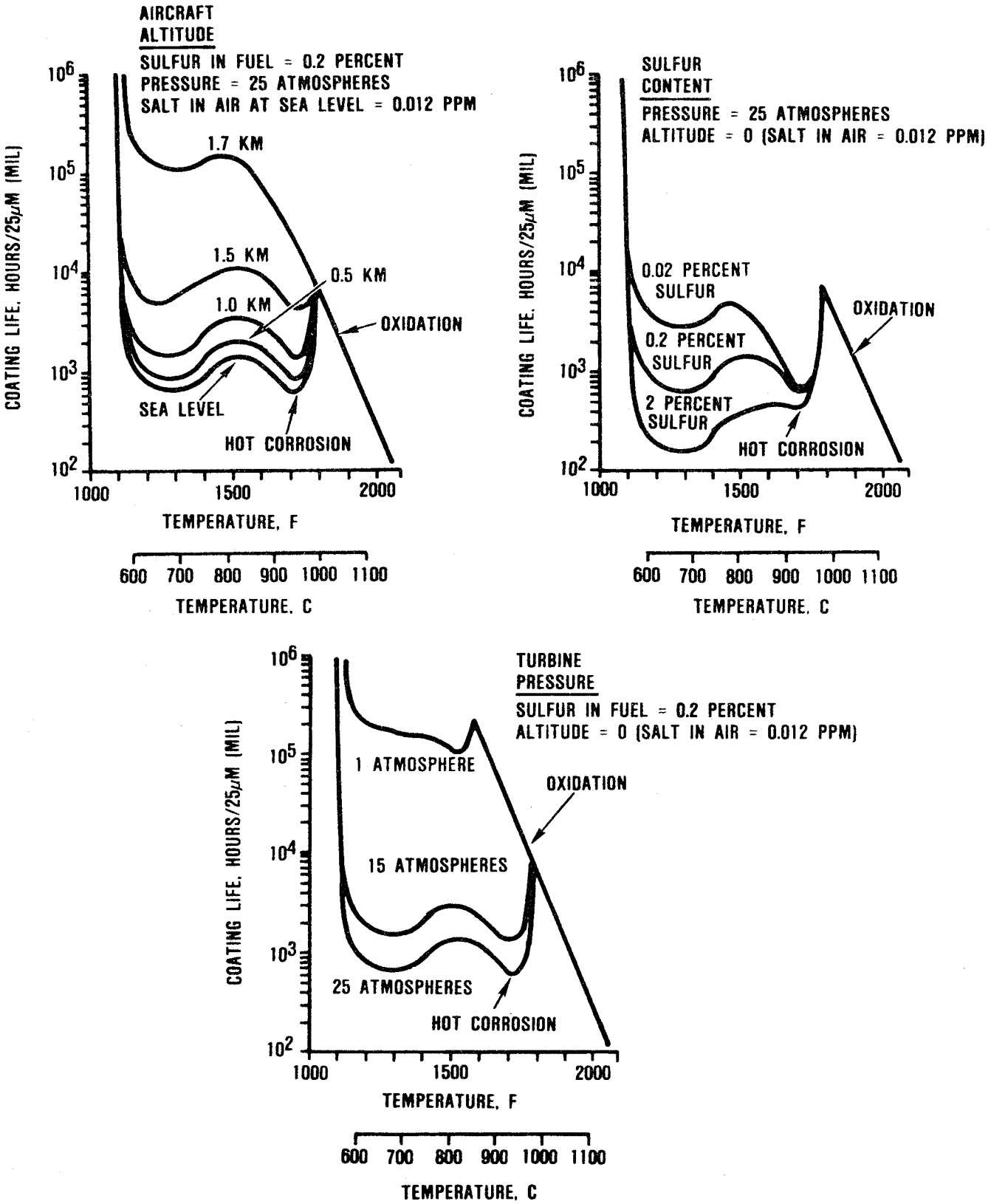

Figure 73. Diffusion Aluminide Coating Life Is Predicted By a Computer Model.

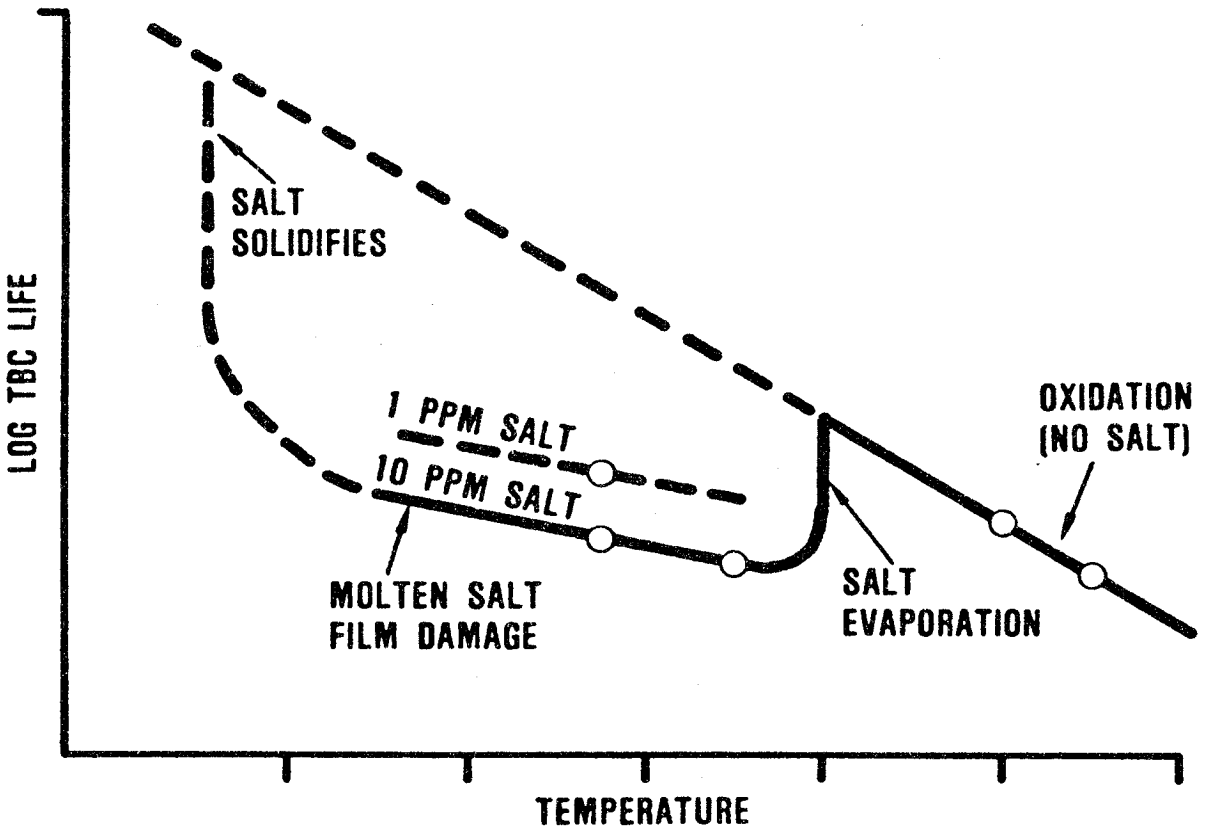

Figure 74. Anticipated Thermochemical TBC Life Prediction Model Will Have Oxidation and Molten Salt Film Damage Modes.

APPENDIX B. TBC LIFE PREDICTION MODEL (TBCLIF.FOR)

The following program was developed at GTEC as a method of quickly predicting the life of a component coated with TBC. It is presented here in VAX VMS FORTRAN77. The program is interactive and provides results to the screen and to a user-defined file. The user I/O required is presented below, and the program with sample input and output is on the following pages:

- o Input
  - **Duty Cycle File**: A text file containing relevant data for the program. A sample is included at the end of the program.
  - **Interactive Input**: Fraction of power at coastal takeoff.

    Choose a material supplier from Klock, Chromalloy, Union Carbide, Temescal

    Give a total time of duty cycle.
- o Output
  - **Results File**: The results file contains the input information plus the predictions for mission segment life and total life. File is echoed to the screen during execution.

```
C-----------------------------------------------------------------------------
       PROGRAM TBC Life Prediction
C
       CHARACTER ANS*1
C
       WRITE(6,900)
       IFLAG = 1
 10    CALL CORR(IFLAG)
       IFLAG = 2
       WRITE(6,900)
       WRITE(6,979)'DO YOU WANT TO PROCESS ANOTHER FILE?(Y/N) '
       READ '(A)',ANS
       IF(ANS .EQ. 'Y')GOTO 10
       WRITE(6,900)
C
       CLOSE(2)
       STOP
 900   FORMAT(/80('*')/)
 979   FORMAT(1X,A,1X,$)
       END
C
CXXXXXXXXXXXXXXXXXXXXXXXXXXXXXXXXXXXXXXXXXXXXXXXXXXXXXXXXXXXXXXXXXXXXXXXXXX
C
       SUBROUTINE CORR(IFLAG)
C
C THIS SUBROUTINE IS THE CORE OF THE PROGRAM
C IT TAKES DUTY CYCLE DATA (SEE END OF PROGRAM) AND
C PREDICTS LIFE OF A TBC SYTEM DUE TO SALT FILM DAMAGE.
C
       DOUBLE PRECISION LIFE,MTBREF
       CHARACTER FNAME*25,TITLE*50,TEMP*50,TITLE1*50,TITLE2*20
       CHARACTER CC*1,LL*10,FORM1*30,FORM2*30,TEMP2*20,TFNAME*30
       CHARACTER MATL*30,MATC*30,ANS*9
C
       DIMENSION C1A(4),C2A(4),BRCFA(4),MTBREF(4),LL(7),MATL(4)
C
C DATA STATEMENTS
C
       DATA ITIME/0/
       DATA MATL/' KLOCK',' CHROMALLOY',' UNION CARBIDE',' TEMESCAL'/
       DATA LL/'  TBOND   ','  TTBC   ','   P     ','   ALT   ',
     +'  TIME   ','   TF    ','   LIFE   '/
       DATA C1A/26.0,25.3,25.3,26.3/
       DATA C2A/61.5,59.0,59.0,62.3/
       DATA BRCFA/1190,383,383,34/
       DATA MTBREF/1.0,0.67,0.27,0.83/
C
       ITIME = 1
C
C GATHER THE NECESSARY INFORMATION FROM THE USER:
C
       WRITE(6,*)'1:  CALCULATE TOTAL LIFE'
       WRITE(6,*)'2:  CALCULATE SEVERAL UNRELATED LIVES'
       WRITE(6,*)
       WRITE(6,979)'WHICH TYPE OF CALCULATION DO YOU WANT? '
       READ(5,*)MPN
C
       WRITE(6,*)'PLEASE ENTER THE TITLE FOR YOUR REPORT (< 50 CHARS)'
       WRITE(6,901)
```

```
        WRITE(6,979)'==> '
        READ(5,905)TITLE1
C
        WRITE(6,*)
 50     WRITE(6,*)'WHAT FRACTION OF THE TOTAL NUMBER OF TAKEOFFS ARE'
        WRITE(6,979)'FROM A COASTAL LOCATION? '
        READ(5,*)CST
        IF(CST .GT. 1)THEN
          WRITE(6,*)'---- THAT IS NOT A FRACTION, TRY AGAIN ----'
          WRITE(6,*)
          GOTO 50
        END IF
C
 51     WRITE(6,*)
        WRITE(6,979)'ENTER TOTAL CYCLE TIME IN MINUTES ==> '
        READ(5,*)TTIME
        WRITE(6,*)'----------------------------------------'
        WRITE(6,*)'1:  KLOCK            3:  UNION CARBIDE'
        WRITE(6,*)'2:  CHROMALLOY       4:  TEMESCAL'
        WRITE(6,*)
        WRITE(6,979)'PLEASE ENTER THE SUPLIER ==> '
        READ(5,*)ISUPLI
        IF(ISUPLI .LT. 1 .OR. ISUPLI .GT. 4)GOTO 51
C
C GET DATA FOR CHOOSEN SUPLIER
C
        C1 = C1A(ISUPLI)
        C2 = C2A(ISUPLI)
        BRCF = BRCFA(ISUPLI)
        TBR = MTBREF(ISUPLI)
        MATC = MATL(ISUPLI)
        LMATC = INDEX(MATC,'  ')
        LMATC = LMATC - 1
C
C
C GET DUTY CYCLE FILE
C
        ASSIGN 811 TO IERROR
        WRITE(6,900)
 811    WRITE(6,979)'ENTER THE FILE NAME OF YOUR DUTY
     +CYCLE FILE ==> '
        READ(5,905)FNAME
        OPEN(1,FILE=FNAME,STATUS='OLD',ERR=999)
C
        IF(IFLAG .NE. 2)THEN
          WRITE(6,*)
          WRITE(6,979)'ENTER THE FILE NAME FOR YOUR OUTPUT
     + FILE ==> '
          READ(5,905)FNAME
          OPEN(2,FILE=FNAME,STATUS='UNKNOWN',ERR=999)
C
          WRITE(6,*)
          WRITE(6,979)'HOW MANY LINES PER PAGE FOR YOUR PRINTER? '
          READ(5,*)NUMLIN
        END IF

C
C START WRITING REPORT TO THE SCREEN THEN TO THE OUTPUT FILE (2)
C
        ICT = 0
```

```
        WRITE(6,'(1H1)')
        WRITE(6,210)TITLE1(:N1)
        WRITE(6,2)CST,MATC(:LMATC)
        WRITE(6,6)
        WRITE(6,3)LL
        WRITE(6,6)
C
        WRITE(2,'(1H1)')
        WRITE(2,210)TITLE1(:N1)
        WRITE(2,12)CST,MATC(:LMATC)
        WRITE(2,16)
        WRITE(2,17)
        WRITE(2,13)LL
        WRITE(2,17)
        WRITE(2,16)
C
C READ DUTY CYCLE FILE
C
        COAST = 0.25 + (0.75*CST)
C
 100    SSP = SSDF
        SHEDP = SHED
        DP = D
        FP = F
C
        READ(1,1,END=300,ERR=989)TITLE2,TB,TC,P,ALT,TI,TF
        IF(MPN .EQ. 2)SRF = 0.0
C
C QUERRY USER FOR CONTINUE AFTER EVERY 12 LINES
C
        ICT = ICT + 1
        IF(MOD(ICT,23) .EQ. 0)THEN
          WRITE(6,979)'HIT CARIAGE RETURN TO CONTINUE ==> '
          READ(5,905)ANS
        END IF
C
C PUT NEW PAGE AND TITLE EVERY numlin LINES
C
        IF(MOD(ICT,NUMLIN) .EQ. 0)THEN
          WRITE(2,16)
          WRITE(2,'(1H1)')
          WRITE(2,*)TITLE1
          WRITE(2,12)CST,MATC(:LMATC)
          WRITE(2,16)
          WRITE(2,17)
          WRITE(2,13)LL
          WRITE(2,17)
          WRITE(2,16)
        END IF
C-----------------------------------------------------------------------
C CALCULATE LIFE
C-----------------------------------------------------------------------
C
C SET UP SOME CONSTANTS
C
        F = TI/TTIME
        TBOND = TB
        TTBC = TC
        TB = TB + 273
        TC = TC + 273
```

```
      ALTM = ALT
      PM = P
C
      AFOO = TF**.25
      BFOO = (-.015*TB) + C1
      CFOO = (-.041*TB) + C2
      DFOO = TBR*(AFOO + .181)
      EFOO = 1/EXP(BFOO)
      FFOO = 1/EXP(CFOO)
      OX = DFOO/(EFOO + FFOO)
C
      FM = 1
      IF(TC .LT. 1157.0)FM = (TC-923)/234
      IF(TC .LE. 923.0)FM = 0
C
      GFOO = .012 - (.007*ALT)
      X = (9.0*GFOO)/(2.0 - GFOO)
      IF(X .LT. 0.0)X = 0.0
      IF(X .GT. 1.0)X = 1.0
C
      HFOO = (0.0276*TC) - 45.54
      VAP = 4.0E5*EXP(HFOO)
      A = P*GFOO/10.0
C
      SSDF = 0.0
      IF(A .GT. VAP)SSDF = (1-X)*(A-VAP)
C
      PI = 0.2*P
      SHED = 0.0
      IF(PI .GT. VAP)SHEDP = ((0.2*P) - VAP)*X
C
      IF(ICT .NE. 1)THEN
        D = FP*(SSP+SHEDP)+ DP - (F*VAP)
        IF(D .GT. 0.0)THEN
          SRF = D*FM
        ELSE
          SRF = 0.0
        END IF
      END IF
C
      SSS = (SSDF+SHED+SRF)*FM
      SFDL = 0.0
      IF(SSS .NE. 0.0)SFDL = COAST*BRCF/SSS
C
      LIFE = 0.0
      IF(SFDL .GT. 2000000.0)SFDL = SFDL - 1
      IF(OX .GT. 2000000.0)OX = OX - 1
C
      IF(SFDL .NE. 0.0 .AND. OX .NE. 0.0)THEN
        OFOO = 1.0/OX
        PFOO = 1.0/SFDL
        LIFE = 1.0/(OFOO+PFOO)
      ELSE
        IF(OX .EQ. 0)LIFE = SFDL
        IF(SFDL .EQ. 0)LIFE = OX
      END IF
C
      IF(LIFE .GT. 1000000.0)LIFE = LIFE - 1
C
      SUM1 = SUM1 + F
```

```
        SUM2 = SUM2 + (F/LIFE)
C
C WRITE RESULTS OF CALCULATIONS TO SCREEN AND UNIT 2
C
        WRITE(3,*)TITLE2,TBOND,TTBC,PM,ALTM,TI,TF,LIFE
        WRITE(6,4)TITLE2,TBOND,TTBC,PM,ALTM,TI,TF,LIFE
        WRITE(2,14)TITLE2,TBOND,TTBC,PM,ALTM,TI,TF,LIFE
C
C READ ANOTHER DUTY CYCLE
C
        GOTO 100
C
C-------------------------------------------------------------------------
C PROGRAM COMES HERE DUTY CYCLE FILE IS DONE BEING READ
C-------------------------------------------------------------------------
C
C CALCUTLATE OVERAL TOTAL LIFE
C
 300    TLIFE = 999999.0
        IF(SUM2 .NE. 0.)TLIFE = SUM1/SUM2
        IF(MPN .EQ. 1)THEN
          WRITE(6,*)'------------------------------'
          WRITE(6,5)TLIFE
          WRITE(2,16)
          WRITE(2,15)TLIFE
        END IF
        WRITE(2,16)
C
C GO BACK TO MAIN PROGRAM
C
        CLOSE(1)
C
        RETURN
C-------------------------------------------------------------------------
C                        FORMAT STATEMENTS
C-------------------------------------------------------------------------
C READ FORMAT
 1      FORMAT(A20,6F10.0)
C TEXT WRITE FORMATS
 2      FORMAT(/8X,'FRACTION COASTAL TAKEOFF',T44,'= ',
     +F8.3/18X,'MATERIAL SYSTEM',T40,'=',A/)
 3      FORMAT(1X,22X,A8,5(A7),A9)
 4      FORMAT(1X,A22,F8.1,5(F7.1),F9.1)
 5      FORMAT(1X,'  TOTAL LIFE = ',F8.0,T101)
 6      FORMAT(1X,60('-'))
C OUTPUT FILE FORMATS
 12     FORMAT(/18X,'FRACTION COASTAL TAKEOFF',T44,'= ',
     +F8.3/18X,'MATERIAL SYSTEM',T40,'=',A/)
 13     FORMAT(11X,'I',22X,'I',A9 ,'I',5(A8,'I'),A10,'I')
 14     FORMAT(11X,'I',A22,'I',F8.1,' I',5(F7.1,' I'),F9.1,' I')
 15     FORMAT(11X,'I  TOTAL LIFE = ',F8.0,T101,'I')
 16     FORMAT(11X,'I',88('-'),'I')
 17     FORMAT(10X,' I',22X,'I',9X,'I',5(8X,'I'),10X,'I')
 199    FORMAT(10X,E11.4)
 210    FORMAT(20X,A)
C
C TERMINAL I/O STUFF
C
 901    FORMAT(' ==> ',50('X'))
 905    FORMAT(A)
```

```
 900     FORMAT(/80('*')/)
 979     FORMAT(1X,A,1X,$)
C
C NOFILE AND BAD FILE SUBROUTINE CALLERS
C
 999     CALL NOFILE(FNAME)
         GOTO IERROR
 989     CALL BADFOR(FNAME)
         GOTO IERROR
         END
C
CXXXXXXXXXXXXXXXXXXXXXXXXXXXXXXXXXXXXXXXXXXXXXXXXXXXXXXXXXXXXXXXXXXXXXXX
         SUBROUTINE NOFILE(FILNAM)
C
C THIS SUBROUTINE JUST BEEPS THE USER AND TELLS HIM HIS FILE
C CAN NOT BE FOUND
C
         CHARACTER FILNAM*24,BEEP*1
         BEEP = CHAR(7)
         LFIL = INDEX(FILNAM,'  ')
         LFIL = LFIL - 1
         WRITE(6,900)
         WRITE(6,*)BEEP
         WRITE(6,1000)FILNAM(:LFIL)
         WRITE(6,*)BEEP
         WRITE(6,900)
         RETURN
 900     FORMAT(80('*'))
 1000    FORMAT(15X,'*****  FILE OPENING ERROR  *****'//10X' THE
     +INPUT FILE <',A,'> CAN NOT BE FOUND'//23X,'PLEASE TRY AGAIN')
         END

C
CXXXXXXXXXXXXXXXXXXXXXXXXXXXXXXXXXXXXXXXXXXXXXXXXXXXXXXXXXXXXXXXXXXXXXXX
         SUBROUTINE BADFOR(FILNAM)
C
C THIS SUBROUTINE JUST BEEPS THE USER AND TELLS HIM HIS FILE
C CAN NOT BE READ PROPERLY
C
         CHARACTER FILNAM*24,BEEP*1
         BEEP = CHAR(7)
         LFIL = INDEX(FILNAM,'  ')
         LFIL = LFIL - 1
         WRITE(6,900)
         WRITE(6,*)BEEP
         WRITE(6,1000)FILNAM(:LFIL)
         WRITE(6,*)BEEP
         WRITE(6,900)
         RETURN
 900     FORMAT(80('*'))
 1000    FORMAT(15X,'*****  FILE READING ERROR  *****'//8X' AN ERROR
     + WAS INCOUNTERED WHILE READING FILE <',A,'>'/23X,
     +'PLEASE TRY AGAIN')
         END

C
CXXXXXXXXXXXXXXXXXXXXXXXXXXXXXXXXXXXXXXXXXXXXXXXXXXXXXXXXXXXXXXXXXXXXXXX
C
C        EXAMPLE FILES|||||||||||||||
C
```

```
C-------------------------------------------------------------------------
C
C DUTY CYCLE INPUT FILE:
C
C FORMAT IS (A20,6F10.0)
C
C MISION PART          BOND       TBC        P         ALT        TIME     HOT TIME
C                     TEMP       TEMP      (ATM)      (KM)       (MIN)  INCREMENTS
C                                                                          (HR)
C------ INPUT BEGINS HERE ----------
C IDLE                  482.       538.     1.26       0.         5.         .083
C TAKE-OFF              788.       871.     8.16       6.096      17.        .283
C CRUISE                760.       821.     5.44       12.192     20.       2.75
C CRUISE                760.       821.     5.44       0.5        95.       2.75
C CRUISE                760.       821.     5.44       12.192     20.       2.75
C PART POWER            760.       821.     4.42       6.096      10        2.75
C LANDING               482.       538.     1.36       0.         5.         .083
C----- INPUT ENDS HERE -------------
C
C-------------------------------------------------------------------------
C END IF PROGRAM
```

APPENDIX C. 3-D FINITE ELEMENT MICROMODEL GENERATOR (DIMPLE.FOR)

The following program was developed by GTEC to create a finite element mesh that models the various layers in a TBC-coated part. Output takes the form of ANSYS PREP7 commands that when read into ANSYS will produce the desired model. The program generates four material layers.

The first layer represents the base metal, which is flat. The second layer represents the bond coat, which changes from flat to sinusoidal. The third is the oxidation layer, which is sinusoidal on the top and bottom. This shape transitions back to flat in the fourth layer, which represents the TBC itself. Input is interactive and consists of requests for the geometric dimensions.

```
C
C       PROGRAM TBC Micromodel
C
CXXXXXXXXXXXXXXXXXXXXXXXXXXXXXXXXXXXXXXXXXXXXXXXXXXXXXXXXXXXXXXXXXX
C
C THIS PROGRAM IS CONSTRUCTED TO PRODUCE ANSYS INPUT FOR A 3-D FINITE
C ELEMENT MODEL FOR A MATERIAL INTERFACE PROBLEM FOR A TBC SYSTEM
C THE PROGRAM GENERATES 4 SEPERATE MATERIAL ZONES:
C
C       MATERIAL 1 => SUBSTRATE, BASE METAL
C       MATERIAL 2 => BOND COATING, BETWEEN METAL AND OXIDE LAYER
C       MATERIAL 3 => OXIDE, BETWEEN BOND AND TBC LAYER
C       MATERIAL 4 => TBC LAYER, GOES FROM DIMPLE TO FLAT ON TOP
C
C DIMENSIONS ARE OBTAINED INTERACTIVELY.  THE OUTPUT FILE IS IN
C ANSYS FILE29 FORMAT AND CAN BE USED TO CREATE GEOMETRY.  ALL OTHER
C FACTORS SUCH AS MATERIAL PROPERTIES AND CONSTRAINTS MUST BE ADDED IN
C ANSYS.
C
CXXXXXXXXXXXXXXXXXXXXXXXXXXXXXXXXXXXXXXXXXXXXXXXXXXXXXXXXXXXXXXXXXX
C
        IMPLICIT DOUBLE PRECISION (A-H,O-Z)
        DOUBLE PRECISION HITE1,HITE2,HITE3
        INTEGER O,P
        CHARACTER INFILE*12,OUTFIL*12,AGAIN*9
C
C  DO I/O STUFF
C
        WRITE(6,900)
 1      WRITE(6,979)'ENTER AN OUTPUT FILE NAME==>'
        READ '(A)',OUTFIL
C
        ASSIGN 1 TO IERROR
        OPEN(9,FILE=OUTFIL,STATUS='UNKNOWN')
C
 2      WRITE(6,900)
        WRITE(6,979)'WHAT IS THE MAXIMUM AMPLITUDE?  (PEAK TO PEAK) '
        READ(5,*)AMPMAX
        WRITE(6,*)
        AMPMAX = AMPMAX/2.DO
C
        WRITE(6,979)'WHAT IS THE LENGTH OF A SIDE OF THE SQUARE? '
        READ(5,*)SLNGTH
        WRITE(6,*)
C
        WRITE(6,979)'HOW MANY LINES OF NODES PER SIDE? (INCLUDING EDGES)'
        READ(5,*)ITIMS
        WRITE(6,*)
C
        WRITE(6,979)'WHAT IS THE HEIGHT OF THE SUBSTRATE? '
        READ(5,*)HITE1A
C
        WRITE(6,*)
        WRITE(6,*)'HOW MANY LAYERS OF NODES ARE THERE IN THE RADIAL '
        WRITE(6,979)'DIRECTION FOR THE SUBSTRATE? '
        READ(5,*)ILAY1A
        WRITE(6,*)
C
        WRITE(6,979)'WHAT IS THE HEIGHT OF THE BOND COATING?'
```

```
      READ(5,*)HITE1
      WRITE(6,*)
C
      WRITE(6,*)'HOW MANY LAYERS OF NODES ARE THERE IN THE RADIAL '
      WRITE(6,979)'DIRECTION FOR THE BOND COATING? '
      READ(5,*)ILAY1
      WRITE(6,*)
C
      WRITE(6,979)'WHAT IS THE HEIGHT OF THE OXIDE? '
      READ(5,*)HITE2
      WRITE(6,*)
C
      WRITE(6,979)'WHAT IS THE HEIGHT OF THE TBC LAYER? '
      READ(5,*)HITE3
      WRITE(6,*)
C
      WRITE(6,*)'HOW MANY LAYERS OF NODES ARE THERE IN THE RADIAL'
      WRITE(6,979)'DIRECTION FOR THE TBC LAYER? '
      READ(5,*)ILAY3
      WRITE(6,900)
C
C  CHECK TO SEE IF ENTERED VALUES ARE OK
C
      HCHK1 = HITE1 + HITE2 + 2*AMPMAX
      HCHK3 = HITE1 + HITE2 + HITE3
      IF (HCHK1 .GE. HCHK3) THEN
         WRITE(6,*)'****************** WARNING ******************'
         WRITE(6,*)
         WRITE(6,*)'YOU HAVE ENTERED GEOMETRY WHICH MAKES THE TOP'
         WRITE(6,*)'OF THE SUBSTRATE AND/OR THE OXIDE LAYER, '
         WRITE(6,*)'POKE THROUGH  THE TOP OF THE TBC COATING'
         WRITE(6,*)'   PLEASE ENTER IN NEW GEOMEOMETRY|'
         WRITE(6,*)
         WRITE(6,979)'WOULD YOU LIKE TO CONTINUE? (Y/N)'
         READ '(A)',AGAIN
         IF (AGAIN .EQ. 'Y')GOTO 2
         GOTO 99
      END IF
C
C  SHOW USER WHAT THEY'VE GOT

      WRITE(6,*)'THE MODEL WILL BE BUILT USING:'
      WRITE(6,*)
      WRITE(6,*)'MAXIMUM AMPLITIUDE =',AMPMAX*2
      WRITE(6,*)
      WRITE(6,*)'SUBSTRATE HEIGHT =>',HITE1A
      WRITE(6,*)'BOND COAT HEIGHT =>',HITE1
      WRITE(6,*)'OXIDE HEIGHT     =>',HITE2
      WRITE(6,*)'TBC LAYER HEIGHT =>',HITE3
      WRITE(6,*)'TOTAL RAD HEIGHT  =>',HCHK3 + HITE1A
      WRITE(6,*)
      WRITE(6,*)'CUBE SIDE LENGTH  =>',SLNGTH,'X',SLNGTH
      WRITE(6,*)'-----------------------------------------------'
C
      A = (ITIMS-1)*(ITIMS-1)
      B = ILAY1 + ILAY3 - 2 + ILAY1A
      C = A*B
C
      WRITE(6,*)'ELEMENTS PER LAYER=>',A
      WRITE(6,*)'NUMBER OF LAYERS=>',B
```

```
      WRITE(6,*)'NUMBER OF TOTAL ELEMENTS=>',C
      WRITE(6,*)
      WRITE(6,979)'CONTINUE WITH THESE VALUES? (Y/N)'
      READ '(A)',AGAIN
      WRITE(6,900)
      IF (AGAIN .EQ. 'N')GOTO 2
C
C SET UP SOME CONSTANTS
C
      ILNGTH = ITIMS - 1
      PI = 3.141592645
      PIOL = 2.D0*(PI/SLNGTH)
C
C CALCULATE NODAL POSITION FOR SUBSTRATE
C
      WRITE(9,*)'/NOPR'
C
      START = 0.D0 - HITE1A
      N = 1
      ZINC = HITE1A/(ILAY1A-1)
      DO 3 K=1,ILAY1A
         WRITE(6,*)'CALCULATING NODES FOR SUBSTRATE, LAYER',K
         ZADD = ZINC*(K-1)
         DO 4 I=1,ITIMS
            AI1 = I - 1
            DO 5 J=1,ITIMS
               AK = J - 1
               X = SLNGTH*(AK/ILNGTH)
               Y = SLNGTH*(AI1/ILNGTH)
               Z = START + ZADD
               WRITE(9,1500)N,X,Y,Z
               N = N + 1
 5          CONTINUE
 4       CONTINUE
 3    CONTINUE
C
C CALCULATE NODAL POSITION FOR MATERIAL 1
C
      AINC = AMPMAX/(ILAY1-1)
      ZINC = HITE1/(ILAY1-1)
      DO 30 K = 2,ILAY1
         WRITE(6,*)'CALCULATING NODES FOR BOND COAT, LAYER',K
         AMP = AINC*(K-1)
         ZADD = ZINC*(K-1)
         DO 10 I = 1,ITIMS
           AI1 = I - 1
           DO 20 J = 1,ITIMS
             AK = J - 1
             X = SLNGTH*(AK/ILNGTH)
             Y = SLNGTH*(AI1/ILNGTH)
             A = (0.D0-AMP*COS(PIOL*Y))+AMP
             Z = (0.D0-A*COS(PIOL*X))+(ZADD)+A
             WRITE(9,1500)N,X,Y,Z
             N = N + 1
 20        CONTINUE
 10      CONTINUE
 30   CONTINUE
C
C  DO THE NODES FOR MATERIAL 2
C
```

```
          WRITE(6,*)'CALCULATING NODES FOR OXIDE LAYER'
          DO 11 I = 1,ITIMS
           AI1 = I - 1
           DO 21 J = 1,ITIMS
             AK = J - 1
             X = SLNGTH*(AK/ILNGTH)
             Y = SLNGTH*(AI1/ILNGTH)
             A = (0.D0-AMP*COS(PIOL*Y))+AMP
             Z = (0.D0-A*COS(PIOL*X))+(ZADD)+(A)+HITE2
             WRITE(9,1500)N,X,Y,Z
             N = N + 1
 21         CONTINUE
 11        CONTINUE
C
C  DO NODES FOR MATERIAL 3
C
         ZINC = HITE3/(ILAY3-1)
         DO 32 K = 1,ILAY3
            WRITE(6,*)'CALCULATING NODES FOR TBC, LAYER',K
            AINC = AMPMAX/(ILAY3-1)
            AMP = AINC*(ILAY3-K)
            ZADD = ZINC*(K-1)
            DO 12 I = 1,ITIMS
              AI1 = I - 1
              DO 22 J = 1,ITIMS
                AK = J - 1
                X = SLNGTH*(AK/ILNGTH)
                Y = SLNGTH*(AI1/ILNGTH)
                A = (0.D0-AMP*COS(PIOL*Y))+(AMP)
                Z = (0.D0-A*COS(PIOL*X))+(ZADD)+(A)+HITE2+HITE1
                WRITE(9,1500)N,X,Y,Z
                N = N + 1
 22           CONTINUE
 12         CONTINUE
 32      CONTINUE
C
C DO ELEMENT CONNECTIVITY FOR THE FIRST ELEMENT
C
         WRITE(9,*)'ET,1,45'
         WRITE(9,*)'/GOPR'
         IT2 = ITIMS*ITIMS
         I = IT2 + ITIMS + 1
         J = IT2 + ITIMS + 2
         K = ITIMS + 2
         L = ITIMS + 1
         M = IT2 + 1
         N = IT2 + 2
         O = 2
         P = 1
         IL2 = ILNGTH*ILNGTH
         IELAY = ILAY1A-1
         WRITE(9,2000)I,J,K,L,M,N,O,P
C
C DO EGENS FOR SUBSTRATE
C
         WRITE(9,3000)ILNGTH,ILNGTH,ITIMS,ILNGTH
         WRITE(9,4000)IELAY,IT2,1,IL2
C
C DO EGENS FOR MATERIAL 1
C
```

```
        IE2 = IL2*IELAY
        IE1 = IE2 - IL2 + 1
        ITM1 = ILAY1
        WRITE(9,4000)ITM1,IT2,IE1,IE2
        IELAY = ILAY1A + ILAY1 - 2
        IA = IE2+1
        IB = IL2 * IELAY - 1
        WRITE(9,5000)IA,IB
        WRITE(9,*)'MAT,2'
        WRITE(9,*)'EMODIF,ALL'
        WRITE(9,*)'EALL'
C
C
C DO EGENS AND MATERIAL TYPE FOR MATERIAL 2
        IE2 = IL2*IELAY
        IE1 = IE2 - IL2 + 1
        WRITE(9,4000)2,IT2,IE1,IE2
        IA = IE2+1
        IB = IE2 + IL2
        WRITE(9,5000)IA,IB
        WRITE(9,*)'MAT,3'
        WRITE(9,*)'EMODIF,ALL'
        WRITE(9,*)'EALL'
C
C DO EGENS AND MATERIAL TYPE FOR MATERIAL 3
C
        IE3LAY = ILAY3
        IE2 = IE2 + IL2
        IE1 = IE1 + IL2
        WRITE(9,4000)IE3LAY,IT2,IE1,IE2
        IA = IE2+1
        IB = IE2 + IL2*IE3LAY
        WRITE(9,5000)IA,IB
        WRITE(9,*)'MAT,4'
        WRITE(9,*)'EMODIF,ALL'
        WRITE(9,*)'EALL'
        WRITE(9,*)'MNUM,1'
C
        WRITE(6,900)
        CLOSE(9)
C
C FORMAT STATEMENTS
C
 1000   FORMAT(6X,2(E16.9,','),E16.9)
 1500   FORMAT('N,',I5,3(',',G16.9))
 2000   FORMAT(1X,'E',8(',',I5))
 3000   FORMAT(1X,'EGEN,',I5,',1,1'/1X,'EGEN,',I5,',',I5,',1,',I5)
 4000   FORMAT(1X,'EGEN',4(',',I5))
 5000   FORMAT(1X,'ESEL,ELEM,',I5,',',I5)
 900    FORMAT(/80('*')/)
 979    FORMAT(1X,A,1X,$)
C
 99     STOP
        END
```

REFERENCES

1. T.E. Strangman and J. Neumann, "Thermal Barrier Coating Life Prediction Model Development - First Annual Report," NASA CR-175002, 1985.

2. J.T. DeMasi and K.D. Sheffler, "Thermal Barrier Coating Life Prediction Model Development - Second Annual Report," NASA CR-179508, 1986.

3. K.E. Wilkes and J.F. Lagedrost, "Thermophysical Properties of Plasma Sprayed Coatings," NASA CR-121144, 1973.

4. W.R. Sevcik and B.L. Stoner, "An Analytical Study of Thermal Barrier Coated First Stage Blades in a JT9D Engine," NASA CR-135360, 1978.

5. J.T. DeMasi and K.D. Sheffler, "Thermal Barrier Coating Life Prediction Model Development - Presentation at the 1985 NASA-HOST Workshop," 1985.

6. K.D. Sheffler, R.A. Graziana, and G.C. Sinko, "JT9D Thermal Barrier Coated Vanes," NASA CR-167964, 1982.

7. Sheffler, K.D. and DeMasi, J.T., "Thermal Barrier Coating Life Prediction Model Development, First Annual Report," NAS3-23944.

8. Anderson, C.A., et al, "Advanced Ceramic Coating Development for Industrial/Utility Gas Turbine Applications," DEN3-110.

9 R.A. Miller, "An Oxidation Based Model for Thermal Barrier Coating Life," J. American Ceramic Society, 67 (1984) 517-521.

10 J.T. DeMasi, "Thermal Barrier Coating Life Prediction Model Development," P. 445-455 in Turbine Engine Hot Section Technology 1985, NASA CP 2405, 1985.

11. R.A. Miller, unpublished research.

12. R.V. Hillery, B.H. Pilsner, T.S. Cook and K.S. Kim "Thermal Barrier Coating Life Prediction Model," NASA CR-179504, 1986.

13. T.E. Strangman, "Life Prediction and Development of Coatings for Turbine Airfoils," Workshop on Gas Turbine Materials in a Marine Environment, Bath, England, 1984.

14. A.H. Woodcock, "Salt Nuclei in Marine Air as a Function of Altitude and Wind Force," Journal of Meterology, 10, Pages 362-371, 1953.

15. C.M. Gordon, E.C. Jones, and R.E. Larson, "The Vertical Distribution of Particulate Na and Cl in a Marine Atmosphere," Journal of Geophysical Research, 82, pages 988-990, 1977.

16. D.J. Jung, E.W. Mihalek, R.E. Ruskin, and C.T. Frazier, "Status of U.S. Navy Gas Turbine Inlet Development Program," pages 105-131 in Proceedings of the 4th Conference on Gas Turbine Materials in a Marine Environment, Annapolis, MD, 1979.

17. R.E. Ruskin, R.K. Jeck, F.K. Lepple, and W.A. VonWald, "Salt Aerosol Survey at Gas Turbine Inlet Aboard USS Spruance," NRL Memorandum Report 3804, 1978.

18. J.G. Tschinkel, "Formation of Sodium Sulfate in Gas Turbine Combustors," Corrosion NACE, 28, pages 161-169, 1972.

19. C.G. McCreath, "The Fate of Sea Salt in a Marine Gas Turbine," Proceedings of the Third Conference on Gas Turbine Materials in a Marine Environment, Bath, England, 1976.

20. C.G. McCreath, "The Fate of Sea Salt in a Marine Gas Turbine - Phase Two," pages 339-356 in Proceedings of the Fourth Conference on Gas Turbine Materials in a Marine Environment, Annapolis, MD, 1979.

21. J.T. Prater, R.W. Knoll, and E. Courtright, "Ceramic Thermal Barrier Coatings With Improved Corrosion Resistance," presented at the International Conference on Metallurgical Coatings, San Diego, CA, 1987.

22. I.E. Sumner and D. Ruckle, "Development of Improved Durability Plasma Sprayed Ceramic Coatings for Gas Turbine Engines," AIAA Paper No. 80-1193, 1980.

23. C.A. Andersson, et al., "Advanced Ceramic Coating Development for Industrial/Utility Gas Turbine Applications," NASA CR-165619, 1982.

24. W.D. Kingery, Introduction to Ceramics, John Wiley & Sons, Inc., New York, 1960, p. 599.

25. I. Zaplatynsky, "Performance of Laser-Glazed Zirconia Thermal Barrier Coatings in Cyclic Oxidation and Corrosion Burner Rig Tests," Thin Solid Films, 95 (1982), 275-284.

26. E. Demaray, "Thermal Barrier Coatings by Electron Beam Physical Vapor Deposition," DOE Contract DE-AC06-76RL01830, 1982.

27. N.E. Ulion and D.L. Ruckle, "Columnar Grain Ceramic Thermal Barrier Coatings on Polished Substrates," U.S. Patent 4,321,310, 1982.

28. T.E. Strangman, "Columnar Grain Ceramic Thermal Barrier Coatings," U.S. Patent 4,321,331, 1982.

29. D.S. Duval, "Processing Technology for Advanced Metallic and Ceramic Turbine Airfoil Coatings," in Proceedings of the Second Conference on Advanced Materials for Alternative-Fuel-Capable Heat Engines, EPRI RD-2369-SR, Monterey, California, 1981.

30. A.G. Evans, G.C. Crumley, and E. Demaray, "On the Mechanical Behavior of Brittle Coatings and Layers," Oxidation of Metals, 20 (1983), 193-216.

31. T.E. Strangman, "Thermal Barrier Coatings for Turbine Airfoils," Thin Solid Films, 127 (1985), 93-105.

32. G. McDonald and R. Hendricks, "Effect of Thermal Cycling on ZrO_2 - Y_2O_3 Thermal Barrier Coatings," NASA TM 81480, 1980.

33. G. McDonald and R. Hendricks, "Effect of Thermal Cycling on ZrO_2-Y_2O_3 Thermal Barrier Coatings," Thin Solid Films, 73 (1980), 491-496.

34. R.A. Miller and C.E. Lowell, "Failure Mechanism of Thermal Barrier Coatings Exposed to Elevated Temperatures," Thin Solid Films, 95 (1982), 265-273.

35. R.A. Miller and C.C. Berndt, "Performance of Thermal Barrier Coatings in High Heat Flux Environments," Thin Solid Films, 119 (1984), 195-202.

36. R.A. Miller, "An Oxidation Based Model for Thermal Barrier Coating Life," J. American Ceramic Society, 67 (1984), 517-521.

37. R.A. Miller, "Analysis of the Response of a Thermal Barrier Coating to Sodium and Vanadium-Doped Combustion Gases," DOE/NASA/2593-79/7, NASA TM-79205, 1979.

APPENDIX C. DISTRIBUTION LIST

D.L. Alger (301-2)
NASA Lewis Research Center
21000 Brookpark Road
Cleveland, OH 44135

L.F. Aprigliano
D. Taylor Shipyard
R&D Center
Annapolis, MD 21402

M.M. Bailey (77-6)
NASA Lewis Research Center
21000 Brookpark Road
Cleveland, OH 44135

Michael Bak (5-16)
Williams International
P.O. Box 200
Walled Lake, MI 48088

H. Beale
Applied Coatings, Inc.
775 Kaderly Drive
Columbus, OH 43228

Robert Beck
Teledyne - CAE
1330 Laskey Road
Toledo, OH 43612

Biliyar N. Bhat (EH-23)
NASA Marshall Space
Flight Center
Huntsville, AL 35812

David Bott
Muscle Shouls Mineral Company
1202 East 2nd Street
Muscle Shoals, AL 35661

R.J. Bratton
Westinghouse Electric R&D
1310 Buelah Road
Pittsburgh, PA 15235

Sherman D. Brown
Chemical Engineering Dept.
University of Illinois
Urbana, IL 61801

Walter Bryzik (RGRD)
U.S. Army Tank-Auto. Command
Diesel Engine Research RMSTA
Warren, MI 48397

R.F. Bunshah
University of California
6532 Boelter Hall
Los Angeles, CA 90024

George C. Chang (MC 219)
Cleveland State University
Cleveland, OH 44115

Jerry Clifford
U.S. Army Applied Tech. Lab.
SAVDL-ATL-ATP
Fort Eustic, VA 23604

Dave Clingman
Detroit Diesel Allison - GMC
Engineering Operations
Indianapolis, IN 46206

Arthur Cohn
E P R I
3412 Hillview Avenue
Palo Alto, CA 94303

Thomas A. Cruse
Southwest Research Institute
P.O. Box 28510
San Antonio, TX 78284

Keith Duframe
Battelle Labs.
Columbus, OH 43216

Mrityunjoy Dutta
U.S. Army AMSAV-EAS
4300 Goodfellow Blvd.
St. Louis, MO 63120

D.S. Engleby
Naval Air Rework Facility
Mail Drop 9, Code 017
Cherry Point, NC 28533

John Fairbanks (FE-22)
Department of Energy
Office of Fossil Energy
Washington, DC 20545

N. Geyer
AFWAL/MLLM
Wright Patterson AFB
Dayton, OH 45433

J.W. Glatz
NAPTC R&D Division
Naval Air Prop. Test Center
Trenton, NJ 08628

G.W. Goward
Coatings Technology Corp.
2 Commercial Street
Branford, CT 06405

M.A. Greenfield (RM)
NASA Headquarters
600 Independence Avenue
Washington, DC 20546

S.J. Grisaffe (49-1)
NASA Lewis Research Center
21000 Brookpark Road
Cleveland, OH 44135

D.K. Gupta
Pratt & Whitney Aircraft
400 Main Street
E. Hartford, CT 06108

William K. Halman
Temescal
2850 Seventh Street
Berkeley, CA 94710

E. Hanink
Detroit Diesel Allison - GMC
Engineering Operations
Indianapolis, IN 46206

Doug Harris
APS - Materials Inc.
153 Walbrook
Dayton, OH 45405

Harold Herman
Argonne National Lab.
9700 South Cass Avenue
Argonne, IL 60439

H. Herman (W-8)
Detroit Diesel Allison - GMC
P.O. Box 894
Indianapolis, IN 46206

M. Herman
Dept. of Materials Science
State Univ. of New York
Stonybrook, NY 11794

Frank Hermanek
Alloy Metals, Inc.
501 Executive Drive
Troy, MI 48084

R. Hillery (M-85)
General Electric Company
MPTL
Cincinnati, OH 45215

J. Stan Hilton
University of Dayton
300 College Park
Dayton, OH 45469

Richard R. Holmes (EH-43)
Marshall Space Flight Center
Huntsville, AL 35812

Lulu Hsu
Solar Turbines, Inc.
2200 Pacific Highway
San Diego, CA 92138

Larry A. Junod
Allison Gas Turbine Division
P.O. Box 420, Plant 8-T12
Indianapolis, IN 46206

C. Kortovich
TRW Inc.
23355 Euclid Avenue
Cleveland, OH 444117

Propulsion Laboratory (302-2)
U.S. Army Res. & Tech. Lab.
21000 Brookpark Road
Cleveland, OH 44135

Sylvester Lee
AFWAL-MLTM
Wright Patterson AFB
Dayton, OH 45433

A.V. Levy
Lawrence Berkely Lab.
University of California
Berkeley, CA 94720

C.H. Liebert (77-2)
NASA Lewis Research Center
21000 Brookpark Road
Cleveland, OH 44135

E.L. Long, Jr.
Oak Ridge National Lab.
P.O. Box X, Bldg. 4508
Oak Ridge, TN 37831

Frank N. Longo
Metco, Inc.
1101 Prospect Avenue
Westbury, L.I., NY 11590

Richard Martin (9W-61)
Boeing Commercial Airplane Co.
P.O. Box 3707
Seattle, WA 98124

R.A. Miller (105-1)
NASA Lewis Research Center
21000 Brookpark Road
Cleveland, OH 44135

T.E. Mitchell
Case Western Reserve Univ.
10900 Euclid Avenue
Cleveland, OH 44106

S. Naik
AVCO-Lycoming Division
550 South Main Street
Stratford, CT 06497

J.A. Nesbitt (49-3)
NASA Lewis Research Center
21000 Brookpark Road
Cleveland, OH 44135

J.W. Patten
Cummins Engine Company
Box 3005
Columbus, IN 47202

Ronne D. Proch
Corning Glass Works
31501 Solon Road
Solon, OH 44139

R.J. Quentmeyer (500-220)
NASA Lewis Research Center
21000 Brookpark Road
Cleveland, OH 44135

Gopal Revanton
Deer & Company
3300 River Drive
Moline, IN 61265

David Rigney (D-83)
General Electric Company
Cincinnai, OH 45215

Joseph Scricca
AVCO-Lycoming Division
550 South Main Street
Stratford, CT 06497

Keith Sheffler
Pratt & Whitney Aircraft
400 Main Street
Hartford, CT 06109

T.P. Shyu
Caterpiller Tractor Company
100 N.E. Adams
Peoria, IL 61629

R.W. Soderquist (165-03)
Pratt & Whitney Aircraft
400 Main Street
E. Hartford, CT 06108

D.E. Sokolowski (49-7)
NASA Lewis Research Center
21000 Brookpark Road
Cleveland, OH 44135

C.A. Stearns (106-1)
NASA Lewis Research Center
21000 Brookpark Road
Cleveland, OH 44135

S. Stecura (49-3)
NASA Lewis Research Center
21000 Brookpark Road
Cleveland, OH 44135

T.E. Strangman
Garrett Turbine Engine Co.
2739 E. Washington
Phoenix, AZ 85010

T.N. Strom (23-2)
NASA Lewis Research Center
21000 Brookpark Road
Cleveland, OH 44135

Richard Stueben
Chromalloy R&T
Chromalloy Amer. Corp.
Orangeburg, NY 10962

T.A. Taylor
Linde Division
Union Carbide Corporation
Indianapolis, IN 46224

Robert P. Tolokan
Brunswick Corporation
2000 Brunswick Lane
DeLand, FL 32724

F.C. Toriz
Rolls Royce, Inc.
1985 Phoenix Blvd.
Atlanta, GA 30349

Donald Whicker
GM Research Laboratory
GM Technical Center
Warren, MI 48090

I. Zaplatynsky (106-1)
NASA Lewis Research Center
21000 Brookpark Road
Cleveland, Ohio 44135